RADIATION DAMAGE IN $KMgF_3$

By

JOHN EVERETT RHOADS

Bachelor of Science
Midwestern University
Wichita Falls, Texas
1968

Master of Science
Oklahoma State University
Stillwater, Oklahoma
1972

Submitted to the Faculty of the Graduate College
of the Oklahoma State University
in partial fulfillment of the requirements
for the Degree of
DOCTOR OF PHILOSOPHY
December, 1974

RADIATION DAMAGE IN $KMgF_3$

Thesis Approved:

Larry E. Halliburton
Thesis Adviser

W. A. Sibley

K. D. Berlin

William J. Lewis

Dean of the Graduate College

To

Garland

and

La Vera

ACKNOWLEDGMENTS

Without the professional assistance and the personal encouragement of Dr. L. E. Halliburton, this work would never have been completed by myself. For the encouragement, the assistance, and the example he set I am deeply grateful. I only hope that time demonstrates this work, the first under his direction as an advisor, to be the worst done under his auspices.

The completion of this work on my part is in reality the result of efforts made by literally hundreds of persons who have been a part of my life, beginning with my parents. I feel this is one place that appreciation for them should be expressed. Garland and La Vera Ray offered a unique and very much appreciated opportunity for me to work my way through Midwestern University, an opportunity that has had a great impact on my life. Grandparents, other uncles and aunts, and cousins all gave unsolicited moral support for all my academic endeavors as well as representing certain ideals to which I could aspire. The same may be said of all members of my wife's family and relatives, especially her parents, Mr. and Mrs. Joseph Mione. I am extremely honored by the support all these individuals have given.

Obviously, teachers have played an integral part in the completion of this work, and I have been uncommonly fortunate to have had

such a high percentage of excellent ones helping me understand the intricacies of this world and its people, from grade one up. Because of their personally deep commitment to excellence in their pupils, two deserve special mention: Mr. R. L. Bradley of the Wichita Falls Public School System and Dr. P. A. Westhaus of the Physics Department of this university--two extremely rare individuals.

I have enjoyed during my residence at OSU what I felt to be an excellent relationship with all members of the Physics faculty, people who answered the little questions and in various ways contributed incalculably to my total enlightenment. Members of the Physics office staff were also of significant assistance in numerous details that arose through the years, most especially Ms. Janet Sallee, to whom enough tributes cannot be paid. Mr. Heinz Hall and Mr. Floyd Vulgamore of the Physics-Chemistry Machine Shop are due a great deal of credit for this work in that quite simply without their excellent work this research project could not have proceeded as smoothly as it did. There were the other graduate students from whom I also learned much, and recognition of Mr. Doyle Fouquet, Mr. Edwin Bradford, and Ms. Sandra Whisenhunt for their invaluable aid with regards programming needs be given. Mr. Fouquet supplied copies of the diagonalization subroutines for complex Hermitian matrices, subroutines which were central to analysis of the experimental data.

And most significantly, I must acknowledge my wife, who has been my closest friend and has played a vital and much appreciated

supporting role for my graduate work. The excellent typing of this work and my M. S. thesis represents only a small portion of her total effort.

Financial support has been provided in the form of a three year National Defense Education Act Fellowship (1970-1973), a National Science Foundation research associateship (1973-1974), and an allowance from the Veteran's Administration for educational purposes. The American people have made all this possible through their hard-earned tax dollars.

For all of this I am grateful.

TABLE OF CONTENTS

LIST OF TABLES

LIST OF FIGURES

CHAPTER I

INTRODUCTION

What appears to be the first observation of radiation-induced effects in materials was that by Wollaston and Berzelius in 1815 (1), preceding by many years the discovery of natural radioactivity itself. These workers found that the black or brown mineral gadolinite ($Be_2FeY_4Si_2O_{13}$) when heated to near incandescence suddenly showed a sharp temperature rise (presumably a phase change) and emitted a brilliant flash of light. This mineral, which incidentally is a source of the constituent elements as well as cerium and erbium, was later found to also contain uranium or thorium at concentrations of greater than 0.1 percent. It is these natural sources of roughly 4 MeV alpha particles that through the eons have bombarded the gadolinite crystal from within, disordering the relatively unstable crystal structure. It is this disorder which is annealed by heating of the mineral.

There were other such observations during the nineteenth century which are covered adequately by Billington and Crawford (1). It appears, however, that the first deliberate attempt by man to disorder a crystal structure by radiation was made by Stackelberg and Rotterbach in 1939 by irradiating a zircon ($ZrSiO_4$) crystal directly

with alpha particles (1). The weak source, however, gave inconclusive results.

The advent of the nuclear reactor in 1943 brought the subject of radiation damage further out of the realm of naturally occurring physical curiosa and deeper into the realm of technological significance. Since 1895, which brought discovery of both X-rays by Roentgen and natural radioactivity by Becquerel, most work in this area concerned itself with the effect on the radiation caused by its interaction with matter. The emphasis shifted to the effects radiation had on matter in 1943. In this year "Wigner's Disease" was predicted, i.e., reactor components could be adversely affected by the high energy products of fission. Fusion reactors, too, now present their own radiation damage problems. To the purist, however, radiation damage and the defects so created have become a means of exploring the intricacies of the solid state.

Two questions that have been addressed almost since the inception of the study of radiation damage to materials are (A) What are the physical and electronic properties of defects induced by radiation and (B) What are the processes and mechanisms that lead to the creation of these defects? It is to the first question that this study will be addressed, but for completeness a discussion of the second question will be included. Point defects, well isolated single defects in materials, are the implicit basis for this discussion, as opposed to extended defects such as cascade displacements, interstitial or

vacancy clusters, loops, etc.

Presently, radiation damage processes in polar crystals are divided into three distinct classes (2, p. 212): (A) electronic processes "in which an electronic state is changed or charge is moved about by the absorption of radiant energy, but in which no ionic or atomic defects are formed"; (B) elastic collisions "in which atoms or ions are displaced due to momentum and energy transfer from irradiating particles"; and (C) radiolysis, "those processes in which atomic or ionic defects are produced by a series of reactions beginning with an electronic excitation." Each of these three classes has its own domain within which it is of importance, and many references concerning each class are available (1, 3, 4). Of these classes, the two that are of importance to this study are the first and third. These will now be discussed in more detail.

Electronic processes are effected by the absorption of energy from incident radiating particles or photons, and the mode of absorption of this energy depends on the type of radiation. For instance, photons may give up their energy to a crystal in a number of ways, depending strongly on the initial energy of the photon. Some representative type mechanisms for the transfer of photon energy are the photoelectric effect, the Compton effect, pair production, and nuclear processes (2).

When the radiation field consists of energetic charged particles, one usually calculates formulae for the energy loss per unit path

length in the material, this energy loss being due to the interaction of the charged particles with the electrons of the crystal. As an example, for 1.5 MeV (relativistic) electrons the differential energy loss in a material may be calculated from (5):

$$-\frac{dE}{dx} = \frac{4\pi e^2}{mc^2} N \left[\ln \frac{2mc^2}{I} - \frac{3}{2} \ln \left[(1 - \beta^2)^{\frac{1}{2}}\right] - \frac{1}{2} \ln 8 + \frac{1}{16}\right]$$

where I is a special average of the excitation and ionization potentials in the atoms of the stopping material, $\beta = \frac{v}{c}$ (v the velocity of the electrons of charge e and rest mass m, c the velocity of light in vacuum), and N is the electronic density of the stopping material.

Regardless of how energy is absorbed from the radiation field by the crystal, the result can be electrons in a normally empty conduction band and holes in a normally occupied valence band, or excitons (bound electron-hole pairs) localized at lattice ions, impurities, or existing defects in the crystal. The production of an electronic defect is effected by the separation and stabilization of either or both the electron and the hole. Stabilizing sites for electrons or holes may be impurities, existing defects, or select sites, which may exist even in the perfect lattice. This motion and subsequent stabilization of electron and hole must produce as an end result a change in the electronic structure of the crystal. One example of an electronic defect is a change due to irradiation in the charge state of an impurity ion in a crystal, yet the one example of particular interest to this study is the self-trapped hole center (6), which will be discussed in more detail later.

The other class of radiation damage processes which is of importance to this study is radiolysis. This class of damage evolved in a natural way in an attempt to explain the production of interstitial-vacancy pairs (Frenkel pairs) created in many alkali halide crystals by ultraviolet photons. These photons lack the physical properties required to transfer sufficient momentum to a lattice atom or ion to displace it directly in an elastic collision; hence, some scheme had to be conceived to explain the experimentally observed radiation damage. This scheme now consists of three elements. First, the photon causes an electronic excitation which results (at least temporarily) in the creation of a polarized or charged electronic defect in the lattice, in essence a product of the first class of radiation damage as discussed above. The second element is the conversion of this electronic excitation energy into kinetic energy of a lattice atom (or ion) in such a way that the latter moves. And the final step in this scheme is the movement of this atom or ion away from its original site and its subsequent stabilization at some other point in the lattice, not necessarily at a normal lattice site.

The majority of the evidence now amassed from years of study of alkali halide materials implies that radiolysis produces Frenkel pairs in the halide sub-lattice and that it is a bulk process that can occur in the perfect lattice. The question as to the precise details or mechanism for radiolysis in the alkali halides consistent with the above evidence, however, has had and continues to have considerable attention

given to it. Some of the questions are (A) How is the electronic excitation energy converted into kinetic energy of a lattice atom? (B) Exactly how does the ejected ion or atom move through the lattice? (C) How far does it move from its original site? and (D) What prevents it from recombining with the vacancy? Through the years various proposals have been submitted in attempts to answer these questions. These began with an Auger process (with subsequent dissociation) described by Platzman (7), followed by another multiple ionization scheme proposed by Varley (8, 9). There were also several variations of Varley's original mechanism (10, 11, 12, 13) as well as the renowned "vacancy pair evaporation" scheme that was proposed by Seitz (14). At present, however, the proposal with the broadest base of support to explain radiation damage by radiolysis at low temperatures in halide-containing crystals is the Pooley-Hersh mechanism, which will now be described in detail.

Pooley (15) first proposed this mechanism following work with potassium iodide (KI). Konitzer and Hersh (16), also working with KI, published essentially the same proposal just a few months later. The more elucidative paper describing this mechanism appears to be that by Hersh (17), which will be outlined.

At the heart of this mechanism are excitons. Hersh states that during X-ray or UV irradiation there exists in a crystal a high steady state population of excitons in the form of $X_2^{=*}$ molecules, which are formed by the following sequence:

$X^- + h\nu$ (X-ray or UV) $\rightarrow X^{-*}$ (primary Frenkel exciton) Eq. 1

$X^{-*} + X^- \rightarrow X_2^{=*}$ (relaxed Frenkel exciton) Eq. 2

or

$X_2^- + e \rightarrow X_2^{=*}$ Eq. 3

where X^- is a halide ion at a normal site and X_2^- is a pre-existing self-trapped hole center. Hersh proposes that these $X_2^{=*}$ molecules are <u>all</u> initially formed in an excited or induced predissociative state and that the successful dissociation of <u>some</u> of them generates vacancies and interstitials by imparting roughly 4 eV kinetic energy to essentially one of the halides, causing a replacement sequence (18) to occur along close-packed rows. The possible fates of this $X_2^{=*}$ entity are:

I Luminescence: $X_2^{=*} \rightarrow 2X^- + h\nu$ Eq. 4

II Heat (phonon): $X_2^{=*} \rightarrow 2X^- + h\nu_\phi$ Eq. 5

III Ionization: $X_2^{=*} \rightarrow X_2^- + e$ Eq. 6

IV Dissociation: $X_2^{=*} \rightarrow X_2^{=**} \rightarrow X_{int} + X^- + \square + e$ Eq. 7

where $X_2^{=**}$ is used to depict the relaxed Frenkel exciton in an excited vibronic predissociative or repulsive state, X_{int} denotes a halide atom at an interstitial site, $\square$ indicates a vacancy at a normally occupied halide site, and e is an electron. Dissociation is the Frenkel pair producer, and it is in this detail that the proposals of Pooley and Hersh as originally reported differ: Pooley postulated an interstitial ion whereas Hersh called for the production of the smaller interstitial atom. In light of work by Ueta, et al., (19), whereby F centers are produced within a 30-nanosecond 60 MeV electron beam pulse, it

appears that the vacancy and electron may actually never appear as separate entities as shown in Equation 7. In fact, Itoh (20) has proposed a model of F center and interstitial atom formation consistent with this latter statement.

The key idea is that the association of an excited and a normal X^- (halide ion) produces an $X_2^{=*}$ (exciton) in a state which is sufficiently excited or predissociative that within one or several vibrations of the newly formed molecule it dissociates. All of the halogen-associated defect centers are believed to arise after the primary photochemical act (Equation 1) from ordinary chemical interactions.

The clue leading to this proposal came from observations by both Hersh and Pooley of the luminescence (Equation 4) in KI <u>during</u> irradiation. Hersh noted that in many systems the onset of a photochemical reaction is accompanied by a drop in luminescence. As the temperature of the KI sample was raised through 100 K during irradiation, this transition was observed: Luminescence desisted; F center production commenced. Hence, an integral relationship was assumed to exist between the emitting center and the production of F centers and interstitials. By using crystals known to contain F and $[X_2^-]$ centers, it was observed in photoconductivity and infrared-stimulated luminescence studies that when a moving electron recombines with a self-trapped hole center, the $[X_2^-]$, the recombination luminescence can be quantitatively correlated with the characteristic excitonic luminescence generated during irradiation. The emitting

center was then conceived of as being due to a transitory molecule composed of an $[X_2^-]$ center and an additional bound electron (the $X_2^{=*}$).

Although the initial observations were made on KI, the identity of luminescence observed during irradiation and that produced during electron/self-trapped hole recombination has been demonstrated as well for RbI and NaI (21). Too, the drop in luminescence with the onset of F center production has been observed by Pooley, et al., (22) for a number of other alkali halides, although explicable exceptions do appear. The most convincing evidence for the Pooley-Hersh mechanism in alkali halides is the work done by Keller and Patten (23). In KCl:Tl containing $[Cl_2^-]$ centers, trapped electrons were released at 25 K by bleaching at 640 nm into the thallium optical band. It was found that the number of interstitials formed was in direct proportion to the number of trapped hole centers destroyed (Equations 3 and 7).

The proposed mechanism appears to explain most of the experimental results, although there are minor details yet to be settled. As Hersh (16, p. 780) states, "The way in which this mechanism seems superior . . . is that it ties together more observations in a simple way and contemplates an excitonic mechanism which has actually been observed."

This process (radiolysis) is of importance to this study because it is the one whereby interstitial-type point defects (H centers) appear to be produced in the alkali halides. It is a question yet to be answered

as to whether or not this mechanism is responsible for creating vacancy-interstitial pairs in other type crystalline structures containing halide ions.

As should be apparent at this point, the two defects of interest here are the self-trapped hole center [X_2^-] and the H center. Hence, an account of these two types of defects needs to be given.

The excellent and original work on self-trapped hole centers in alkali halides was done by Castner and Känzig, and their analysis of EPR (Electron Paramagnetic Resonance) and optical data is given in a paper published in 1957 (24). It should be pointed out, however, that the original report of this defect was made by Känzig two years earlier (6).

The self-trapped hole center is created by the interaction of the primary Frenkel exciton (Equation 1) (itself created by radiation) and a nearest neighbor halogen ion. The resulting $X_2^{=*}$ becomes ionized (Equation 6), and the two halide cores approach each other slightly to form a molecular ion. Because the two halides leave their original sites, there is a local lattice distortion which is of such a nature that the hole becomes "self-trapped"--as long as the hole is present, there will be the lattice distortion to stabilize the hole.

Since the original work by Castner and Känzig, much work concerning self-trapped holes in alkali halides has been done, much of it by C. J. Delbecq and P. H. Yuster. An excellent review article on self-trapped hole centers is that by Kabler (25). A rather complete

article with a rather extensive bibliography of all work concerning $[X_2^-]$ type centers in alkali halides is that by D. Schoemaker (26).

In 1966 the existence of a self-trapped hole in the cubic perovskite structured material $KMgF_3$ was reported by T. P. P. Hall (27). The perovskite[1] structure is shown in Figure 1 along with the configuration of the self-trapped hole as determined by Hall from EPR experiments. (Figure 1(b) neglects lattice distortion.) For comparison, Figure 2(a) shows a well-known cubic alkali halide crystal structure, while Figure 2(b) shows the configuration of the $[Cl_2^-]$ center in this type crystal (KCl). The immediately obvious difference between the centers in the two materials is the "bent bond" of the intrinsic center in the perovskite material as opposed to the linear center in the alkali halide lattice. This bending reflects the lower symmetry (C_{2v}) of the $[F_2^-]$ in $KMgF_3$ as opposed to the D_{2h} symmetry of the center in the alkali halides. The origin of this bending may be simply thought of as a repulsion of the self-trapped hole away from the doubly charged positive magnesium ion. This bending of the molecular bond is detected experimentally by observing that the principal axis of the hyperfine tensor on each constituent fluorine is not colinear with the line of centers between the two fluorines.

---

[1] Perovskite applies to crystalline substances having the basic $CaTiO_3$ structure, $CaTiO_3$ being the "original" perovskite. The material was so named in honor of the Russian Count L. A. Perovski.

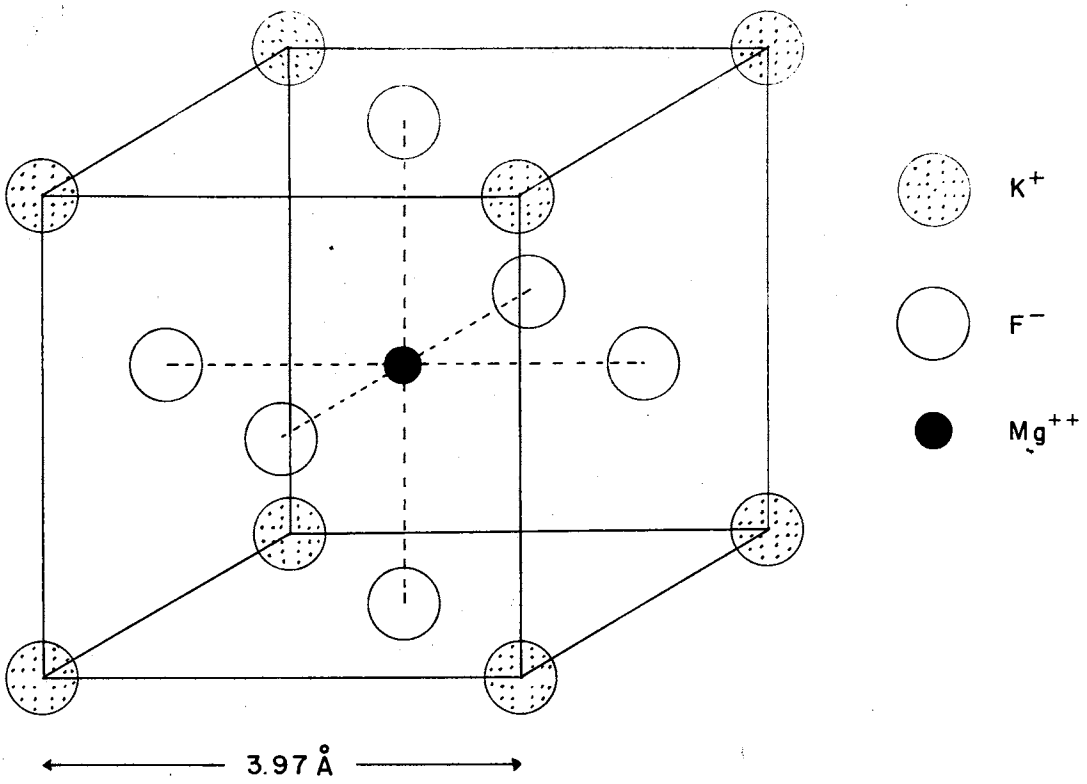

Figure 1(a). Conventional Unit Cell for the Cubic Perovskite $KMgF_3$

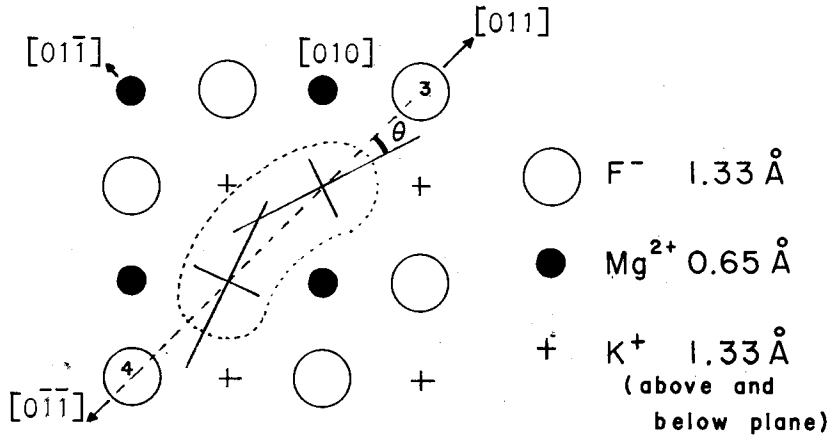

Figure 1(b). Configuration of the $[F_2^-]$ Center in $KMgF_3$

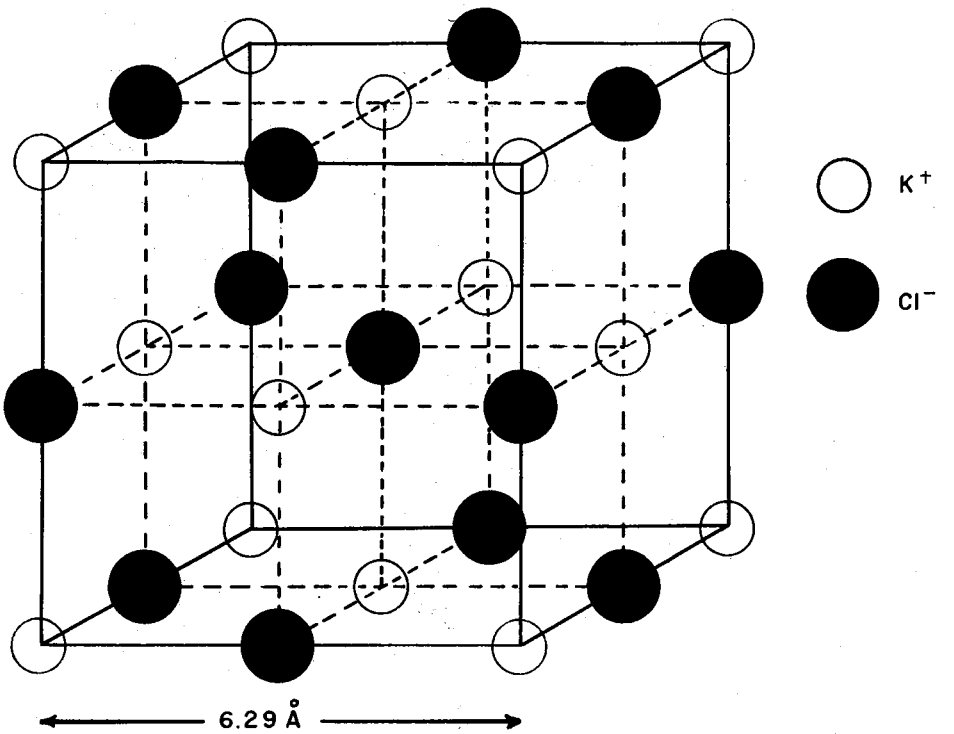

Figure 2(a). Crystal Structure of the Cubic Alkali Halide KCl

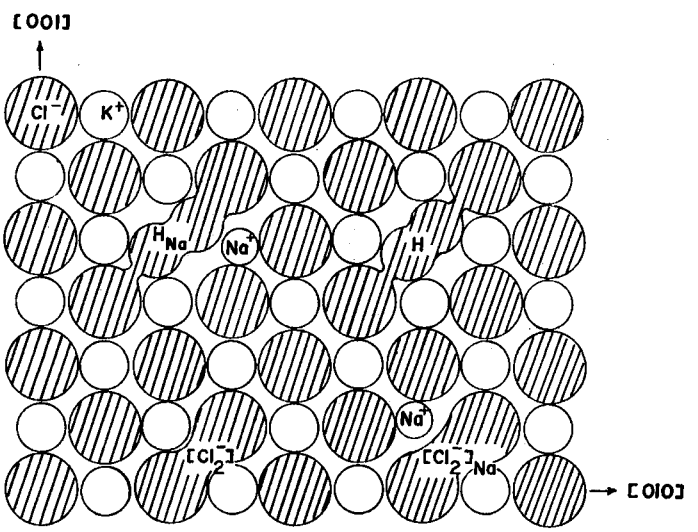

Figure 2(b). The Configuration of the $[Cl_2^-]$ Center as Well as Other Reported Point Defects of Interest in KCl

The bending of the molecular bond of the $[F_2^-]$ center in $KMgF_3$ was not an entirely new idea. Känzig (28, 29) had reported on this bending effect on the axis of $[F_2^-]$ centers in LiF caused by nearby Li^+ vacancies, the so-called V_F centers. Bass and Mieher (30) did an excellent EPR and ENDOR (Electron Nuclear Double Resonance) study on the self-trapped hole associated with lithium impurities in NaF, which also showed a bending of the normally linear axis of $[F_2^-]$ centers in NaF.

A logical relation may now be drawn. The intrinsic $[X_2^-]$ center in alkali halides has a linear molecular axis. Perturbations on this intrinsic center, such as substitutional impurities or nearby lattice imperfections, lead to a bending of the molecular bond; that is, to effects observable with EPR. Similarly, in $KMgF_3$ the intrinsic $[F_2^-]$ center already has a bent bond. One may expect then that perturbations on this system will lead to yet other effects observable with EPR. In fact, the existence of perturbed $[F_2^-]$ centers has been reported by Kappers and Halliburton (31) in $KZnF_3$ and by Lewis, et al., (32) in $KMgF_3$. It is one aim of this study to create and to characterize the properties of perturbed $[F_2^-]$ centers (denoted as $[F_2^-]_A$ [2]) in $KMgF_3$

---

[2] This notation, suggested by Sonder and Sibley (2), is used to denote a perturbed self-trapped hole center, where A is the perturbing entity. The notations suggested by this reference are used throughout the present study with the exceptions of Appendixes E and F, where for convenience the older notation for the point defect $[F_2^-]_A$ is used: V_{KA}(VKA).

beyond that point possible in $KZnF_3$; the $KZnF_3$ samples available to Kappers and Halliburton contained impurity resonances which obscured the crucial center portion of the EPR spectrum of the $[F_2^-]_A$. The $KMgF_3$ samples can be more easily grown with a higher degree of purity, and hence observation of the complete EPR spectrum of the $[F_2^-]_A$ should be possible.

Having introduced the $[F_2^-]$ centers, the other center of interest needs now to be discussed. The original identification of the H center was done by Känzig and Woodruff (33), using basically EPR data obtained from X-rayed crystals of KCl and KBr. Essentially it was found that this paramagnetic center consisted of a molecular ion $[X_2^-]$, located on a single halide site, with the axis of the molecule parallel to a crystallographic <110> axis (Figure 2(b)). This center requires the existence of an interstitial atom, whose origin has already been discussed in conjunction with the Pooley-Hersh mechanism. This is to be distinguished from the $[X_2^-]$ center, which is located on two adjacent halide sites and requires no interstitial atom. The general appearance of the EPR spectrum of the H center is quite similar to that for the $[X_2^-]$ center; normally, however, the overall anisotropic hyperfine splitting is larger in the H center than in the corresponding $[X_2^-]$ center, reflecting the fact that the halide cores must approach each other to a larger degree in the H center than in the $[X_2^-]$ center (e.g., in KCl compare the values A_z = 101 Gauss for the $[Cl_2^-]$ center with A_z = 109 Gauss for the H center) (33).

There have been several investigations concerning H centers in alkali halides since the original report. Using ENDOR Dakss and Mieher (34, 35) were able to conclusively show that the H center in LiF as originally reported by Känzig and Woodruff was in fact not the intrinsic defect but rather an H center associated with a sodium substitutional impurity, an $H_A(Na^+)$ center (Figure 2(b)). The intrinsic H center in LiF was reported by Chu and Mieher (36, 37), again using ENDOR data. Its distinguishing feature turned out to be a <111> symmetry as opposed to the <110> symmetry of the intrinsic H center in the other alkali halides. Other reports have given descriptions of: the $H_A(Na^+)$ center in KCl (38, 39); the $H_A(Li^+)$ in KCl (40); and the $H_A(K^+)$ and $H_A(Li^+)$ in NaF (41).

Given $[F_2^-]$, $[F_2^-]_A$, H, and H_A centers in the alkali halides, and given $[F_2^-]$ and $[F_2^-]_A$ centers in the material $KZnF_3$, one may expect to find the existence of H and/or H_A centers in the perovskite material $KMgF_3$. It is another aim of this study to create and to study with EPR an H center type defect in $KMgF_3$.

To recapitulate, the aims of this study are as follow: (A) to create and to characterize with EPR a perturbed self-trapped hole center $[F_2^-]_A$ in $KMgF_3$ and (B) to create and to characterize with EPR an H type center in this same material.

The $KMgF_3$ samples will be electron irradiated with a Van de Graaff Electrostatic Generator/Accelerator and the EPR resonances of the paramagnetic defects so created will be observed with an X-band

homodyne EPR spectrometer. In the alkali halides the H type centers are characteristically produced at a slow rate, compared with that for the $[X_2^-]$; hence, it is expected that relatively long periods of irradiation will be required to fulfill objective two. The complete experimental procedure as well as the apparatus employed in this study will be presented in rather full detail in the next chapter. It will be supplemented in the area of experimental apparatus by Appendixes A, B, C, and D. Chapter III will be a simple and straightforward presentation of experimental observations of interest, and in Chapter IV this data will be analyzed in depth. The final chapter will consist of a recapitulation of the entire study, observations made during the course of this study that were not pursued, suggestions for further study, and other such pertinent comments.

CHAPTER II

EXPERIMENTAL APPARATUS AND PROCEDURE

During the course of this investigation several single crystals of $KMgF_3$ from different sources were examined. Dr. W. A. Sibley supplied what were believed to be pure $KMgF_3$ crystals, denoted henceforth as $KMgF_3$(ORNL), and Dr. J. T. Lewis supplied crystals doped with ytterbium, $KMgF_3$:Yb. All of these crystals were originally grown at the Oak Ridge National Laboratory. Other crystals that were examined during the course of this study were grown by the Stockbarger method in the Crystal Growth Laboratory of this university by Nicholas Koumvakalis. The starting materials were purified KF and MgF_2 crystal cuttings purchased from the British Drug House and Harshaw Chemicals, respectively. To this material was added approximately 0.1% NaF by weight in one case; in another growth an attempt was made to add 0.05% LiF by weight. Crystals cut from these two grown boules were designated as $KMgF_3$:Na and $KMgF_3$:Li, respectively. Samples from these two boules were submitted for impurity analysis to the Oak Ridge National Laboratory. The results are given in Chapter III, Table III. It is clear from this analysis that $KMgF_3$:Li is

somewhat of a misnomer, having ten times more Na than Li, but the nomenclature will be retained for ease of reference.

The major crystallographic axes of all samples had to be determined. Samples taken from the boules were closely examined for visual indications of (100) planes; occasionally small cleavage planes could be seen on various surfaces of these crystals. Once one plane was determined, Laue patterns[1] were taken to ascertain the directions of the remaining two <100> axes. If no visual observation of a (100) cleavage plane presented itself, the orientation of a sample was much more difficult. Here the determination of the three <100> directions was obtained from a series of Laue patterns. Once a single sample had been oriented, knowing the relative orientation of the sample to the boule, the orientation of the boule itself was fairly well established, making subsequent samples cut from this boule much easier to orient. A Laue pattern of a (100) plane is presented in Figure 3 for a $KMgF_3$:Li sample.

Having oriented a piece of the boule, there remained the matter of cutting or cleaving these pieces into sizes convenient for EPR and compatible with size restrictions of the experimental apparatus, to wit in some experiments samples were required to fit into 5 mm I.D. tubing. Hence, typical sample sizes were cut or cleaved to the

---

[1] A detailed listing of manufacturer and model for most equipment used in this study is given in Appendix A.

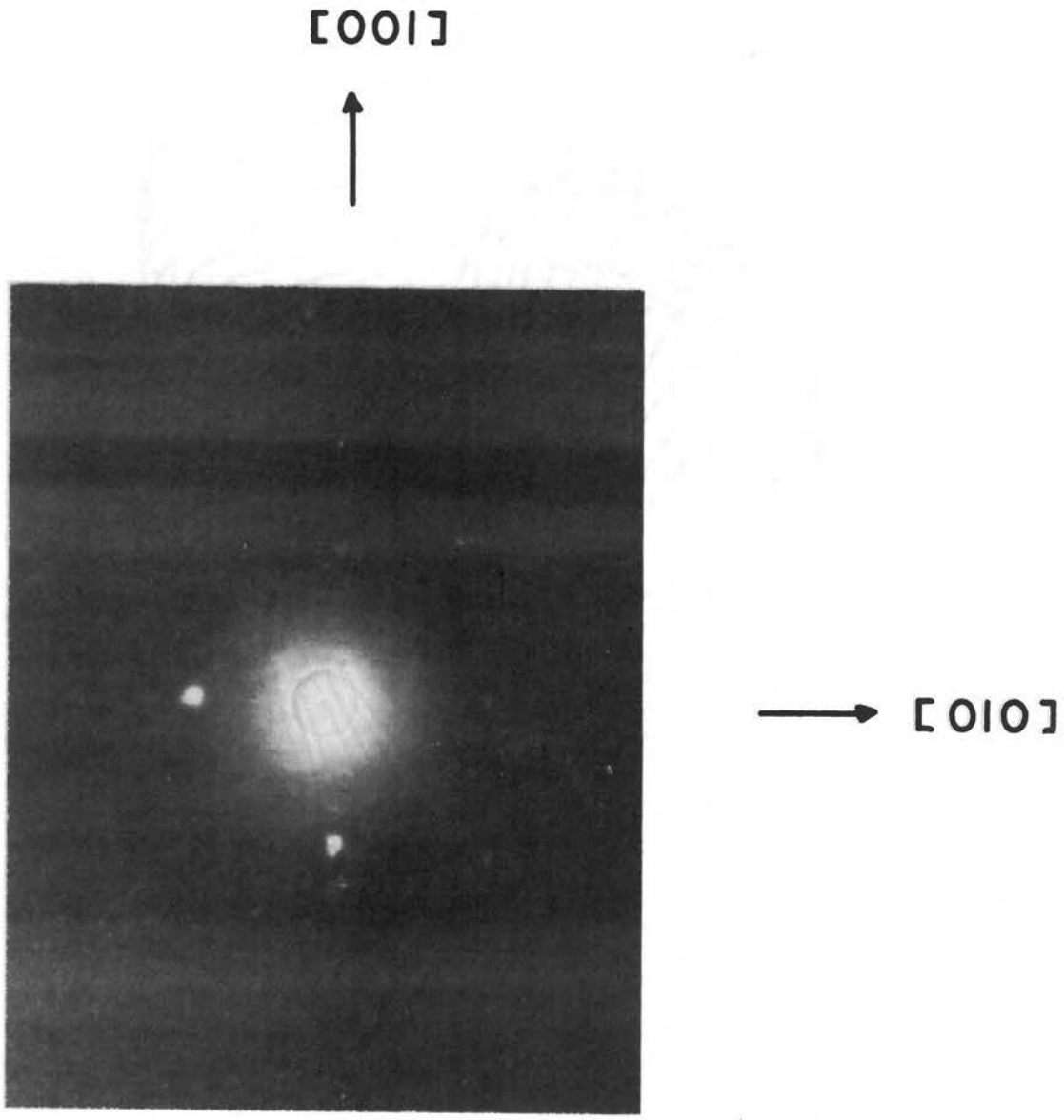

Figure 3. Laue Pattern of a (100) Plane of $KMgF_3$:Li

dimensions 6mm x 3.5mm x 3mm. Most of the sample surfaces were cut with a diamond saw along (100) planes. However, an attempt was usually made to cleave one surface of a sample (3mm x 3.5mm) along a (100) plane; this plane would be used for mounting samples into or onto experimental apparatus. This material will cleave along (100) planes but not as easily as many of the alkali halides. This cleavage plane made orientation of the sample in the magnetic field of the EPR spectrometer much more simple.

Irradiation of EPR samples was normally carried out by one of two means. For much of the work concerning $[F_2^-]_A$ centers, samples were mounted by their cleaved surfaces onto the end of a 1/8" copper rod (3½" long) with a small amount of silicon high vacuum grease. This ensemble was then immersed into an eight-ounce styrofoam cup of liquid nitrogen. This mounting technique was satisfactory, but the bond between the rod and sample was brittle at liquid nitrogen temperature (LNT). Hence, care in handling was necessary. Use of General Electric 7031 varnish was limited since it, too, at LNT provided an extremely brittle bond; moreover, it required a drying period at room temperature before use. It was found that both the silicon grease and the varnish develop large EPR resonances in the $g \sim 2$ region upon prolonged irradiation. Hence, minimal amounts were used.

The first means of irradiating samples was to place the cup of nitrogen with the rod-sample ensemble inside at a distance of 3-4 cm

in air from the electron beam output window (aluminum of thickness 0.010") of the Van de Graaff accelerator. The sample was placed next to the inside wall of the styrofoam cup which faced the beam output window. All irradiations were performed with 1.5 MeV electrons and typically a total beam current of 10 μamperes. Under these conditions and with the stated nitrogen volume it was possible to irradiate directly into the liquid nitrogen for up to ten minutes. The rod-sample assembly was then transferred into unirradiated liquid nitrogen and the electron irradiated liquid nitrogen discarded before any untoward reaction could occur. This cycle could be repeated as many times as necessary. When a sufficient dose had been obtained, this rod-sample ensemble was screwed into a 3/16" x 7" stainless steel rod. It was this arrangement that could be used in either a modified Varian finger Dewar (see Figure 4) or in the Varian variable temperature accessory in conjunction with the Varian V-4531 rectangular EPR cavity.

The second means of irradiation involved the use of a stainless steel Dewar, described in detail in Appendix B. The sample was mounted upright on its cleavage plane on the bottom plate near the window in the narrow wall of the TE_{102} cavity (see Figure 22). This window was faced by holes in each of the heat shields and by the 0.006" aluminum window in the outer wall of the Dewar. This latter window was placed 3-4 cm in front of the electron beam output window to accomplish electron irradiations of a sample <u>in situ</u> in the EPR cavity. Both the helium and nitrogen reservoirs of the Dewar were

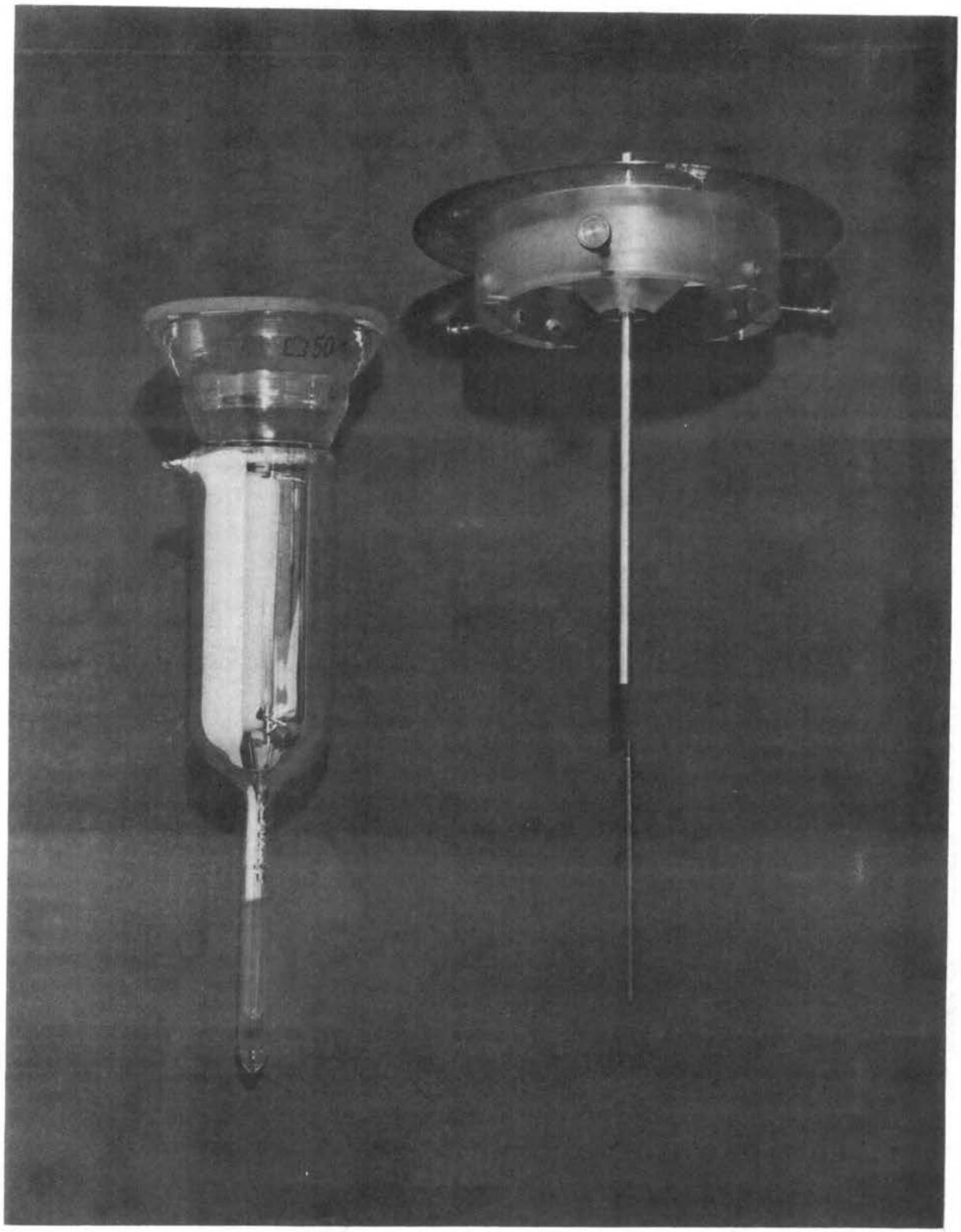

Figure 4. Nitrogen Finger Dewar Arrangement for Use With the Varian V-4531 Rectangualr EPR Cavity

filled with liquid nitrogen during these irradiations. The steady state temperature of the bottom plate of the resonant cavity during irradiation was approximately 85 K.

Facilities were also constructed to irradiate at temperatures above LNT. Basically this consisted of a nitrogen gas/liquid nitrogen heat exchange apparatus (Varian Associates Variable Temperature Accessory). The cooled gas was directed through a ¼" hole bored through a length (~ 40 cm) of styrofoam which was placed perpendicular to the electron beam path. The sample, mounted on the 1/8" copper rod, was placed inside the styrofoam at the intersection of the gas stream and the electron beam path, again about 3-4 cm from the beam output window. The temperature of the gas stream could be changed by varying the rate of gas flow through the heat exchanger. The temperature of the gas at the sample was monitored by a copper vs. constantan (Type T) thermocouple.

Standard potentiometric techniques were employed for monitoring temperatures. The stainless steel Dewar was equipped with a gold-iron vs. chromel thermocouple attached to the bottom plate of the resonant cavity; the calibrated table for the wire used in this thermocouple was obtained from Dr. J. J. Martin. All other thermocouples used in this study were copper vs. constantan. The revised table of EMF vs. T (National Bureau of Standards--1971) for copper vs. constantan thermocouples was used. Both tables were referenced to a 0 C reference junction, whereas the reference junctions in this work

were left at ambient temperatures. Since this temperature could not be known accurately, especially when using the stainless steel Dewar, the temperatures quoted in this work must be viewed as very approximate. They are perhaps accurate to ±2 K.

The Varian Variable Temperature Accessory was also used in conjunction with the Varian V-4531 rectangular microwave cavity in pulse anneal studies. Typically the temperature of the gas would be raised from a base temperature (between 94 K and 106 K, depending on gas flow rate) to a temperature T_0 over a time period of 3-5 minutes by use of the heater element, keeping the gas flow rate constant. This higher temperature T_0 would be held for three minutes, after which the heater would be turned off, the base temperature regained, and an EPR spectrum obtained. Obviously, it is this same assembly that was used to observe EPR spectra at various temperatures above 77 K. The heater and gas flow could be easily adjusted to maintain any temperature from 94 K to 270 K while an EPR spectrum was being obtained.

On occasion the need arose to irradiate a sample with ultraviolet light after having been electron irradiated. This was accomplished by placing the rod and sample into the finger Dewar and placing the quartz tail of this Dewar close to the unfiltered and unfocused output of a 100 watt mercury arc lamp.

If the sample was mounted in the metal Dewar, the following procedure was employed. The Dewar would be placed onto a vacuum

pumping station and the retaining ring for the aluminum irradiation window removed such that only the Dewar vacuum held the window in place. By valving off the diffusion pump and then flushing the Dewar vacuum space with nitrogen gas, the window would be forced out. The gas flow would then be stopped, a quartz window inserted in the space previously occupied by the aluminum window, and then the Dewar would be re-evacuated. The entire procedure utilized two workers and required less than 30 seconds to complete, sufficiently fast that the measured temperature of the resonant cavity did not rise appreciably (less than 3 K). Through this quartz window samples in the metal Dewar could also be bleached with UV light. In this case focusing of the UV upon the sample was accomplished with a large glass lens.

The EPR spectra of these irradiated samples were obtained with an X-band homodyne spectrometer utilizing a 100 KHz magnetic field modulation unit (Varian Associates) which contained its own phase sensitive detector (PSD, lock-in amplifier). The magnet was a Varian six-inch current regulated model. A block diagram of the spectrometer is provided in Figure 5 with emphasis on the microwave network. The lettered components are described further in Appendix D.

Magnetic field positions were measured in one of two ways. Data for the $[F_2^-]_A$ center were taken with an NMR marginal oscillator (Appendix C), while that for the interstitial type center were taken with a rotating coil magnetometer. The accuracy of the latter

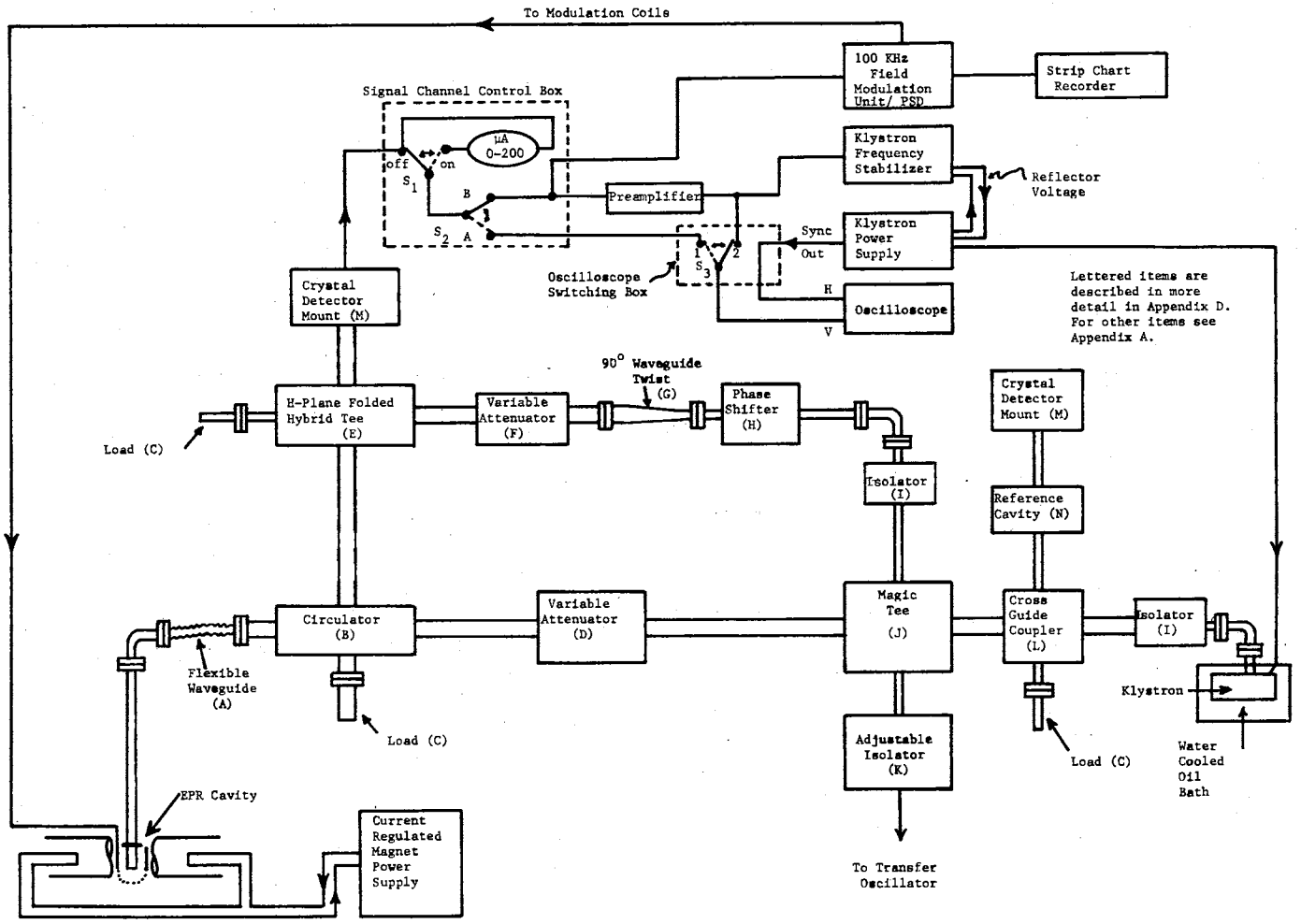

Figure 5. Block Diagram of EPR Spectrometer: The Lettered Components Are Described Further in Appendix D

was given as 0.05 percent, whereas the quoted resolution was one part in 20,000 at full scale. The measured field positions of resonant lines were corrected so as to result in the true magnetic field at the sample by means of DPPH (2, 2-diphenyl-1-picrylhydrazyl). This standard was placed inside the cavity with the sample when using the metal Dewar and was taped to the tail of the finger Dewar (outside) at the same level as the sample when using the Varian rectangular cavity. The g value of the DPPH was taken as 2.0037 ± 0.0002.

One final procedure needs to be mentioned; this concerns the criterion for determining absolute alignment of a sample in the static magnetic field. Essentially it consisted of maximizing certain resonant lines in each spectrum. Which line of each spectrum will be designated as each is presented in the following chapter.

CHAPTER III

EXPERIMENTAL RESULTS

This chapter will be divided into two sections. The first will deal with the study of the $[F_2^-]_A$ center while the second will contain experimental results of the study of an H type center. By nature, this chapter is less dialogue and more results. Most comments concerning these results are withheld for Chapter IV.

The $[F_2^-]_A$ Center

Upon brief (4-12 minutes) electron irradiation and the taking of an EPR spectrum at LNT, all $KMgF_3$ samples studied displayed a rather intense spectrum that appeared to be identical with that reported by Hall in 1966 (27). For convenience and later for comparison, the [100] and [110] spectra of the intrinsic $[F_2^-]$ center in $KMgF_3$ are displayed in Figure 6. The stick diagrams identify those resonances which are due to $[F_2^-]$ centers whose major axes (defined as the line of centers between the two constituent fluorines) make angles of 0°, 45°, 60°, and 90° with respect to the externally applied magnetic field. It is the high field zero degree line of the [110] spectrum that exhibits a well resolved hyperfine interaction with the two fluorine

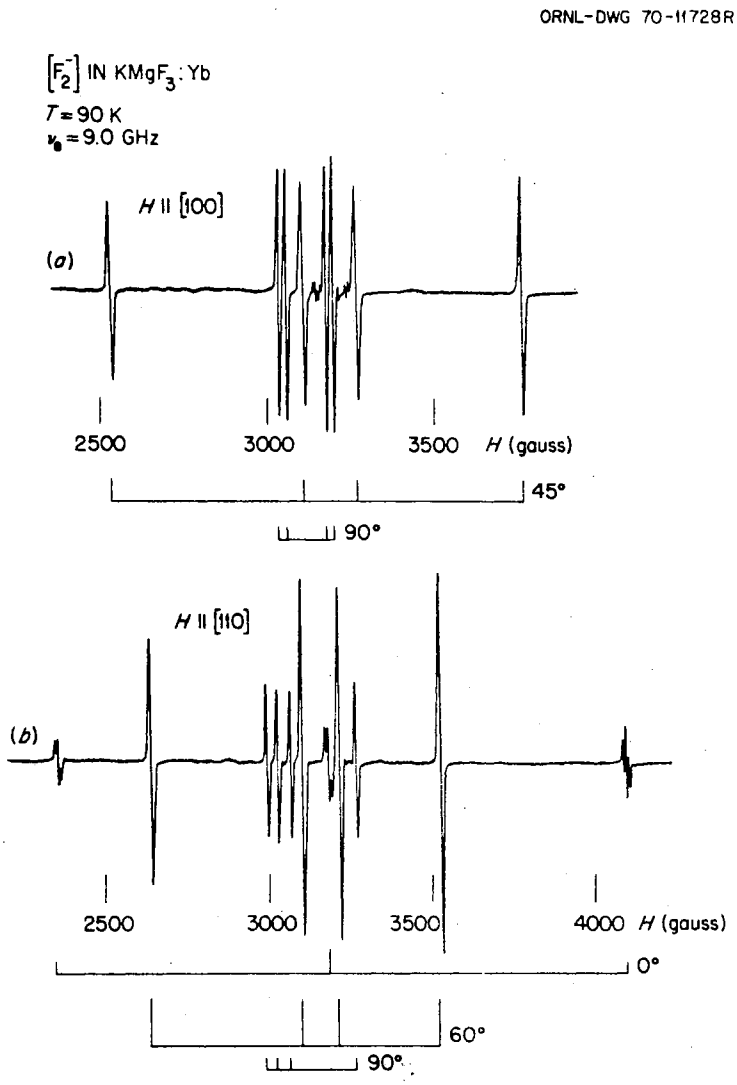

Source: 42, p. 69.

Figure 6. The [100] and [110] Spectra of the Intrinsic $[F_2^-]$ Center in $KMgF_3$

nuclei (commonly referred to as 3 and 4; see Figure 1(b)) that lie at each end of the $[F_2^-]$ center along the [110] direction. Using the Varian variable temperature accessory, a series of three-minute pulse anneals were performed, the base temperature regained, and the EPR of this [110] high field line observed. A portion of this data is shown in Figure 7 for samples $KMgF_3$:Na, $KMgF_3$:Li, and $KMgF_3$ (ORNL). Resonances were observed at pulse anneal temperatures intermediate and higher than those shown. It was found that the decay temperatures (the temperatures at which the resonances changed from the first to the second patterns, and from the second to the third) occurred at ~108 K and ~150 K. That is, the intrinsic $[F_2^-]$ center appears to decay at approximately 108 K, giving rise to two perturbed type $[F_2^-]$ centers, one of which decays at roughly 150 K. The remaining center was still observable even after pulse anneals to 260 K. This agrees well with values reported by Kappers and Halliburton (31) in $KZnF_3$, by Riley and Sibley (43) from optical data in $KMgF_3$, and by Lewis, et al., (32) in $KMgF_3$. In an attempt to enhance the concentration of these more stable $[F_2^-]_A$ centers, the $KMgF_3$:Na sample was irradiated at approximately 110 K. It appears that this procedure did not lead to a readily observable increase in concentration of these centers. This finding implies an efficient conversion of $[F_2^-]$ centers into $[F_2^-]_A$ centers, to a point where all perturbing entities capable of stabilizing self-trapped holes are utilized for that purpose.

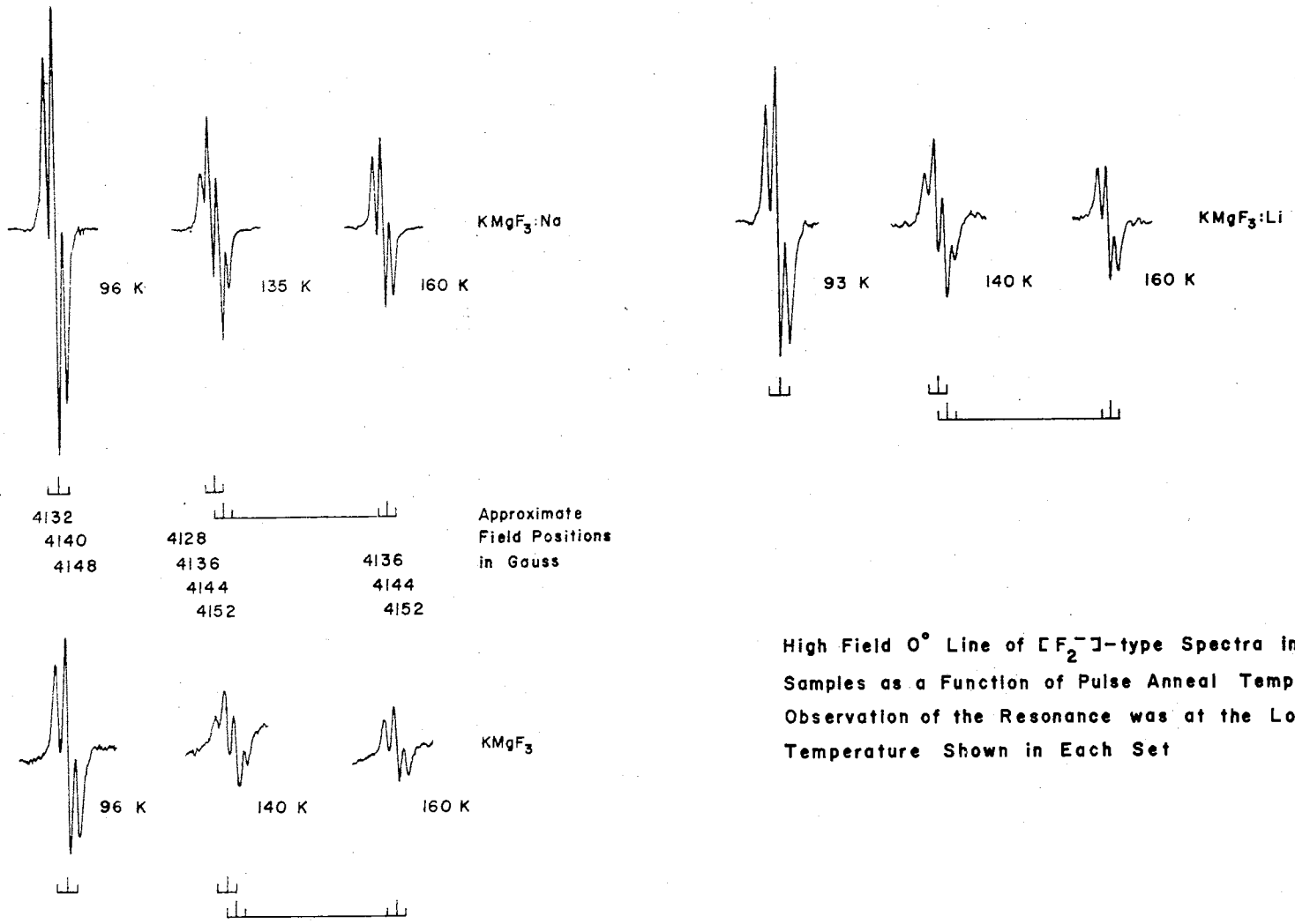

High Field 0° Line of $[F_2^-]$-type Spectra in Three Samples as a Function of Pulse Anneal Temperature Observation of the Resonance was at the Lowest Temperature Shown in Each Set

Figure 7. Three-Minute Pulse Anneal Data of $[F_2^-]$ and Various $[F_2^-]_A$ Centers in Three Different $KMgF_3$ Samples

As has been noted, there are two contributions to the zero degree lines in the temperature range from 108 K to ~150 K. Above 160 K there appears to be only one paramagnetic center contributing to the resonance; moreover, its structure is akin to that for the intrinsic $[F_2^-]$ center. It was this center alone that could be examined in more detail since a means of destroying it while retaining the other $[F_2^-]_A$ center (stable to ~150 K) did not present itself. Henceforth, in this study the designation $[F_2^-]_A$ center will be reserved for the perturbed self-trapped hole center that is stable to near room temperature.

The [100] and [110] spectra of the $[F_2^-]_A$ center in $KMgF_3$:Na at LNT are given in Figure 8. Alignment criterion was based upon the maximization of the intensity of the high field sixty-degree line in the [110] spectrum. The [100] spectrum was obtained by a subsequent rotation of the magnet by 45^o. By comparison with Figure 6, it is seen that the only obvious distinguishing feature of the $[F_2^-]_A$ center EPR spectra is the presence of six sixty-degree lines in the [110] spectrum as opposed to four for the intrinsic $[F_2^-]$ center. An explanation for the existence of these additional resonances is given in the next chapter.

The field positions of the resonant lines in these two spectra were measured with the NMR marginal oscillator and the corrected values are reported in Table I. It is from this data that a detailed model of the $[F_2^-]_A$ center will be drawn.

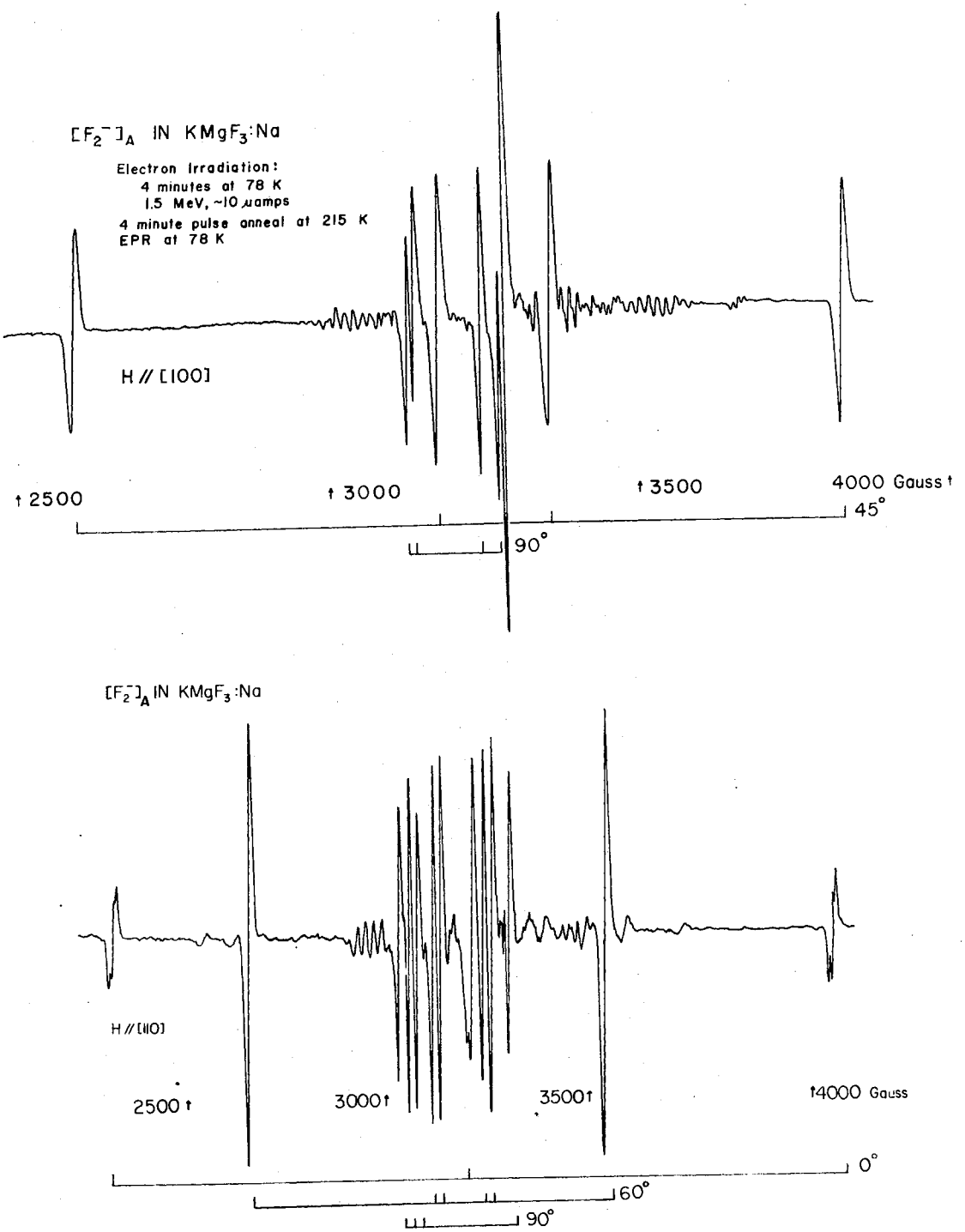

Figure 8. The [100] and [110] Spectra of the $[F_2^-]_A$ Center in $KMgF_3$ at LNT

TABLE I

CORRECTED FIELD POSITIONS (IN GAUSS) OF RESONANT LINES OF THE $[F_2^-]_A$ CENTER EPR SPECTRA

[100] Data		[110] Data	
Experimental	Calculated	Experimental	Calculated
45° Lines		0° Lines	
2590.5	2591.0	2404.4	2404.2
3176.1	3177.1		3282.7
3355.2	3354.7		3283.0
3823.7	3824.2	4166.8	4166.4
90° Lines		90° Lines	
3128.2	3127.8	3105.6	3105.1
3139.9	3138.1	3131.9	3130.4
3245.9	3246.0	3148.9	3148.4
3274.4	3274.7	3376.9	3376.3
Microwave Frequency: 9210.20 MHz (both [100] and [110])		60° Lines	
		2737.8	2737.7
$g_{DPPH} = 2.0037 \pm 0.0002$		3187.9	3187.8
		3206.9	3207.5
$H = 234.87 * \nu$ Gauss, MHz where ν is the measured NMR resonant frequency		3312.5	3313.6
		3332.3	3331.8
		3608.8	3608.9

Another experiment of perhaps only incidental interest was performed by observing the EPR of the lowest field 45° line of the [100] spectrum of the $[F_2^-]_A$ center as a function of temperature. There was an evident reversible reduction in amplitude of the EPR line with increasing temperature that apparently cannot be attributed simply to a Boltzmann effect. The amplitude of this line at ~208 K relative to the amplitude at ~100 K was approximately as three to thirty-seven. At 250 K this line was not observable whereas upon subsequent recooling to 100 K, the original intensity was regained.

By UV irradiation at LNT a preferential population among the various possible orientations of $[F_2^-]$ centers in $KMgF_3$ may be obtained (43). By monitoring the various EPR resonances pertinent to each orientation as a function of pulse anneal temperature, the activation energies for reorientation may be obtained (32). This experiment was briefly tried for all $[F_2^-]$ type centers in $KMgF_3$. There was apparent agreement in results for the intrinsic $[F_2^-]$ center when compared with that of Lewis, et al., (32). However, the experiments with the perturbed $[F_2^-]$ centers were inconclusive; it appeared that UV irradiation at LNT caused reorientation of the perturbed $[F_2^-]$ center that decays around 150 K whereas UV light simply destroyed the remaining $[F_2^-]_A$ centers.

The H_A Center

At this stage the designation H_A center is adopted to represent

the other radiation induced point defect that has been studied. The experimental observations underlying this designation will become apparent as the data and analysis are presented.

If the electron irradiation was carried to larger doses than that necessary to produce $[F_2^-]$ centers, small resonances with an overall hyperfine splitting slightly larger than that of the $[F_2^-]$ center began to appear. For this study it was found that this spectrum could be enhanced to a usable level by continuing the irradiation at 77 K for approximately four hours (see Figure 15). At the end of that period, the EPR spectrum observable at 77 K was a composite of $[F_2^-]$ center and H_A center resonances.

The first question to be addressed was that of the thermal stability of the H_A center. The pulse anneal procedure was again employed and results are incorporated in Figures 9 and 10 where the line monitored was the lowest field line in the H_A [100] spectrum at ~96 K. The $[F_2^-]_A$ line monitored was the low field 45° line of the [100] spectrum. The H_A resonance is essentially lost after a three-minute pulse anneal to 210 K, whereas the $[F_2^-]_A$ line has increased slightly in amplitude. This high thermal stability of the H_A was exploited in that it allowed thermal annealing (at 165 K, 4-5 minutes) of a large percentage of the intrinsic $[F_2^-]$ centers and the perturbed $[F_2^-]$ centers stable to ~150 K. It was also found that by a three to four hour UV irradiation at 77 K subsequent to this thermal anneal the remaining $[F_2^-]_A$ centers could be severely reduced in number with

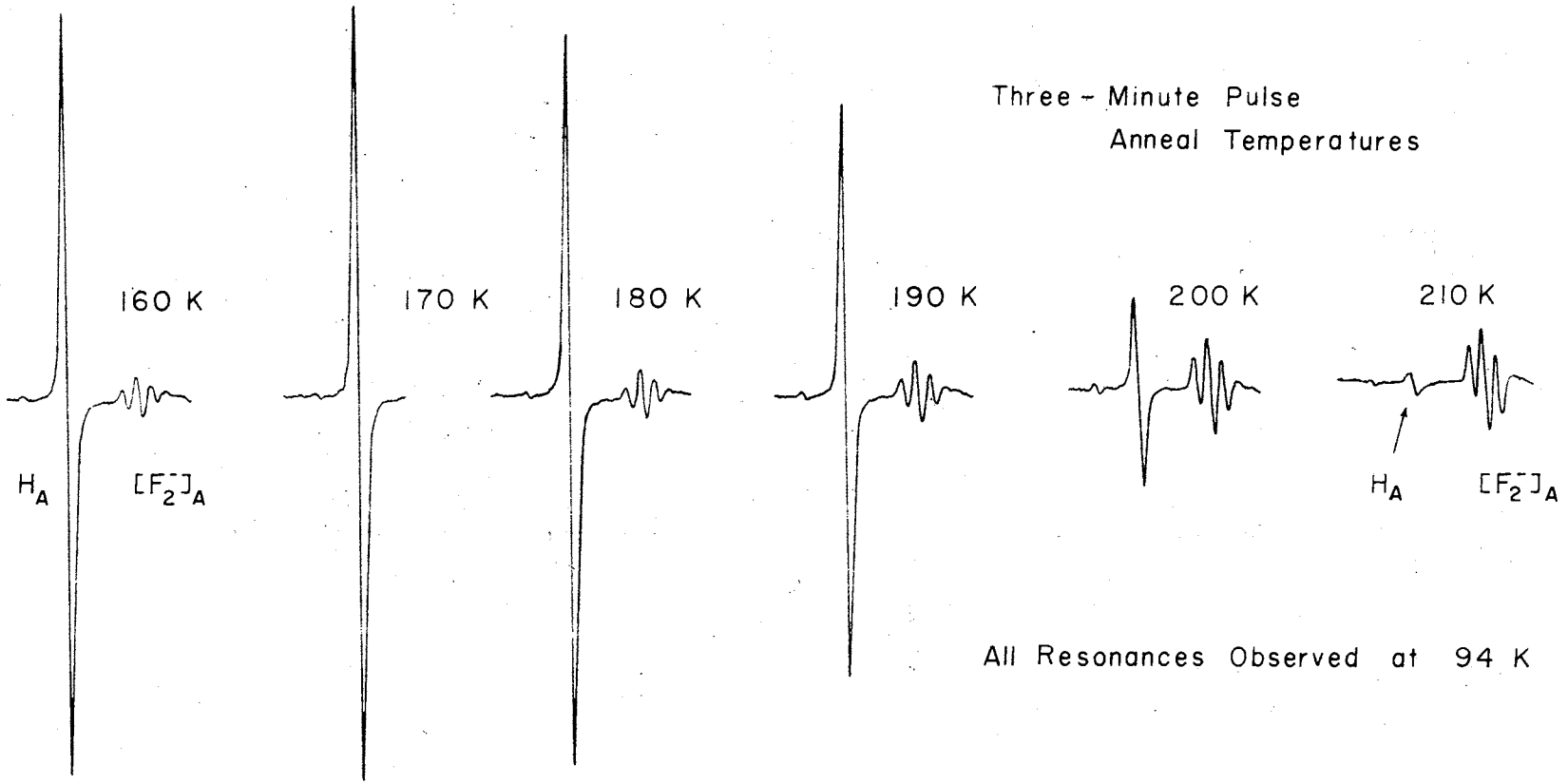

Figure 9. Pulse Anneal Data for H_A Center in $KMgF_3$

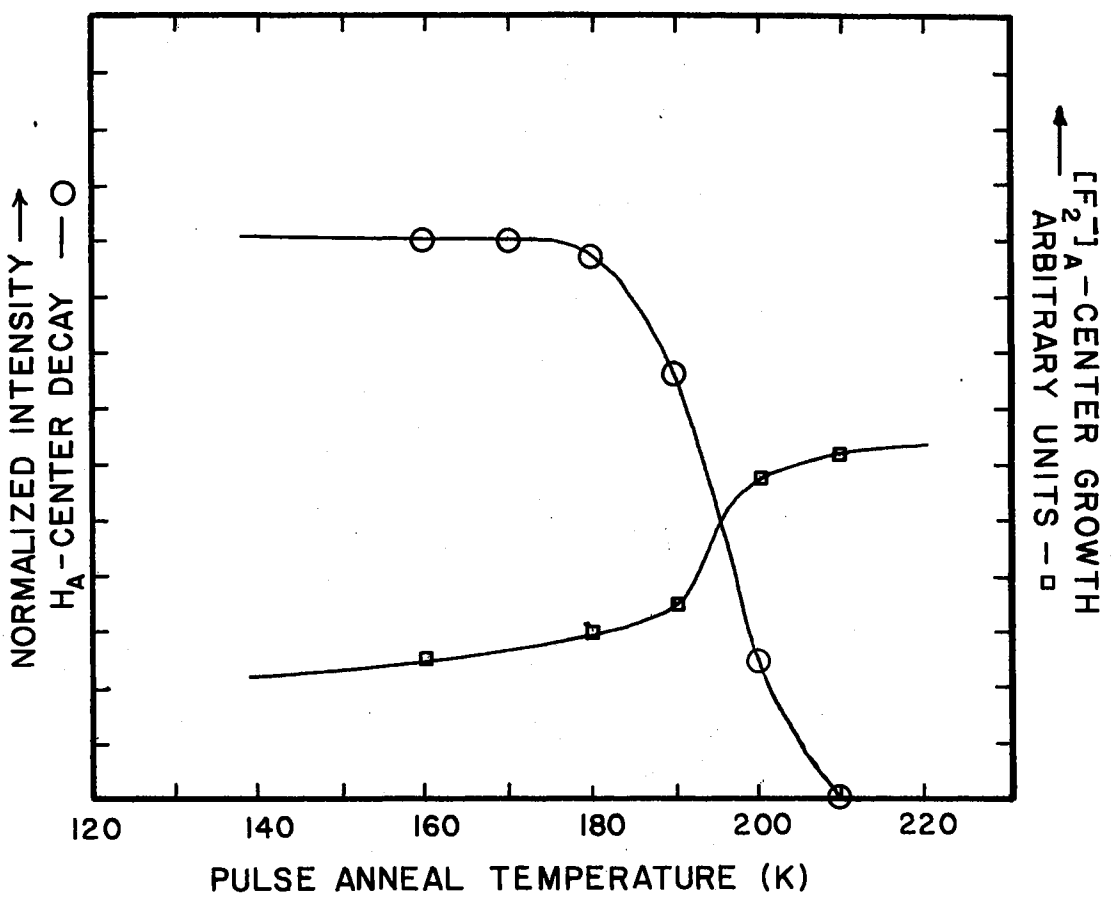

Figure 10. Plot of Experimental Data in Figure 9: The left ordinate applies to the anneal of the H_A center whereas the right ordinate applies to the $[F_2^-]_A$ center growth as the H_A decays.

only a slight degradation in the H_A center concentration.[1] This made observation of the complete H_A center EPR spectra much more tractable. In fact, this treatment was effected prior to taking the data shown in Figures 9 and 10.

When a sample was prepared in the manner just described, there resulted at 10 K EPR spectra which are displayed in Figures 11 and 12 for the magnetic field parallel to [100] and [110] directions, respectively. The 10 K temperature was also helpful in the further demise of the $[F_2^-]_A$ signals via severe saturation of these resonances at this temperature, leading to even "cleaner" H_A center spectra. The orientation designations in these figures are discussed in the following chapter, specifically in Figure 17. In the [100] spectrum alignment was based upon the maximization of the two high field lines belonging to the E, F, K, L oriented H_A centers whereas in the [110] spectrum the criterion was the maximization of any of the outer resonant lines, since all these lines were sensitive to alignment. The major observation to be made from this data is the existence of sets of doublets. The [100] spectrum was found to consist of three sets of lines, each set consisting of four doublets (some coalescing into one line); the [110] spectrum was similarly found to consist of four such sets of lines. The field positions of both spectra were measured with

---

[1] An additional UV irradiation of the sample at 10 K after this treatment, however, did produce an effect. The effect is tentatively believed to be a conversion of the H_A centers into intrinsic H centers.

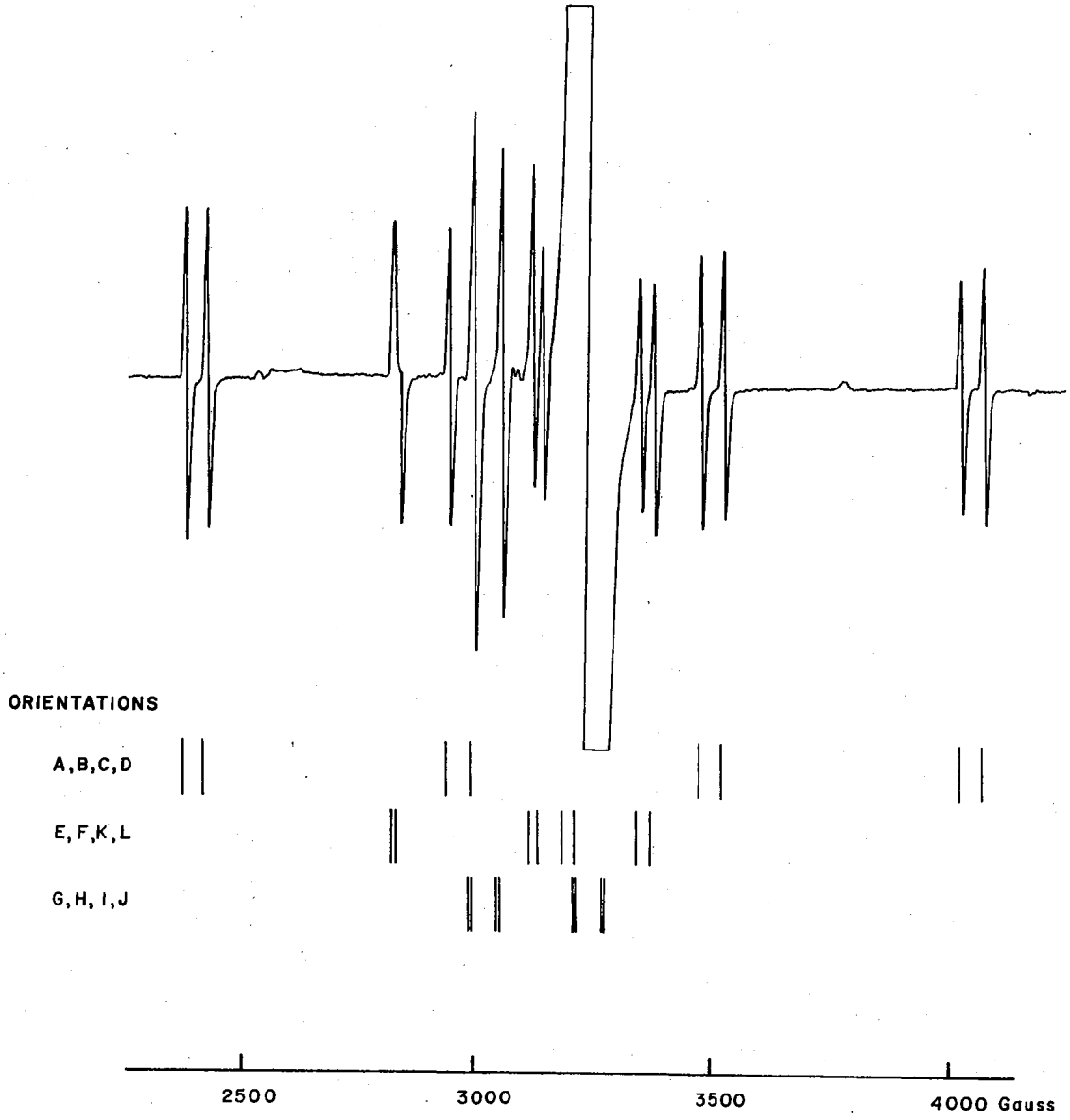

Figure 11. The [100] EPR Spectrum of the H_A Center in $KMgF_3$ at 10 K: The microwave frequency was 9070.0 MHz; the orientation labels are taken from Figure 17.

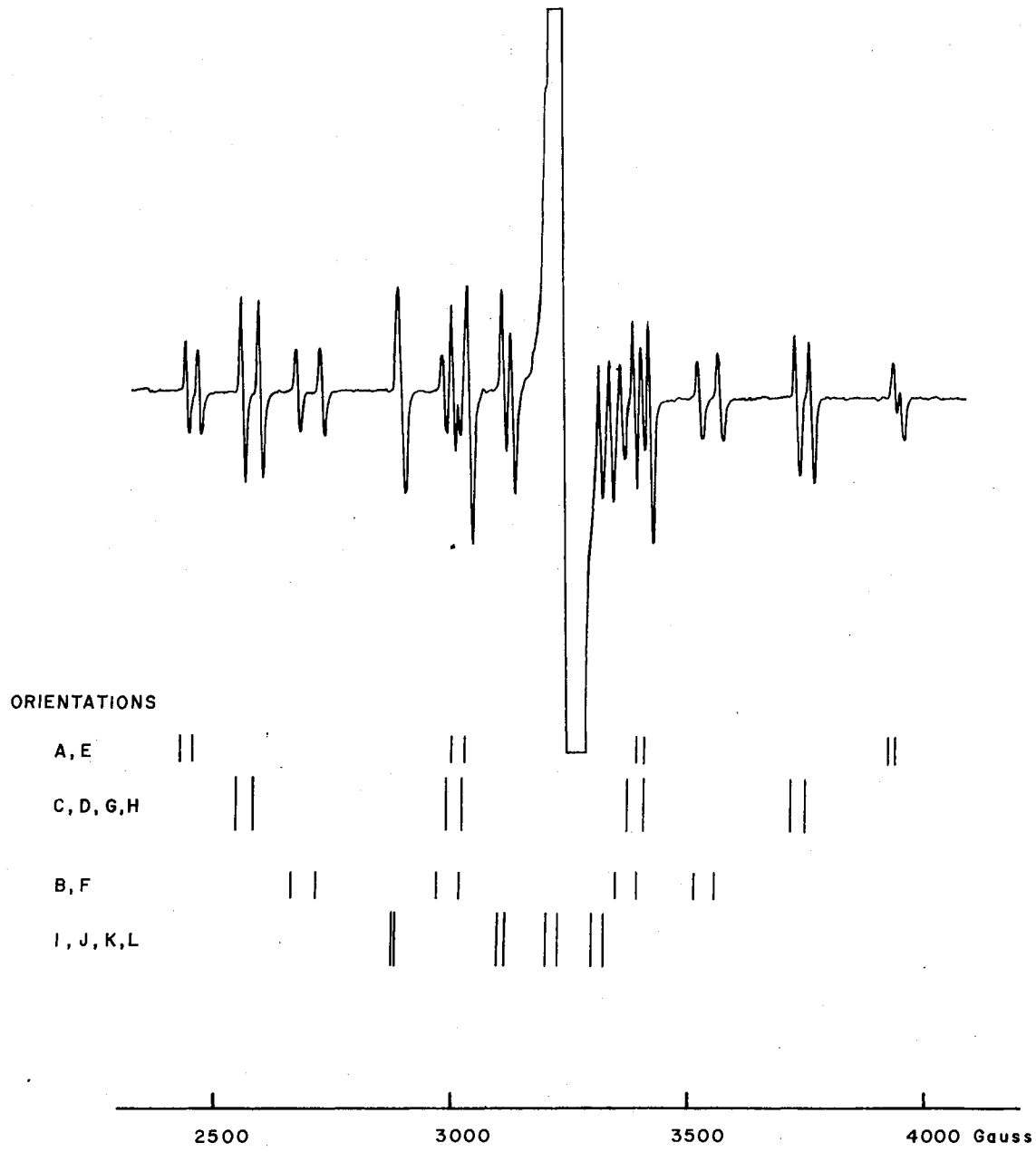

Figure 12. The [110] EPR Spectrum of the H_A Center in $KMgF_3$ at 10 K: The microwave frequency was 9070.0 MHz; the orientation labels are taken from Figure 17.

the rotating coil magnetometer. The corrected field positions are given in Table II.

If the temperature of the sample was raised from 10 K to ~30 K, there occurred an interesting metamorphosis. Since 30 K was unavailable as a stable temperature, these transformed spectra were observed at temperatures of 77 K and above. The [100] and [110] spectra of the H_A center at 77 K are presented in the lower portions of Figures 13 and 14, respectively. It should be noted again that the thermal annealing studies of the H_A center (Figures 9 and 10) were performed by monitoring the lowest field resonance of the [100] transformed spectrum. The relationship between the spectra at 10 K and at 77 K will be discussed in the following chapter.

There was also observed an effect upon the EPR spectra if the observations were made at temperatures above 77 K. In the 77 K to 120 K range there was observed a narrowing of select lines with increasing temperature, resonances which will be shown to be a specific averaging of lines which are distinct in the 10 K spectra. All the H_A center resonances decreased in amplitude (broadened) with increasing temperature above ~120 K, up to ~160 K, when the resonances were no longer observable. These resonances did not reappear as a single averaged line (44) before the annealing temperature at ~195 K was reached, precluding an absolute statement regarding the origin of this broadening. If the sample was recooled to lower

TABLE II

CORRECTED FIELD POSITIONS (IN GAUSS) OF RESONANT LINES OF THE H_A CENTER EPR SPECTRA AT 10°K

[100] Data		[110] Data	
Experimental	Calculated	Experimental	Calculated
Orientations A,B,C,D		Orientations I,J,K,L	
2379.3	2379.5	2889.5	2883.8
2424.4	2424.6	2889.5	2892.8
2942.1	2941.3	3104.4	3104.8
~2988.8	2988.1	3122.8	3122.6
3475.3	3475.3	~3197.3*	3197.3
3522.6	3522.2	~3218.3*	3216.2
4019.7	4020.8	3308.8	3309.9
4068.6	4069.2	3332.2	3332.2
Orientations E,F,K,L		Orientations B,F	
~2825.2	2824.5	2670.1	2669.9
~2835.8	2836.2	2721.3	2720.4
3117.2	3117.8	2979.2	2978.1
3138.9	3138.7	~3027.0**	3025.4
~3182.9*	3187.1	3354.6	3354.5
~3212.1*	3211.1	3398.8	3399.6
3347.2	3346.5	3518.5	3518.3
3377.1	3376.2	3561.1	3560.6
Orientations G,H,I,J		Orientations A,E	
2993.5	2989.5	2436.2	2436.9
2993.5	2998.1	2461.6	2462.3
3052.9	3048.7	~3022.0**	3009.0
3052.9	3057.5	~3042.0**	3031.7
~3212.9*	3212.7	3398.8	3397.5
~3212.9*	3221.9	3415.1	3415.8
~3271.1*	3271.5	3928.2	3927.0
~3271.1*	3281.0	3942.8	3943.6
Microwave Frequency: 9070.0 MHz (both [100] and [110])		Orientations C,D,G,H	
		2553.8	2553.7
		2591.3	2591.0
$g_{DPPH} = 2.0037 \pm 0.0002$		2998.1	2997.6
		3032.6	3032.7
		3382.3	3382.7
		3415.1	3414.3
		3722.7	3722.7
		3752.7	3752.5

*Not used in analysis.

**Not used in analysis; crude measurements from data taken without DPPH.

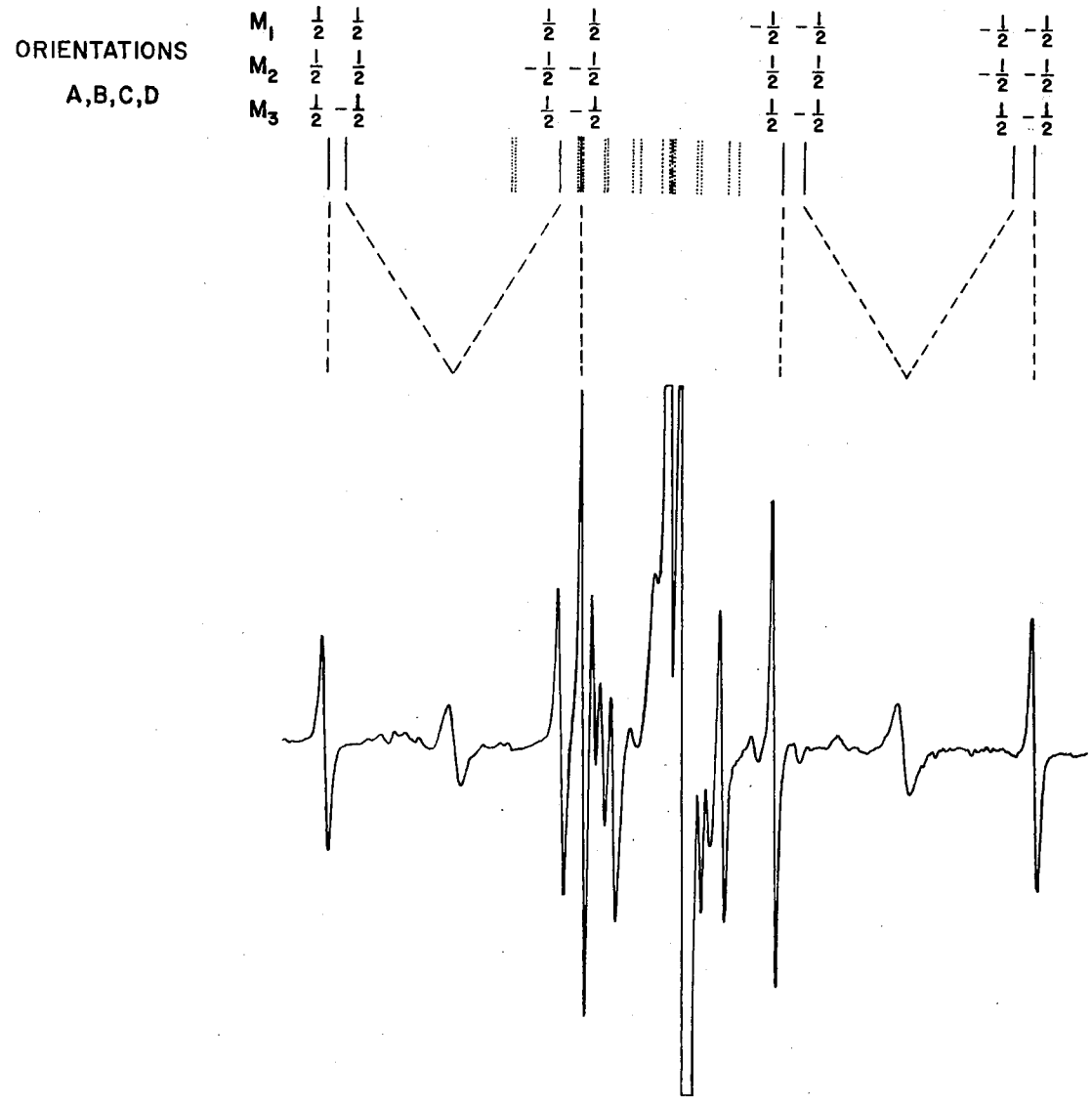

Figure 13. The 77 K [100] Spectrum of the H_A Center in $KMgF_3$: The "stick" diagram of the 10 K spectrum is shown in the upper portion of this figure; the magnetic field strength increases from left to right.

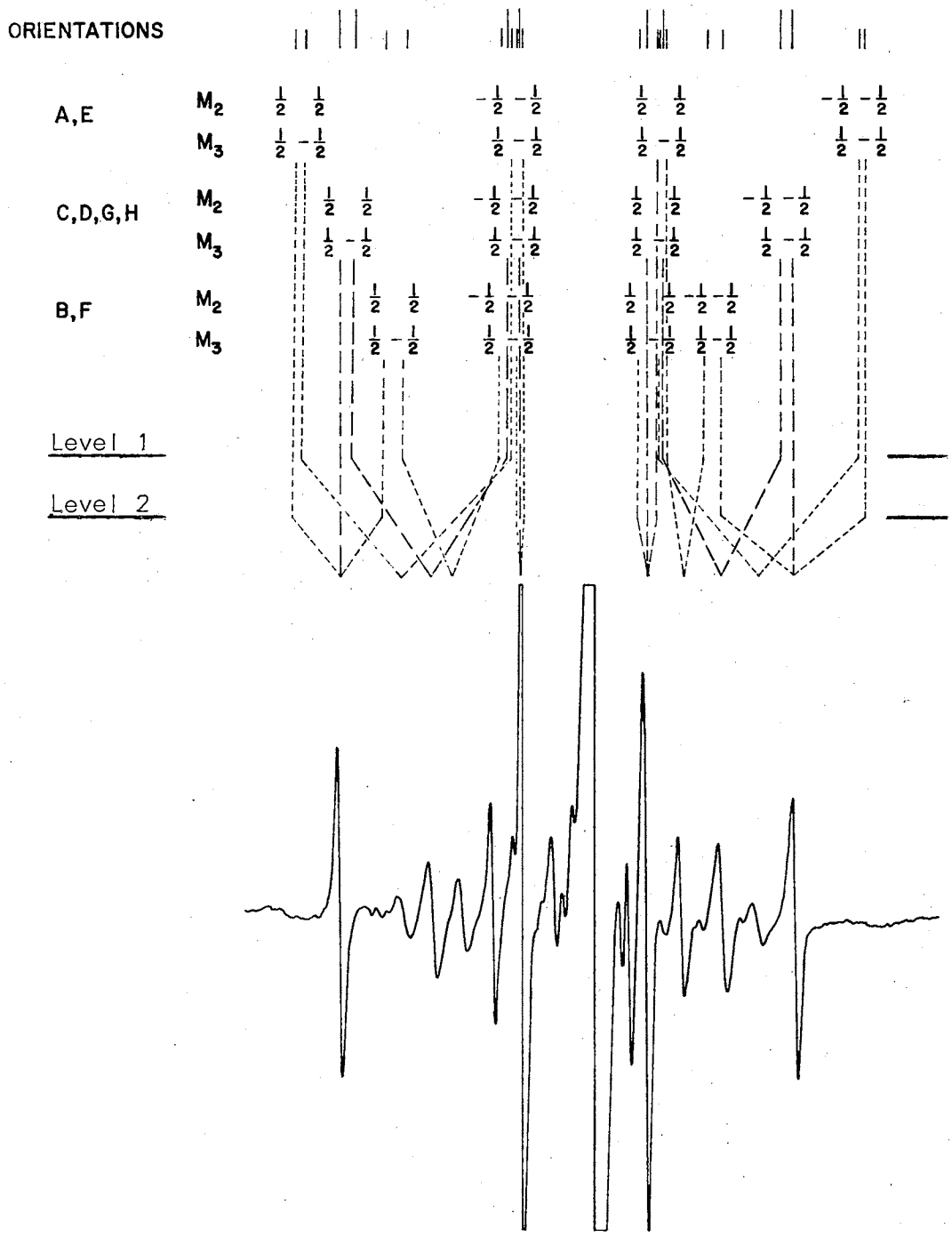

Figure 14. The 77 K [110] Spectrum of the H_A Center in $KMgF_3$: The "stick" diagram of the 10 K spectrum is shown in the upper portion of the figure; the magnetic field strength increases from left to right.

temperatures without exceeding the annealing stage, the resonances would reappear.

The H_A center designation implies an H center perturbed by the nearby presence of a perturbing entity A. Some data was taken in an attempt to implicate sodium impurities as this perturbing agent. This is displayed in Figure 15. The rationale was, given a series of different $KMgF_3$ samples, if a saturation level of H_A center concentration (as determined by EPR) could be obtained by prolonged irradiation of a crystal, then intuitively this level for each sample, normalized to a unit sample weight, should be a "measure" of the concentration of the perturbing entity A. From Table III the ratio of sodium in the $KMgF_3$:Na boule to that in the $KMgF_3$:Li boule was reported as three to two, a ratio not found from Figure 15. It should be pointed out that the low saturation level of H_A concentration in the $KMgF_3$:Yb sample may be attributable to the massive ytterbium concentration (~25,000 ppm).

This essentially completes the presentation of experimental data. In the following chapter analyses of these results are presented and explanations offered.

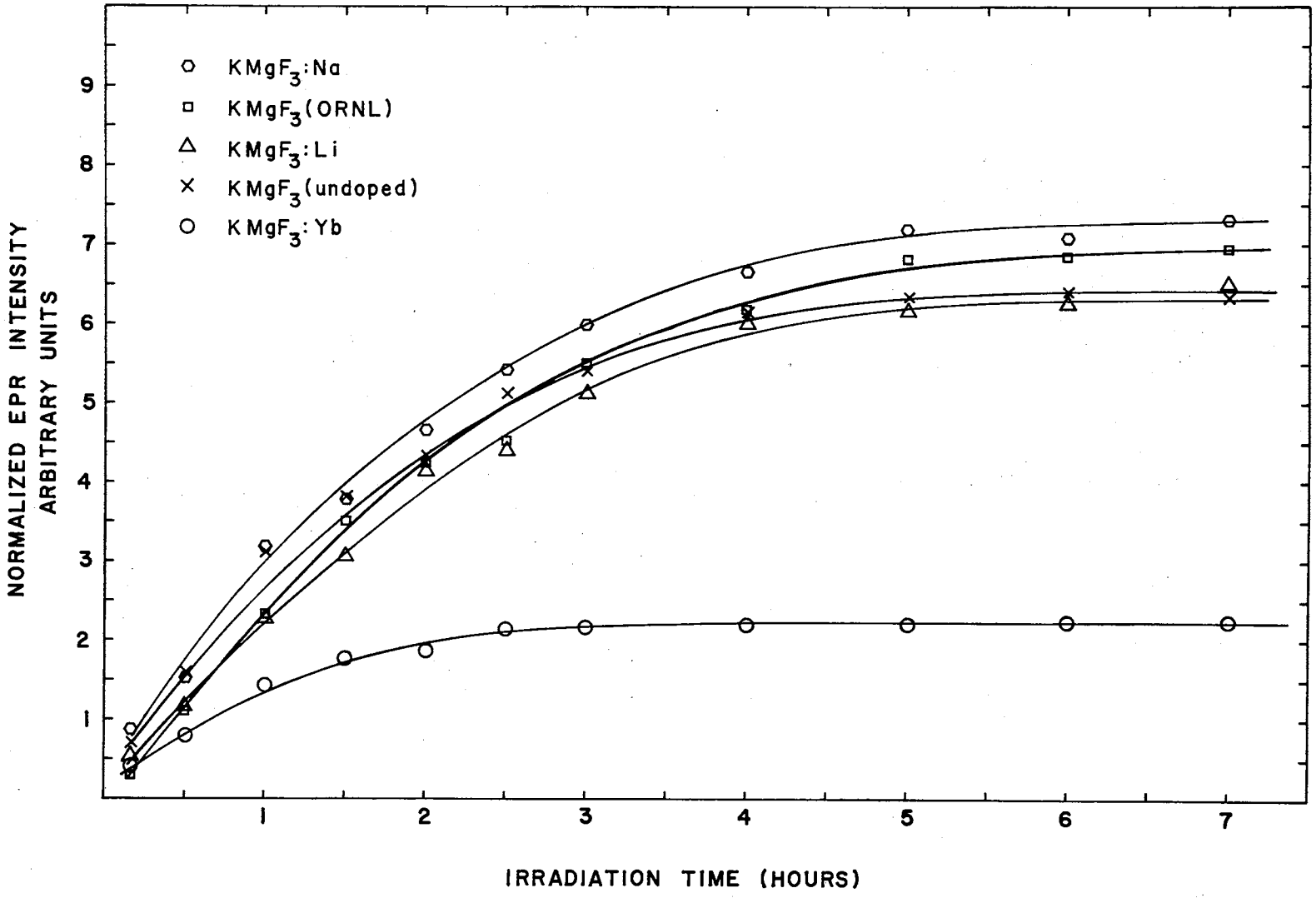

Figure 15. Saturation of H_A Center Concentration Normalized to Unit Weight in Various Samples as a Function of Irradiation Time

TABLE III

IMPURITY ANALYSES FOR SAMPLES CUT FROM TWO DIFFERENT BOULES (ppm)

Impurity	Sample Concentration (ppm)	
	$KMgF_3$:Li	$KMgF_3$:Na
Ag	< 1	< 1
Al	75	100
Au	< 5	< 5
B	< 1	< 1
Ba	< 2	10
Be	< 15	< 1
Bi	< 2	< 2
Ca	15	< 2
Cd	< 2	< 2
Co	< 5	< 5
Cr	< 2	< 2
Cu	1	2
Fe	5	3
Ga	< 1	< 2
Ge	< 2	< 2
Hg	< 5	< 5
Gd	< 5	< 5
Eu	< 5	< 5
Li	60	10
Mn	< 1	< 1
Mo	25	
Na	600	900
Nb	< 10	< 10
Ni	< 5	< 1
Pb	< 1	< 2
Pt	< 5	< 5
Rb	90	
Sb	< 10	< 10
Si	2	10
Sn	< 2	< 2
Sr	< 25	
Ti	20	< 1
V		< 2
W	< 5	< 10
Zn	< 200	< 200
Zr		< 5

CHAPTER IV

ANALYSIS

As in the previous chapter, there will be a division of this chapter into two major sections dealing with the $[F_2^-]_A$ center and the H_A center, respectively.

Analysis of the $[F_2^-]_A$ Center Data

The model of the $[F_2^-]$ center as proposed by Hall has already been introduced in Chapter I. It was also stated at that point that perturbations on this system may be expected to lead to effects observable with EPR. Indeed, effects have evolved in the form of additional resonances (to wit, the lifting of degeneracies) in the [110] spectrum as well as in the relatively high thermal stability of the $[F_2^-]_A$ centers, both effects implying a stabilizing perturbation.

The data does not favor the proposition of a perturbation located on the magnesium site nearest the $[F_2^-]$ center since this would appreciably affect the positions of certain lines in the $[F_2^-]_A$ spectra (those lines most sensitive to the bond angle in Hall's paper, which are the inner 45° lines in the [100] spectrum and the 90° lines in the [110] spectrum), but more importantly this would not lead to the

observed additional resonances since the symmetry of this perturbed defect would not be reduced from that of the intrinsic defect. As may be seen from Table III of the preceding chapter, predominant substitutional impurities in the $KMgF_3$:Na sample are sodium and lithium, both monovalent and hence both capable of substituting for potassium ions. They are also endowed with smaller ionic radii than the potassium ion and should therefore, at least intuitively, serve as a stabilizing perturbation on any nearest neighbor self-trapped hole center. Assuming a perturbation at the potassium site leads to a reduction in the symmetry of a nearest neighbor $[F_2^-]$ and hence to a splitting of certain resonant lines, an effect that is observed. Although there is no hard evidence to implicate them, vacancies at these potassium sites would appear to be extremely effective in stabilizing these centers in that the effective "positive" charge of the vacancy would strongly attract the effective "negative" charge of the $[F_2^-]_A$ center.

Hence, the data is consistent with a model in which some perturbation is present at a nearest neighbor potassium site, which, of course, may be above or below the (100) plane containing the two fluorines comprising the $[F_2^-]_A$ center (see Figure 1). As in the intrinsic $[F_2^-]$ center, the two fluorines remain equivalent whereas the symmetry of the environment of the $[F_2^-]_A$ center is reduced when compared to the C_{2v} symmetry of the intrinsic center.

The intrinsic $[F_2^-]$ center (27) is well described by the spin Hamiltonian (45, 46):

$$\hat{H} = \beta\vec{H}\cdot\overleftrightarrow{g}\cdot\hat{\vec{S}} + \hat{\vec{I}}_1\cdot\overleftrightarrow{A}_1\cdot\hat{\vec{S}} + \hat{\vec{I}}_2\cdot\overleftrightarrow{A}_2\cdot\hat{\vec{S}} - g_{NF}\beta_N\vec{H}\cdot(\hat{\vec{I}}_1 + \hat{\vec{I}}_2) \qquad \text{Eq. 8}$$

where

β = Bohr magneton = 9.274096×10^{-21} erg/Gauss

$\hat{\vec{S}}$ = the spin operator for this spin $\frac{1}{2}$ system

$\overleftrightarrow{g}$ = the g tensor for the system

$\vec{H}$ = the direction and magnitude of the externally applied dc magnetic field

$\overleftrightarrow{A}_i$ = the hyperfine tensor representing basically the dipole-dipole interaction of the spin with nucleus $i = 1, 2$, as well as a Fermi contact interaction

$\hat{\vec{I}}_i$ = the nuclear spin operator for nucleus $i = 1, 2$

$g_{NF}\beta_N$ = the gyromagnetic ratio pertinent to fluorine nuclei times Planck's constant h divided by $2\pi = 2.654144 \times 10^{-20}$ erg/Gauss

and $|\overleftrightarrow{A}_1| = |\overleftrightarrow{A}_2|$ by equivalence.

As a result of the rather high symmetry of the intrinsic center, the principal axes of its A and g tensors are found to lie in {100} planes; two axes, which shall be referred to as x and z, lie in the (100) plane of the molecular ion (i.e., in the plane of the page in Figure 1(b)), whereas the y principal axis lies along the [100]. The z principal axes of the A tensors were found by Hall to deviate some 7^o from the <110> directions.

The model of the $[F_2^-]_A$ is envisioned to be the same as that for the $[F_2^-]$ center and is described by the same spin Hamiltonian, with only one additional parameter needed to describe an intact rotation

by an angle δ (ELTA)[1] of the intrinsic molecular ion out of the (100) plane and about an [011] direction (Figure 1(b)), colinear with a line joining the two constituent fluorines. The absolute sense of the rotation was not determined but is assumed to be towards the perturbation at the potassium site. The y principal axes of all tensors remain parallel but no longer lie along a [100]; instead, they deviate from this direction by the angle δ. The plane of the perturbed molecular ion is normal to the direction of the y axes.

For the specific orientation in Figure 1(b), diagrammatic cross sectional views through the (011) plane looking along an [011] direction for the $[F_2^-]$ and $[F_2^-]_A$ centers are:

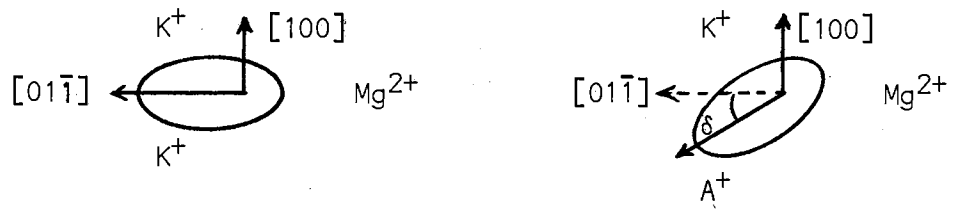

$[F_2^-]$ $\qquad$ $[F_2^-]_A$

The deviation of the $[F_2^-]_A$ from (100) planes doubles the number of distinguishable orientations of this molecular ion in $KMgF_3$ from six in the intrinsic case to twelve and is the fact responsible for the "splitting" of the inner 60° resonances observed in the [110] spectrum. From calculations it was found that this deviation leads to

---

[1] Capitalized and spelled Greek letters as well as capitalized abbreviations denote the various quantities as expressed in the program listings in Appendixes E through H.

a small (~2 Gauss) yet unresolvable splitting of the outer 60° resonances and resulted in no splitting in any of the other resonances in the [110] or [100] spectrum.

The analysis of the experimental data in terms of the proposed model will now be presented, along with all the assumptions employed.

The starting point is the spin Hamiltonian given by Equation 8. On the basis of equivalence, it is assumed that $|\overleftrightarrow{A}_1| = |\overleftrightarrow{A}_2|$ for the $[F_2^-]_A$ center. A crystallographic coordinate system is defined with the x-, y-, and z-axes along the $[0\bar{1}1]$, [100], and $[0\bar{1}\bar{1}]$ directions, respectively (Figure 1(b)). The principal axis coordinate system of the g tensor is assumed to be such that its z-axis lies along the line of centers joining the two fluorines and colinear with the $[0\bar{1}\bar{1}]$ direction, an assumption also employed by Hall; the x-axis lies in the plane of the molecular ion perpendicular, of course, to the z-axis, the positive direction being toward the nearest neighbor Mg^{2+} ion; the y-axis is normal to both, forming a right-handed cartesian coordinate system. Two more coordinate systems are introduced, both with their y-axes parallel to the y-axis of the $\overleftrightarrow{g}$ tensor principal axis coordinate system, and defined as the principal axis coordinate systems of the $\overleftrightarrow{A}_1$ and $\overleftrightarrow{A}_2$ tensors, centered on nuclei one and two, respectively. Again, by equivalence it is assumed that these z-axes both make an angle α = ALPHA (θ in Figure 1(b)) with respect to the line of centers between nuclei one and two. One final coordinate system is introduced, the magnetic field coordinate system where $\vec{H} = H\hat{k}$.

The first step is to express the hyperfine tensors $\overleftrightarrow{A}_1$ and $\overleftrightarrow{A}_2$ in the $\overleftrightarrow{g}$ tensor principal axis coordinate system. This is done via the matrices $\overleftrightarrow{T}_1$ and $\overleftrightarrow{T}_2$ such that:

$$\overleftrightarrow{A}_I = \overleftrightarrow{T}_i^{-1} \cdot \overleftrightarrow{A}_i \cdot \overleftrightarrow{T}_i , \qquad I = i = 1,2 \qquad \text{where}$$

$$\overleftrightarrow{T}_1 = \begin{pmatrix} \cos\alpha & 0 & \sin\alpha \\ 0 & 1 & 0 \\ -\sin\alpha & 0 & \cos\alpha \end{pmatrix}$$

$$\overleftrightarrow{T}_2 = \begin{pmatrix} \cos\alpha & 0 & -\sin\alpha \\ 0 & 1 & 0 \\ \sin\alpha & 0 & \cos\alpha \end{pmatrix} , \quad \text{and of course}$$

$$\overleftrightarrow{A}_i = \begin{pmatrix} A_{ix} & 0 & 0 \\ 0 & A_{iy} & 0 \\ 0 & 0 & A_{iz} \end{pmatrix}$$

An additional transformation is now needed to transform all three tensors $\overleftrightarrow{g}$, $\overleftrightarrow{A}_1$, and $\overleftrightarrow{A}_2$ from the $\overleftrightarrow{g}$ tensor system to the magnetic field coordinate system. The transformation may be thought of as bringing the z-axis of the $\overleftrightarrow{g}$ tensor into coincidence with the positive direction of the magnetic field. The general form of the transformation matrix is given by Goldstein (47) in terms of Euler angles which are measured with respect to the crystallographic coordinate axes. Note that the value of ψ is immaterial in this particular situation and has been set to zero in the program listings in Appendixes E and F. The value of δ has been treated explicitly:

$$\overleftrightarrow{K} = \begin{pmatrix} \cos\psi\cos(\phi-\delta) - \cos\theta\sin\psi\sin(\phi-\delta) & -\sin\psi\cos(\phi-\delta) - \cos\theta\cos\psi\sin(\phi-\delta) & \sin\theta\sin(\phi-\delta) \\ \cos\psi\sin(\phi-\delta) + \sin\psi\cos\theta\cos(\phi-\delta) & -\sin\psi\sin(\phi-\delta) + \cos\psi\cos\theta\cos(\phi-\delta) & -\sin\theta\cos(\phi-\delta) \\ \sin\theta\sin\psi & \cos\psi\sin\theta & \cos\theta \end{pmatrix}$$

Hence, a tensor $\overleftrightarrow{S}'$ in the $\overleftrightarrow{g}$ tensor principal axis coordinate system becomes $\overleftrightarrow{S} = \overleftrightarrow{K}^{-1} \cdot \overleftrightarrow{S}' \cdot \overleftrightarrow{K}$ in the magnetic field coordinate system.

To be explicit, the spin Hamiltonian now takes the following form in the magnetic field coordinate system:

$$\hat{H} = \beta(0,0,H) \cdot \overleftrightarrow{K}^{-1} \cdot \begin{pmatrix} g_x & 0 & 0 \\ 0 & g_y & 0 \\ 0 & 0 & g_z \end{pmatrix} \cdot \overleftrightarrow{K} \cdot \begin{pmatrix} \hat{S}_x \\ \hat{S}_y \\ \hat{S}_z \end{pmatrix}$$

$$+ (\hat{I}_{1x}, \hat{I}_{1y}, \hat{I}_{1z}) \cdot \overleftrightarrow{K}^{-1} \cdot \overleftrightarrow{T}_1^{-1}(\alpha) \cdot \overleftrightarrow{A}_1 \cdot \overleftrightarrow{T}_1(\alpha) \cdot \overleftrightarrow{K} \cdot \begin{pmatrix} \hat{S}_x \\ \hat{S}_y \\ \hat{S}_z \end{pmatrix}$$

$$+ (\hat{I}_{2x}, \hat{I}_{2y}, \hat{I}_{2z}) \cdot \overleftrightarrow{K}^{-1} \cdot \overleftrightarrow{T}_2^{-1}(\alpha) \cdot \overleftrightarrow{A}_2 \cdot \overleftrightarrow{T}_2(\alpha) \cdot \overleftrightarrow{K} \cdot \begin{pmatrix} \hat{S}_x \\ \hat{S}_y \\ \hat{S}_z \end{pmatrix}$$

(continued to next page)

$$- g_{NF}\beta_N(0,0,H) \cdot \begin{pmatrix} \hat{I}_{1x} + \hat{I}_{2x} \\ \hat{I}_{1y} + \hat{I}_{2y} \\ \hat{I}_{1z} + \hat{I}_{2z} \end{pmatrix} \qquad \text{Eq. 9}$$

This expression was expanded in terms of the basic quantities H, g_x, g_y, g_z, A_x, A_y, A_z ($|\vec{A}_1| = |\vec{A}_2|$), α and δ, and in terms of the general Euler angles (θ, ϕ, ψ). For the x and y components of the angular momentum operators the raising and lowering (ladder) operators were introduced:

$$\hat{J}_x = \tfrac{1}{2}(\hat{J}_+ + \hat{J}_-) \qquad \hat{J}_y = \frac{1}{2i}(\hat{J}_+ - \hat{J}_-), \quad i = \sqrt{-1}$$

With this spin Hamiltonian and the basis kets $|M_s, M_{I_1}, M_{I_2}\rangle$, an eight by eight complex Hermitian matrix was calculated in terms of the basic quantities and the Euler angles. If values are assumed for these quantities, the matrix may be numerically diagonalized by a computer and eigenvalues obtained.

Two distinct yet essentially similar programs were written to analyze the experimental data. They are listed in Appendixes E and F. The calculated matrix elements may be found in these listings, as well as references to the various algorithms employed in the diagonalization and fitting subroutines.

The first program (Appendix E) assumes that the parameters (g's, A's, and angles) are known; the magnetic field strengths H, or the field positions of the resonant lines comprising the spectra are calculated by an iteration scheme, the gist of which follows.

An initial value of H is assumed. The orientation of the magnetic field relative to the molecular ion is specified by the angles θ and ϕ, and for each set of Euler angles there are four resonances. For instance the 0° resonances in the [110] spectrum are calculated when these angles are all zero such that $\vec{H}$ is parallel to the z-axis of the $\overleftrightarrow{g}$ tensor principal axis coordinate system. Similarly, the other sets of resonances are calculated by specifying the appropriate Euler angles. Once specified the matrix is then diagonalized and eight energy eigenvalues D(I) obtained, given in order of ascending value. At this point four resonances could be predicted if four microwave frequencies (NUMHZ) ν_I were available experimentally, where:

$$h\nu_1 = D(8) - D(1)$$
$$h\nu_2 = D(7) - D(2)$$
$$h\nu_3 = D(6) - D(3)$$
$$h\nu_4 = D(5) - D(4)$$

However, in EPR experiments it is the magnetic field that is normally varied while the experimental microwave frequency ν(FREQ) is held fixed. To calculate the first or lowest field value at which a resonance is predicted with a given set of parameters and for a given orientation of the magnetic field, the value of H is varied and the matrix repeatedly diagonalized until the calculated microwave frequency ν_1 lies within 0.5 MHz of the experimental microwave frequency. For the second field value of this set of four, H is again varied until ν_2 lies within 0.5 MHz of the experimental microwave frequency, and so on until all four resonances have been

calculated.[2] The orientation of the magnetic field relative to the molecular ion is then appropriately changed so that the resonances for inequivalent orientations of the defect in the crystal may be calculated as above. This procedure is reiterated until resonances for all inequivalent orientations of the $[F_2^-]_A$ in the crystal for H along the [100] and [110] directions have been calculated.

The "best" set of parameters (as found in the following paragraph) were used in this program along with the experimental microwave frequency to calculate the field positions of these resonances. These are included with the experimentally observed values in Table I.

Obviously, if the values of the parameters are in error, the calculated field positions will not agree with the experimentally observed field positions. The second program (Appendix F) is designed to systematically vary the values of the parameters until there exists good agreement between the calculated and observed values. As in the preceding program, an initial set of parameters is assumed, but the experimental orientations and magnitudes of the magnetic fields pertinent to each resonance are here furnished as experimental data. With this information the energy eigenvalues are obtained and as before the microwave frequency (NUMHZ) that will produce each resonance is calculated. If all the assumed parameters were correct, then each calculated microwave frequency NUMHZ

---

[2] Note that only two of the eight eigenvalues D(I) are utilized each time the matrix is diagonalized. This represents a tremendous computational inefficiency.

would have the same value as the experimental microwave frequency (MWFRQ). In general, however, they do not coincide, and a DELTA(J) = NUMHZ - MWFRQ is calculated for each resonance. After all the experimentally observed resonances have been considered, a sum of squares of the DELTA(J) is formed. It is this sum that was minimized by a systematic variation of the parameters, and the set that minimizes this sum is the reported set of parameters (Table IV).

TABLE IV

SPIN HAMILTONIAN PARAMETERS AT 77 K FOR THE $[F_2^-]$ AND $[F_2^-]_A$ CENTERS IN $KMgF_3$

$[F_2^-]_A$	$[F_2^-]$
$g_x = 2.025 \pm 0.001$	$g_x = 2.024 \pm 0.001$
$g_y = 2.020 \pm 0.001$	$g_y = 2.018 \pm 0.001$
$g_z = 2.0029 \pm 0.0005$	$g_z = 2.0024 \pm 0.0002$
$A_x = 85 \pm 10$ MHz	$A_x = 160 \pm 16$ MHz
$A_y = 96 \pm 10$ MHz	$A_y = 160 \pm 16$ MHz
$A_z = 2495 \pm 3$ MHz	$A_z = 2479 \pm 6$ MHz
$\alpha = 8.2^\circ \pm 0.2^\circ$	$\alpha = 7^\circ \pm 0.2^\circ$
$\delta = 6.2^\circ \pm 0.5^\circ$	

The results of the fitting program are given in Table IV along with the parameters reported by Hall (27). The error limits on the parameters listed in this table are such that if any one is changed to the upper or lower limit the calculated position of at least one resonance differs by one or more Gauss from that given in Table I. This criterion was employed since experimentally line positions could be measured to at least within one Gauss. The quoted limits are considered conservative.

There is no great disparity in the calculated parameters which are common to both the $[F_2^-]$ and $[F_2^-]_A$, lending more credence to the proposed model of the $[F_2^-]_A$ defect.

Analysis of the H_A Center Data

The determination of a model for the $[F_2^-]_A$ center was a relatively easy task in that it was simply an extension of the model of the intrinsic $[F_2^-]$ center. However, there existed no precursor model on which a model of the H_A center in $KMgF_3$ could be based, and hence the configuration had to be deduced completely from the experimental data.

In the deduction of a model consistent with all the experimental data, heavy reliance was placed upon analogies with interstitial halide centers in the alkali halides. For example, relatively large doses are required to produce significant numbers of the interstitial type

centers in the alkali halides (25) when compared with the production of self-trapped hole centers, a relationship observed to exist between the $[F_2^-]$ centers and what have come to be called the H_A centers in this study. As pointed out on page 15, the overall anisotropic hyperfine splitting for the H center is larger than in the corresponding $[X_2^-]$ center in an alkali halide, which is again a relationship observed to exist between the $[F_2^-]$ and H_A centers in $KMgF_3$. And only the interstitial centers that are stabilized by various perturbations, basically substitutional cations, in the alkali halides show strong resistance to thermal annealing; the intrinsic interstitial centers decay at temperatures well below 100 K. The H_A center, as has been shown, also possesses this high thermal stability, decaying at 195 K (the pulse anneal temperature at which the concentration of H_A centers is one half that of the original; see Figure 10). A most important observation is that at this decay temperature (195 K) Riley (48) has reported a large F center decay stage, suggesting a recombination of interstitial fluorine atoms and F centers. Finally, arguments may be advanced that interstitial type point defects, being uncharged, are not readily susceptable to destruction by UV light, which light normally has the effect of releasing electrons from various electron traps in a crystal, allowing their recombination with defects that are positively charged relative to the crystalline lattice. Long periods of irradiation with UV light at 77 K did indeed reduce the $[F_2^-]$ concentration in $KMgF_3$, whereas the H_A concentration remained virtually unaffected.

The experimental data is then consistent with an interstitial fluorine point defect stabilized by the nearby presence of some perturbing entity A. From the 10 K [100] and [110] EPR spectra of the H_A center and from a study of the angular variation of the spectra upon rotation in a (100) plane, a more detailed model of the H_A center is deduced. It is envisioned to be a composite of three fluorines (one interstitial and two located at approximately normal fluorine sites) and one unpaired spin that is unequally shared among the three fluorines. This hyperfine interaction is strongest with the interstitial fluorine, strong with the nearest normal fluorine, and weak with the third fluorine, this latter interaction basically giving rise to the observed doublets in the 10 K spectra. The defect lies in the (100) planes containing the potassium ions, as illustrated in the top portion of Figure 16. For comparative purposes, the $H_A(Na^+)$ center in KCl is depicted in the lower portion of Figure 16.

Since there are three different such (100) planes, there will be three inequivalent orientations of the H_A centers relative to an external magnetic field applied along a [100] direction, as noted in Figure 11. For $\vec{H}$//[110] there are four inequivalent orientations, as noted in Figure 12.

If the magnetic field is confined to a (100) plane and at some arbitrary direction other than the [100] or [110] directions, there are eight distinguishable orientations, whereas for a completely arbitrary direction of the magnetic field there are twelve distinguishable

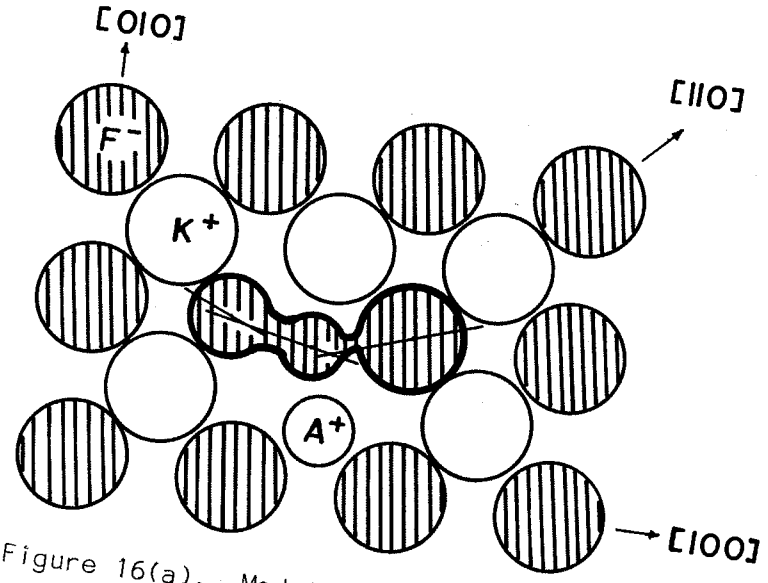

Figure 16(a). Model of H_A Center in $KMgF_3$: The defect lies in the (100) planes of the potassium ions.

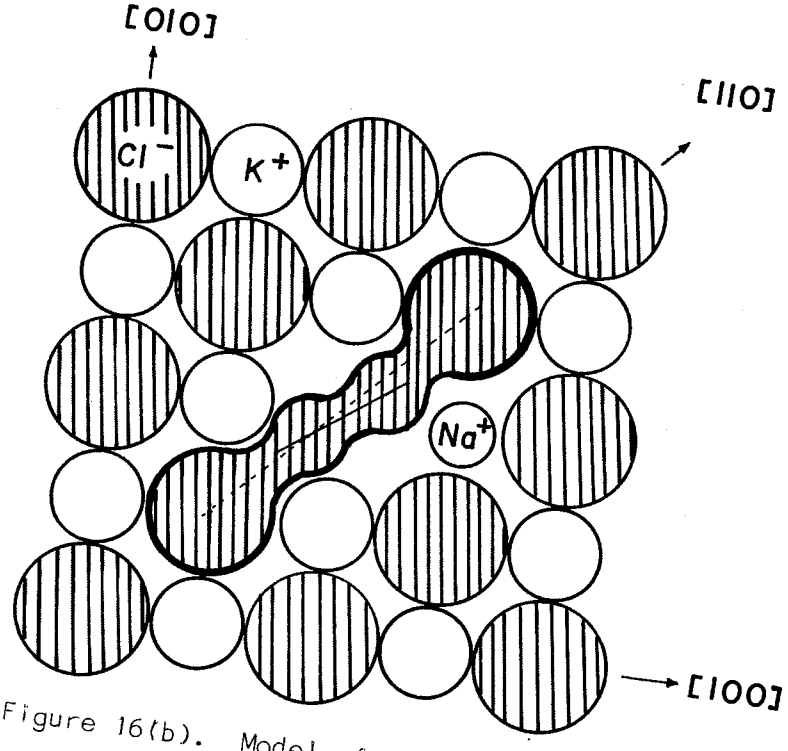

Figure 16(b). Model of the $H_A(Na^+)$ Center in KCl

orientations of the H_A center in $KMgF_3$, and these are displayed in Figure 17. The labeling of the sets of resonances in Figures 11 and 12 are taken from this figure.

The observed EPR resonances are consistent with the following spin Hamiltonian:

$$\hat{H} = \beta \vec{H} \cdot \overleftrightarrow{g} \cdot \hat{\vec{S}} + \hat{\vec{I}}_1 \cdot \overleftrightarrow{A}_1 \cdot \hat{\vec{S}} + \hat{\vec{I}}_2 \cdot \overleftrightarrow{A}_2 \cdot \hat{\vec{S}} + \hat{\vec{I}}_3 \cdot \overleftrightarrow{A}_3 \cdot \hat{\vec{S}} - g_{NF}\beta_N \vec{H} \cdot (\hat{\vec{I}}_1 + \hat{\vec{I}}_2 + \hat{\vec{I}}_3) ,$$

where the terms are basically the same as those introduced earlier in conjunction with the $[F_2^-]_A$ center analysis. The constants are identical. To be completely general, sixteen parameters are needed to describe quantitatively the H_A center in this material, four parameters for each of the four tensors. The principal axis coordinate systems of these tensors and their orientations relative to a crystallographic [100] direction are shown diagrammatically in Figure 18. The y-axes of all four tensors lie along the [010] direction, right-handed cartesian coordinate systems being implied. It is to be noted that θ_3 in the figure is considered as a negative quantity in the analysis below.

All four tensors are first transformed into the crystallographic coordinate system, which is defined with the z-axis along the [100] direction in Figure 18 and the y-axis out of the plane of the page along the [010], colinear with the y-axes of all four tensors. The general transformation matrix is:

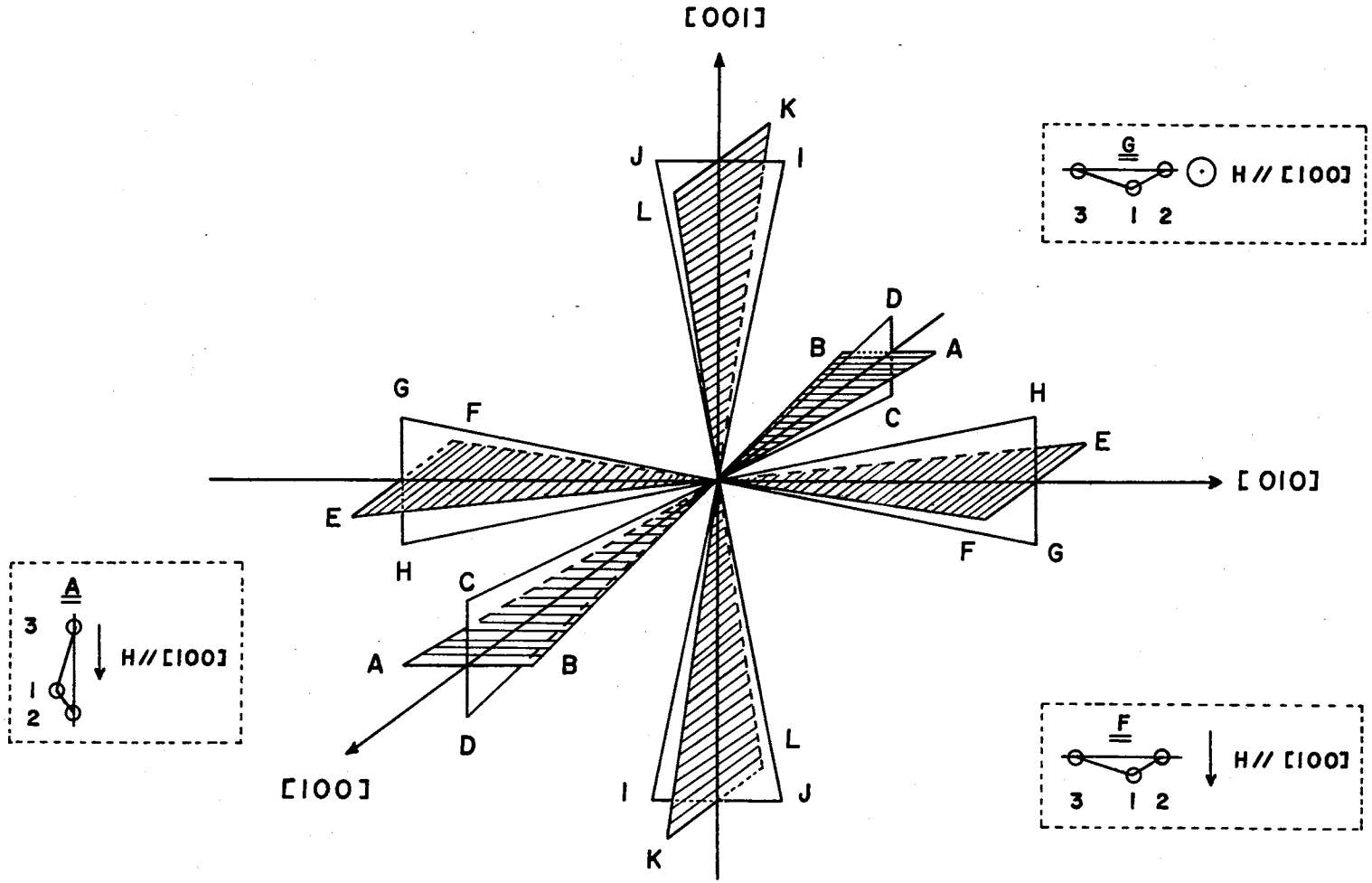

Figure 17. Various Inequivalent Orientations of the H_A Center in $KMgF_3$

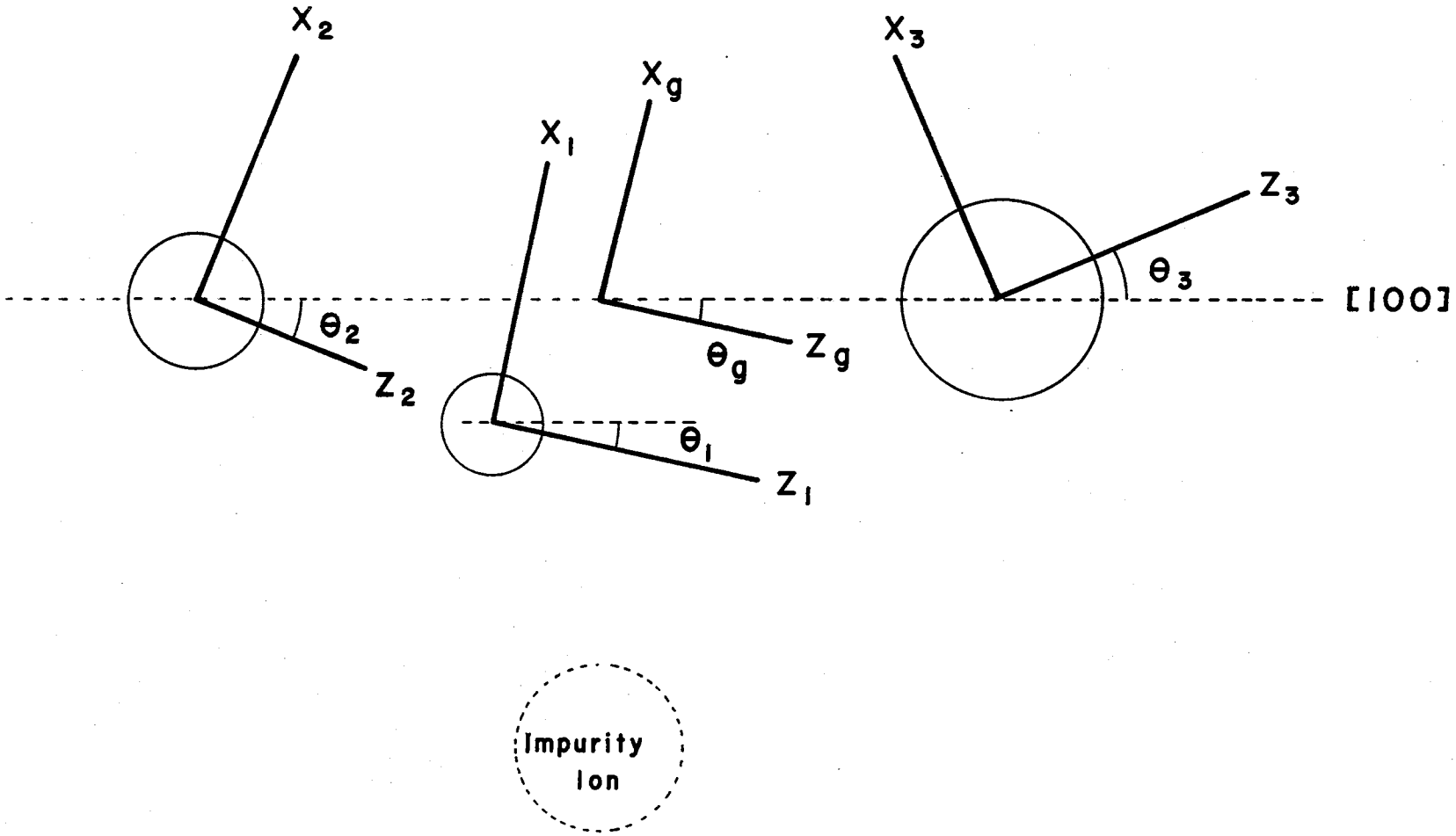

Figure 18. Schematic Representation and Orientation of the Four Principal Axis Coordinate Systems Pertinent to the $\overleftrightarrow{g}$, $\overleftrightarrow{A}_1$, $\overleftrightarrow{A}_2$, and $\overleftrightarrow{A}_3$ Tensors

$$\overleftrightarrow{R}(\theta_i) = \begin{pmatrix} \cos\theta_i & 0 & \sin\theta_i \\ 0 & 1 & 0 \\ -\sin\theta_i & 0 & \cos\theta_i \end{pmatrix}$$

such that, for instance, the $\overleftrightarrow{g}$ tensor in the crystallographic coordinate system assumes the form:

$$\overleftrightarrow{g} = \overleftrightarrow{R}^{-1} \cdot \begin{pmatrix} g_x & 0 & 0 \\ 0 & g_y & 0 \\ 0 & 0 & g_z \end{pmatrix} \cdot \overleftrightarrow{R}(\theta_g \equiv \text{CHI}),$$

and similarly for the three hyperfine tensors:

$$\overleftrightarrow{A}_1 = \overleftrightarrow{R}^{-1} \cdot \begin{pmatrix} A_{1x} & 0 & 0 \\ 0 & A_{1y} & 0 \\ 0 & 0 & A_{1z} \end{pmatrix} \cdot \overleftrightarrow{R}(\theta_1 \equiv \text{ALPHA1}),$$

etc.

The next step is the further transformation of these tensors into the magnetic field coordinate system where $\vec{H} = H\hat{k}$. Rather than perpetuate the redundancy of three angles as was done in the analysis of the $[F_2^-]_A$ center data, the following transformation was defined in terms of two angles $\theta \equiv$ THETA and $\phi \equiv$ PHI. The angle θ defines a counterclockwise rotation of the positive crystallographic z-axis about the crystallographic y-axis, the vantage point for the sense of the rotation being on the positive y-axis looking toward negative y values. Having made this rotation there exist new x- and z-axes. The angle ϕ defines a clockwise rotation of the new positive z-axis about the new x-axis, the vantage point being on the new positive x-axis

looking toward negative x values. The result of these two rotations brings the positive crystallographic z-axis into coincidence with the direction of the magnetic field. The matrix defining these rotations is given by:

$$\overleftrightarrow{E}(\theta \equiv \text{THETA},\ \phi \equiv \text{PHI}) = \begin{pmatrix} \cos\theta & -\sin\phi\sin\theta & \sin\theta\cos\phi \\ 0 & \cos\phi & \sin\phi \\ -\sin\theta & -\sin\phi\cos\theta & \cos\theta\cos\phi \end{pmatrix}$$

The original $\overleftrightarrow{g}$ tensor then takes the following form in the magnetic field coordinate system:

$$\overleftrightarrow{g} = \overleftrightarrow{E}^{-1} \cdot \overleftrightarrow{R}^{-1} \cdot \begin{pmatrix} g_x & 0 & 0 \\ 0 & g_y & 0 \\ 0 & 0 & g_z \end{pmatrix} \cdot \overleftrightarrow{R}(\theta_g \equiv \text{CHI}) \cdot \overleftrightarrow{E},$$

Again, to be explicit, the spin Hamiltonian takes the following form in the magnetic field coordinate system:

$$\hat{H} = \beta(0,0,H) \cdot \overleftrightarrow{E}^{-1} \cdot \overleftrightarrow{R}^{-1} \cdot \begin{pmatrix} g_x & 0 & 0 \\ 0 & g_y & 0 \\ 0 & 0 & g_z \end{pmatrix} \cdot \overleftrightarrow{R}(\theta_g \equiv \text{CHI}) \cdot \overleftrightarrow{E} \cdot \begin{pmatrix} \hat{S}_x \\ \hat{S}_y \\ \hat{S}_z \end{pmatrix}$$

$$+ (I_{1x}, I_{1y}, I_{1z}) \cdot \overleftrightarrow{E}^{-1} \cdot \overleftrightarrow{R}^{-1} \cdot \begin{pmatrix} A_{1x} & 0 & 0 \\ 0 & A_{1y} & 0 \\ 0 & 0 & A_{1z} \end{pmatrix} \cdot \overleftrightarrow{R}(\theta_1 \equiv \text{ALPHA1})$$

$$\cdot \overleftrightarrow{E} \cdot \begin{pmatrix} \hat{S}_x \\ \hat{S}_y \\ \hat{S}_z \end{pmatrix}$$

$$+ (I_{2x},I_{2y},I_{2z}) \cdot \overleftrightarrow{E}^{-1} \cdot \overleftrightarrow{R}^{-1} \cdot \begin{pmatrix} A_{2x} & 0 & 0 \\ 0 & A_{2y} & 0 \\ 0 & 0 & A_{2z} \end{pmatrix} \cdot \overleftrightarrow{R}(\theta_2 \equiv \text{ALPHA2})$$

$$\cdot \overleftrightarrow{E} \cdot \begin{pmatrix} \hat{S}_x \\ \hat{S}_y \\ \hat{S}_z \end{pmatrix}$$

$$+ (I_{3x},I_{3y},I_{3z}) \cdot \overleftrightarrow{E}^{-1} \cdot \overleftrightarrow{R}^{-1} \cdot \begin{pmatrix} A_{3x} & 0 & 0 \\ 0 & A_{3y} & 0 \\ 0 & 0 & A_{3z} \end{pmatrix} \cdot \overleftrightarrow{R}(\theta_3 \equiv \text{ALPHA3})$$

$$\cdot \overleftrightarrow{E} \cdot \begin{pmatrix} \hat{S}_x \\ \hat{S}_y \\ \hat{S}_z \end{pmatrix}$$

$$- g_{NF}\beta_N(0,0,H) \cdot \begin{pmatrix} I_{1x} + I_{2x} + I_{3x} \\ I_{1y} + I_{2y} + I_{3z} \\ I_{1z} + I_{2z} + I_{3z} \end{pmatrix}$$

This expression was expanded, again introducing the raising and lowering operators for x and y components of angular momentum operators, and a sixteen by sixteen complex Hermitian matrix calculated using the basis kets $|M_s,M_{I_1},M_{I_2},M_{I_3}>$. Assuming numerical values for all the quantities allows numerical computer diagonalization of this matrix, or equivalently allows the eigenvalues to be obtained.

The two programs used in the analysis of the H_A data are listed in Appendixes G and H, and these listings both contain the calculated matrix elements $<M_s',M_{I_1}',M_{I_2}',M_{I_3}'|\ \hat{H}\ |M_s,M_{I_1},M_{I_2},M_{I_3}>$. The

functions of these two programs are equivalent to those listed in Appendixes E and F, respectively. That is, the program in Appendix G is designed to calculate the magnetic field positions or field strengths at which resonances occur for the H_A center when values for the sixteen parameters are assumed and a microwave frequency value furnished. And the program in Appendix H is designed to accomplish the reverse task: to take the experimentally measured line positions and microwave frequency and calculate the values of the sixteen parameters. The logic of the programs in Appendixes E and G is identical, as is the logic of the programs listed in Appendixes F and H. Reference may be made to the earlier discussions of Appendixes E and F, and if desired more information may be ascertained through a study of the programs, which are further explained through many comment cards in the listings.

Using the experimental data tabulated in Table II, which in this form gives not only the field values of the resonances but implicitly the values of $\theta \equiv$ THETA and $\phi \equiv$ PHI as well (i.e., the orientation of the magnetic field relative to the various H_A centers depicted in Figure 17), the fitting program in Appendix H calculates the sixteen parameters to have the values listed in Table V. The criterion for the error limits is the same as in the preceding section, and again they are considered conservative.

The consistent inequivalence between x and y subscripted values, not found in the alkali halides, reflects well the lack of

rotational symmetry of the H_A center. It is also to be noted that there were no constraints on the signs of any of the parameters. Except for the angle $\theta_3 \equiv$ ALPHA3, all values were calculated to be positive. However, the absolute signs of A_{ix} and A_{iy} could not be determined.

TABLE V

SPIN HAMILTONIAN PARAMETERS AT 10 K FOR AN H_A CENTER IN $KMgF_3$

$g_x = 2.033 \pm 0.001$	$A_{2x} = 182 \pm 12$ MHz
$g_y = 2.026 \pm 0.001$	$A_{2y} = 193 \pm 12$ MHz
$g_z = 2.0018 \pm 0.0005$	$A_{2z} = 1680 \pm 5$ MHz
$\theta_g = \chi = 12^\circ \pm 1^\circ$	$\theta_2 = \alpha_2 = 22.3^\circ \pm 0.2^\circ$
$A_{1x} = 508 \pm 10$ MHz	$A_{3x} = 13 \pm 15$ MHz
$A_{1y} = 542 \pm 10$ MHz	$A_{3y} = 17 \pm 15$ MHz
$A_{1z} = 3121 \pm 3$ MHz	$A_{3z} = 142 \pm 4$ MHz
$\theta_1 = \alpha_1 = 12.4^\circ \pm 0.1^\circ$	$\theta_3 = \alpha_3 = -23^\circ \pm 2^\circ$

With these parameters and the experimental microwave frequency, the program in Appendix G was utilized to calculate at

what magnetic field values these parameters would predict EPR resonances. These values are recorded in Table II where they may be easily compared with the experimentally observed values.

The intriguing effects observed in the H_A center EPR spectra as the temperature of the sample is raised must now be explained. To a large extent all that will be written is compactly summarized in Figures 13, 14, and 19, with reference to Figure 17 possibly being necessary.

The observed EPR spectra of the H_A center at 77 K and its relationship to the spectra at 10 K can be explained in terms of a restricted interstitial motion (R.I.M.), which in $KMgF_3$ is found to consist of a restricted motion of the interstitial fluorine along the <100> direction, (A) causing an alternating out-of-phase (one increases while the other decreases) strong-weak hyperfine interaction with nuclei two and three, respectively, as depicted in Figure 19, and (B) resulting in a possible change between two distinguishable (with EPR) orientations of the H_A center relative to an arbitrary direction of the external magnetic field. Notice that in case (A) the hyperfine interaction with the interstitial fluorine is assumed to remain essentially constant. This concept of R.I.M. is not a new one in the solid state; the observation and nomenclature was introduced in the study of the $H_A(Na^+)$ in KCl by Delbecq, et al., (38). What does appear to be a noteworthy observation is the clarity of this effect in the solid state caused by the alternating hyperfine interaction. This effect was first

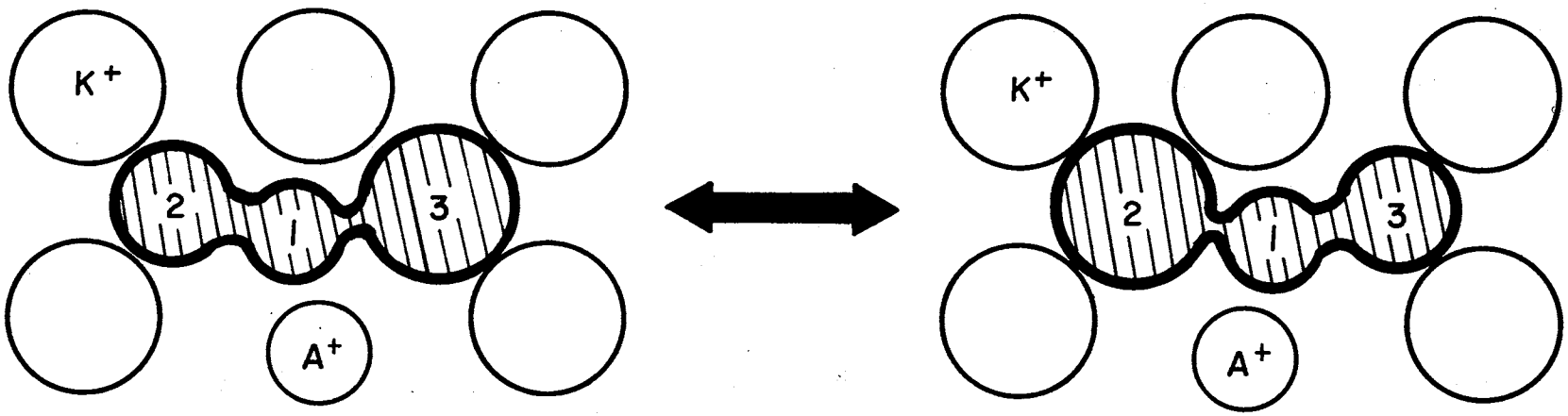

Figure 19. Interconversion of an H_A Center Between Two Thermodynamically Equivalent Configurations

observed in the EPR of solutions; to wit, in the spectra of the dihydroxydurene cation (49) and of the dinitrodurene anion (50) and is labeled as the alternating-linewidth effect, for which the designation should soon become apparent. This is discussed and demonstrated rather clearly by Wertz and Bolton (51) to which the interested reader is strongly referred. This out-of-phase modulation of the two hyperfine splittings due to nuclei two and three, leading to the alternating-linewidth effect, will here be discussed and further elaborated upon in terms of the R.I.M. observed for the H_A center in $KMgF_3$.

An examination of the 10 K and 77 K spectra of the H_A for $\vec{H}$//[100] (Figures 11 and 13, pages 41 and 45) in terms of the above concepts should help clarify these ideas. The discussion is limited to consideration of resonances due to those H_A centers whose "z" axes are essentially parallel to the applied magnetic field (i.e., orientations A, B, C, and D). For such centers first order perturbation theory gives good agreement with experiment (24), and the quantum numbers M_s, M_{I_1}, M_{I_2}, and M_{I_3} are still relatively valid. The nuclear quantum numbers may then be used to label the particular resonances in the 10 K spectrum, as has been done in the "stick" diagram in Figure 13. As the temperature is raised from 10 K, the interconversion shown in Figure 19 becomes more prominent; that is, the roles of nuclei two and three continually interchange and the rate increases with temperature. This is of no consequence for the first, fourth, fifth, or eighth resonance due to these "parallel type"

H_A centers, for the nuclear quantum numbers of nuclei two and three for these resonances are identical. However, upon interconversion, these numbers interchange for the second and third and the sixth and seventh resonances. For a slow rate of interconversion, there is no noticeable effect; the second and sixth resonances simply become the third and seventh resonances, respectively, and no averaging occurs. For a slightly faster rate, effects are noticeable in that the amplitudes of the second, third, sixth, and seventh resonances are somewhat reduced relative to those of the first, fourth, fifth, and eighth resonances, indicating the beginning of an averaging effect. This may be observed in the experimental data recorded in Figure 11. At a much faster rate what is experimentally observed with EPR is an averaged line midway between the second and third and midway between the sixth and seventh resonances. This averaging is clearly denoted in Figure 13. As pointed out by Wertz and Bolton (51), the linewidths of these averaged lines depend upon the size of the field shift between the two unaveraged resonances as well as upon the temperature dependent reorientation rate: These averaged lines are broader for larger shifts and narrow with increasing temperature. The former effect is clearly demonstrated in the 77 K [110] spectrum of the H_A center to be explained next, and the latter was reported in Chapter III (page 43). Hence, for the "parallel type" H_A center, the 77 K [100] spectrum consists of an unaveraged and hence relatively sharp low field (first) resonance with an averaged and hence broadened

(originally second and third) resonance occurring just upfield, followed by the unaveraged original fourth resonance. The same scheme applies to resonances five through eight. At this point the alternating linewidth effect should be self-evident.

This same effect can be observed in the 77 K [110] spectrum of the H_A center. Yet there is another effect that presents itself in this case that must be distinguished from the first, thus making both effects less obvious. This other effect is the averaging of two distinct resonances in the 10 K spectrum as a result of the interconversion between two distinguishable orientations of a particular H_A center relative to the external magnetic field. For instance, upon interconversion orientation A becomes orientation B and similarly for E and F (See Figure 17, page 66). For $\vec{H}$//[100] this is of no consequence, but for $\vec{H}$//[110] these two orientations are distinguishable; that is, they give rise to two different sets of eight resonances in the [110] spectrum as denoted in the lower portion of Figure 12 (page 42) or in the upper portion of Figure 14 (page 46). Hence, resonances from each of these distinct sets which possess identical quantum numbers $[M_1(A) = M_2(A) = M_3(A) = M_1(B) = M_2(B) = M_3(B)]$ will average. This may be seen in Figure 14 where the original first resonance is shown averaged with the fifth at the third resonance to result in a single low field resonance in the 77 K spectrum. This type of averaging gives rise to four such resonances in the [110] spectrum and these are distinguished in the upper portion of Figure 14 by the fact that the

dashed lines indicating this averaging "break" at Level 2 (those lines which "break" at Level 1 are averaging because of the alternating hyperfine interaction as discussed previously). These four resonances are an excellent example of the statement by Wertz and Bolton reported earlier regarding the linewidths of averaged lines and their dependence upon the size of the field shift between the two unaveraged resonances: The narrower the shift, the sharper the averaged resonance.

This completes the analysis of the experimental data. The final chapter will attempt to summarize this entire study, point to its weaknesses, and make suggestions for future study.

CHAPTER V

SUMMARY AND DISCUSSION

It was basically observations on the high field zero degree line of the [110] spectrum of the $[F_2^-]$ type centers that led to the more complete investigation of the $[F_2^-]_A$. At the left in each of the three sets in Figure 7, page 32, the resolved "superhyperfine" interaction of the intrinsic self-trapped hole center with the equivalent nuclei three and four (Figure 1(b)) can be clearly seen, this interaction giving rise to the observed one-two-one intensity ratios depicted in the "stick" diagrams. When these samples were raised to temperatures just above ~108 K and returned to lower temperatures, there was observed a pronounced reduction in amplitude of the observed resonance as well as a loss of the simple one-two-one intensity ratio, the result being shown in the central portion of each set in Figure 7. The reduction in amplitude indicates the decay of the intrinsic $[F_2^-]$ resonance, and the resulting resonance is explicable as a superposition of <u>two</u> new sets of resonances, each (similar to the original) having a one-two-one intensity ratio. These were viewed as arising from two different types of perturbed self-trapped hole centers that were created during the migration of the intrinsic center during its decay

stage,[1] the perturbations "quenching" the mobility of the holes at the temperatures in question. These two different perturbations cause a slightly different hyperfine interaction of the hole with nuclei one and two, and this is detected by the two sets of resolved resonances. This view of two different defects was further substantiated by raising the temperature of the samples to 160 K or above and noting the loss of one set of resonances, leaving only one set that displayed a simple one-two-one intensity ratio, much like the original resonance yet occurring at a slightly higher field value. It was this subtle evidence which indicated that two different types of perturbed self-trapped hole centers existed in all $KMgF_3$ samples studied.

It was, of course, the more stable $[F_2^-]_A$ that was studied in more detail. And evidence of not so subtle a nature was found to more completely distinguish this defect from the intrinsic center; to wit, the splitting of the inner 60° resonances in the [110] spectrum. This evidence led to the postulation of a perturbation at a nearest neighbor potassium site, a proposition that accounts equally well for the observed thermal stability and the splitting of the 60° resonances.

With this model for the $[F_2^-]_A$, the g values, hyperfine parameters, and angles were calculated from the experimental data and

---

[1] Hall (27) reported an annealing of intrinsic $[F_2^-]$ centers at 77 K due to unstable or shallow electron traps (electron to hole recombination). Lewis, et al., (32) reported that hole migration caused $[F_2^-]$ decay in the 100-120 K range (hole to electron trap recombination).

are reported in Table IV, page 60. The agreement with the values reported by Hall (27) is encouraging, and the values reported here are reasonable. The larger A_z value is indicative of a closer approach of the two halide cores comprising the $[F_2^-]_A$ than in the intrinsic defect, again compatible with the concept of a nearby perturbation that allows for this closer approach.

The raison d'etre for the study of this $[F_2^-]_A$ is basically for completeness and to compliment the previous work done with $KMgF_3$. Unfortunately, the exact nature of the perturbation A was not ascertainable in this study. This result will require the application of the ENDOR technique, which is a logical next step. Too, for completeness, optical absorption experiments need to be performed for this defect and compared with results for the intrinsic center.

As has been noted, heavy reliance was placed upon analogies with interstitial type centers that have been studied in the alkali halide materials when determining the model of the interstitial center reported in this study. There was the requirement for relatively long periods of irradiation to produce these defects; the overall anisotropic hyperfine splitting was larger than for the $[F_2^-]$ type centers; there was reported (48) a large F center decay stage at the decay temperature of the H_A; the high thermal stability (195 K) strongly implies a stabilizing perturbation A; and the effects of UV irradiation at 77 K imply an uncharged (relative to the local crystalline lattice) point defect. All these facts support the claim that the observed H_A spectra

in $KMgF_3$ are due to an interstitial type point defect stabilized by some perturbation A.

From a study of the 10 K spectra it became apparent that the defect was composed of three inequivalent fluorines and one hole that interacted with the nuclei of all three. Studying the behavior of the spectrum upon rotation in a (100) plane, the major axis of this defect was found to lie in a general <100> direction. The most logical set of (100) planes (of the two available in $KMgF_3$) in which a three-fluorine center could lie is the set containing the potassium ions. Too, it is the potassium sites that are most likely to be the site of the perturbation A, in the form of substitutional impurities (see Table III) or vacancies.

Given all these considerations, the H_A model was proposed (Figure 16(a), page 64). The study of the motional effects (the averaging) at 77 K and the interpretation given to these effects certainly supports the proposed model. Accepting the model, it should be noted that this defect has features which distinguish it from the interstitial centers that have been studied in the alkali halides. This H_A model proposes the existence of a "true" interstitial (the number "one" fluorine) as opposed to the split interstitial configuration found in the alkali halides. And the symmetry of this H_A center in $KMgF_3$ is much reduced from the intrinsic H centers in the alkali halides. This fact is reflected in the consistent inequality between the A_{ix} and A_{iy} hyperfine values.

As noted on page 47, an attempt was made to implicate sodium impurities as the perturbation A. A sodium concentration analysis was performed (via atomic absorption) on the five samples employed in taking the data displayed in Figure 15, page 48. Dividing each sample into two parts, two trials were made for each sample. Although blank, standard, and background samples were simultaneously run during both determinations, there was in some of the samples some 50 percent disparity between the two trials. Hence, these numbers were not reported, although there was found to be a factor of two or more difference in some of the concentrations (excluding the $KMgF_3$:Yb), a fact not reflected in Figure 15. This rather null result should be compared with results found by Delbecq, et al., (38) in their study of the $H_A(Na^+)$ in KCl. In that study there was indeed a growth of the $H_A(Na^+)$ optical band with increasing Na^+ concentration up to 15.2 ppm Na^+. Above this concentration, this band failed to grow correspondingly. It is highly unlikely that any of the samples employed in this study contained less than 100 ppm Na^+. Hence, the determination of the perturbation A must await the results of ENDOR.

Another rather incidental point to be made relates to the statement by Delbecq, et al., (38) on page 1114: ". . . The hyperfine interactions of a given molecule decrease with increasing temperature." It was found that the overall hyperfine splitting of the H_A in $KMgF_3$ at 10 K was noticeably larger than at 77 K.

There remains yet to be done the optical study of the H_A center as well as the aforementioned ENDOR work. There is room for more detailed information regarding the interstitial motion at all temperatures and the possible study of tunneling behavior at low temperatures. There are the intriguing effects brought about by UV irradiation at 10 K of $KMgF_3$ samples containing H_A centers; to wit, their conversion into intrinsic and/or other perturbed interstitial centers. These latter effects are being pursued further.

An effect not being pursued is the dark (dark blue or black) coloration that occurred when $KMgF_3$ samples used in this study were irradiated at LNT. This coloration anneals in room light but appears to be stable in darkness at this temperature. There were no obvious EPR resonances that could be attributed to this coloration.

In the study of both the $[F_2^-]_A$ and H_A, data was not obtained for $\vec{H}//[111]$. It is felt that this does not invalidate or cast serious doubt on either of the proposed defect models or the values of the parameters. This data might possibly have made determination of the models somewhat easier.

Finally, mention might be again made of the fact that only two of the eight ($[F_2^-]_A$) or sixteen (H_A) eigenvalues were utilized each time the subroutines HTRIDI and IMTQL1 were called. This was of only slight consequence for the $[F_2^-]_A$ problem where the matrix to be diagonalized was only eight by eight. For the H_A computations, however, repeated ($\sim 10^4$) complete diagonalization of the sixteen by

sixteen matrix required a not insignificant amount of computer time even at FORTRAN IV, Level H. If by restricting the subroutines in some manner to calculate only the two eigenvalues of interest, a considerable amount of computer time might have been saved.

SELECTED BIBLIOGRAPHY

(1) Billington, D. S., and J. H. Crawford, Jr. Radiation Damage in Solids. Princeton, New Jersey: Princeton University Press, 1961.

(2) Sonder, E., and W. A. Sibley. "Defect Creation by Radiation in Polar Crystals." Point Defects in Solids, Volume I, General and Ionic Crystals. J. H. Crawford, Jr., and L. M. Slifkin, eds. New York: Plenum Press, 1972, pp. 201-283.

(3) Chadderton, Lewis T. Radiation Damage in Crystals. London: Methuen & Co., Ltd., 1965.

(4) Kelly, B. T. Irradiation Damage to Solids. Oxford: Pergamon Press, 1966.

(5) Segrè, E. Nuclei and Particles. New York: W. A. Benjamin, Inc., 1964.

(6) Känzig, W., Phys. Rev., 99, 1890 (1955).

(7) Platzman, R. T. "Chapter 7." Symposium on Radiobiology, The Basic Aspects of Radiation Effects on Living Systems. James J. Nickson, ed. New York: John Wiley & Sons, Inc., 1950, pp. 97-108.

(8) Varley, J. H. O., Journal of Nuclear Energy, 1, 130 (1954).

(9) Varley, J. H. O., Nature, 174, 886 (1954).

(10) Dexter, D. L., Phys. Rev., 118, 934 (1960).

(11) Howard, R. E., S. Vosko, and R. Smoluchowski, Phys. Rev., 122, 1406 (1961).

(12) Klick, C. C., Phys. Rev., 120, 760 (1960).

(13) Williams, F. E., Phys. Rev., 126, 70 (1962).

(14) Seitz, F., Reviews of Modern Physics, 26, 7 (1954).

(15) Pooley, D., Solid State Communications, 3, 241 (1965).

(16) Konitzer, J. D., and H. N. Hersh, J. Phys. Chem. Solids, 27, 771 (1966).

(17) Hersh, H. N., Phys. Rev., 148, 928 (1966).

(18) Silsbee, R. H., J. Appl. Phys., 28, 1246 (1957).

(19) Ueta, M., Y. Kondo, M. Hirai, and T. Yoshinary, J. Phys. Soc. Japan, 26, 1000 (1969).

(20) Itoh, N., and M. Saidoh, J. de Physique, 34, C9-101 (1973).

(21) Murray, R. B., and F. J. Keller, Phys. Rev., 153, 993 (1967).

(22) Pooley, D., and W. A. Runciman, J. Phys. C: Solid State Phys., 3, 1815 (1970).

(23) Keller, F. J., and F. W. Patten, Solid State Communications, 7, 1603 (1969).

(24) Castner, T. G., and W. Känzig, J. Phys. Chem. Solids, 3, 178 (1957).

(25) Kabler, M. N. "Hole Centers in Halide Lattices." Point Defects in Solids, Volume I, General and Ionic Crystals. J. H. Crawford, Jr., and L. M. Slifkin, eds. New York: Plenum Press, 1972, pp. 327-378.

(26) Schoemaker, D., Phys. Rev. B, 7, 786 (1973).

(27) Hall, T. P. P., Brit. J. Appl. Phys., 17, 1011 (1966).

(28) Känzig, W., Phys. Rev. Letters, 4, 117 (1960).

(29) Känzig, W., J. Phys. Chem. Solids, 17, 80 (1960).

(30) Bass, I. L., and R. L. Mieher, Phys. Rev., 175, 421 (1968).

(31) Kappers, L. A., and L. E. Halliburton, J. Phys. C: Solid State Phys., 7, 589 (1974).

(32) Lewis, J. T., J. L. Kolopus, E. Sonder, and M. M. Abraham, Phys. Rev. B, 7, 810 (1973).

(33) Känzig, W., and T. O. Woodruff, J. Phys. Chem. Solids, 9, 70 (1958).

(34) Dakss, M. L., and R. L. Mieher, Phys. Rev. Letters, 18, 1056 (1967).

(35) Dakss, M. L., and R. L. Mieher, Phys. Rev., 187, 1053 (1969).

(36) Chu, Y. H., and R. L. Mieher, Phys. Rev. Letters, 20, 1289 (1968).

(37) Chu, Y. H., and R. L. Mieher, Phys. Rev., 188, 1311 (1969).

(38) Delbecq, C. J., E. Hutchinson, D. Schoemaker, E. L. Yasaitis, and P. H. Yuster, Phys. Rev., 187, 1103 (1969).

(39) Patten, F. W., and F. J. Keller, Phys. Rev., 187, 1120 (1969).

(40) Schoemaker, D., and J. L. Kolopus, Phys. Rev. B, 2, 1148 (1970).

(41) Plant, W. J., and R. L. Mieher, Phys. Rev. B, 7, 4793 (1973).

(42) Lewis, J. T. "Electron Paramagnetic Resonance and Optical Absorption Studies of Color Centers and Impurity Ions in $KMgF_3$ and MgF_2." (Unpub. Ph.D. dissertation, University of Tennessee, 1971.)

(43) Riley, C. R., and W. A. Sibley, Phys. Rev. B, 1, 2789 (1970).

(44) Hughes, R. C., and Z. G. Soos, J. Chem. Phys., 52, 6302 (1970).

(45) Pryce, M. H. L., Proc. Phys. Soc. (London), A63, 25 (1950).

(46) Abragam, A., and M. H. L. Pryce, Proc. Roy. Soc. (London), A205, 135 (1951).

(47) Goldstein, H. Classical Mechanics, 7th ed. Reading, Massachusetts: Addison-Wesley Publishing Company, Inc., 1965.

(48) Riley, C. R. "Color Centers in Irradiated Potassium Magnesium Fluoride and Potassium Manganese Fluoride." (Unpub. Ph.D. dissertation, University of Tennessee, 1970.)

(49) Bolton, J. R., and A. Carrington, Mol. Phys., 5, 161 (1962).

(50) Freed, J. H., and G. K. Fraenkel, J. Chem. Phys., 37, 1156 (1962).

(51) Wertz, J. E., and J. R. Bolton. Electron Spin Resonance: Elementary Theory and Practical Applications. New York: McGraw-Hill Book Company, 1972.

APPENDIXES

APPENDIX A

LIST OF MAJOR EQUIPMENT

USED

LIST OF MAJOR EQUIPMENT USED

High Voltage Engineering Corporation Electrostatic Generator/Van de Graaff Accelerator Model AN2000 (with Electron Quick Converter Unit)

Cryogenic Technology Incorporated Liquid Nitrogen Cryogenerator Model A

Varian Associates:
- Model V-4007-1 Six Inch Rotating Electromagnet
- Model V-2200 A (Current) Regulated Magnet Power Supply
- Model V-4560 100 KHz Field Modulation and Control Unit
- Model V-4531 Multi-Purpose EPR Cavity
- Model V-4553 Wave Guide Bend
- Model V-4547 Variable Temperature Accessory With Heater Control Unit
- Model V-153C Reflex Klystron

Varian Vacuum Division/NRC Operation Model HS-2 Two-Inch Oil Diffusion Pump

Leeds and Northrup:
- Speedomax XL 620 Strip Chart Recorder
- K-3 Universal Potentiometer No. 7553-5
- D-C Electronic Null Detector No. 9834

Hewlett Packard:
- Frequency Counter Model 5327C
- Transfer Oscillator Model 540B
- Klystron Power Supply Model 716B
- Oscilloscope Model 130B
- Microwave Variable Attenuator Model X382A
- Hand Calculator Model 35

Tektronix: Type 122 Low Level Preamplifier
Type 125 Power Supply

Circuits Processing Apparatus Inc. Model 7061-A Liquid Nitrogen Cold Trap

Micro-Now Instruments Company, Inc. Model 210 Klystron Frequency Stabilizer

Veeco Helium Leak Detector Model MS90

Veeco Vacuum Gauge Control Panel Type RG

Princeton Applied Research Corporation Model JB-5 Lock-In Amplifier

Duo Seal Mechanical Vacuum Pump Welch Scientific Model 1397

General Electric Model XRD Type 1 X-Ray Diffraction Unit

Metals Research, Ltd., Macrotome II (Diamond Saw)

Lindberg Hevi-Duty Furnace Control Unit Model 59744

Hevi-Duty Electric Multiple Unit Furnace Type MK-3012, 54000 Series

Andonian Cryogenics Inc. Standard Helium Transfer Tube

Rotating Coil Magnetometer, Rawson-Lush Type 780, No. 18994 With Probe #18993

Cenco 100-Watt Mercury Arc Lamp

Perkin-Elmer 403 Atomic Absorption Spectrophotometer

Stainless Steel Liquid Helium Dewar (detailed in Appendix B)

NMR Marginal Oscillator (detailed in Appendix C)

Microwave Components (detailed in Appendix D)

APPENDIX B

DESCRIPTION OF STAINLESS STEEL CRYOSTAT

DESCRIPTION OF STAINLESS STEEL CRYOSTAT

The cryostat used in this study was the result of designs by the author and his advisor and was built in the Oklahoma State University Physics and Chemistry Machine Shop by Floyd Vulgamore. The major features of this Dewar are illustrated in the figures and photographs of this appendix. The Dewar was constructed almost exclusively with 304 stainless steel. The Dewar was fusion welded at all stainless-to-stainless junctions by Jim Bolinger of the Badger Meter Company of Tulsa. Leak tests with the Veeco Helium Leak Detector revealed no noticeable leaks. Subsequent experience with this Dewar confirmed this test in that with reasonable care the Dewar would maintain a usable vacuum for many hours, upwards of eight to ten.

The major feature of this cryostat was its simplicity. The insulating vacuum was common throughout and extended through the resonant cavity up through the stainless steel waveguide to the square top flange where it was terminated with a microwave vacuum window (Varian Associates V-1100B) seated on an O-ring in this flange. A large (1-inch) pump out valve allowed rapid evacuation of the Dewar. The liquid helium reservoir was surrounded by the conventional

nitrogen jacket whose usable capacity was approximately 2¼ liters. The usable capacity of the helium reservoir was approximately two liters. A teflon spacer with three contacts was provided to prevent contact of these two reservoirs at the bottom of the Dewar (see Figure 20). Removable copper heat shields extended from the bottom of each reservoir around the waveguide and resonant cavity that extended from the bottom of the helium reservoir (Figures 22 and 23). This entire ensemble was placed inside the outer jacket shown in Figure 21.

As indicated by Figure 20, the thin-walled (0.025") stainless steel waveguide leading to the rectangular TE_{102} resonant cavity was placed so as to lead through the helium reservoir. Two 3/16" stainless steel tubes were positioned along each broad side of the waveguide to accommodate electrical leads. At the outside termination of these two tubes the vacuum was sealed with the hermetically sealed electrical feed-through terminals. The leads from these terminals were taken directly to connectors mounted directly on the Dewar (Figure 24(b)). Heat sinks for the electrical leads were not provided beyond their loose contact with the feed-through tube and the waveguide at the bottom of the Dewar (Figure 22).

The waveguide terminated inside the Dewar with a circular brass flange to which the resonant cavity was afixed with four screws. A 0.010" brass iris plate with a ¼" iris was placed between this flange and the resonant cavity brass flange. The cavity itself was of brass

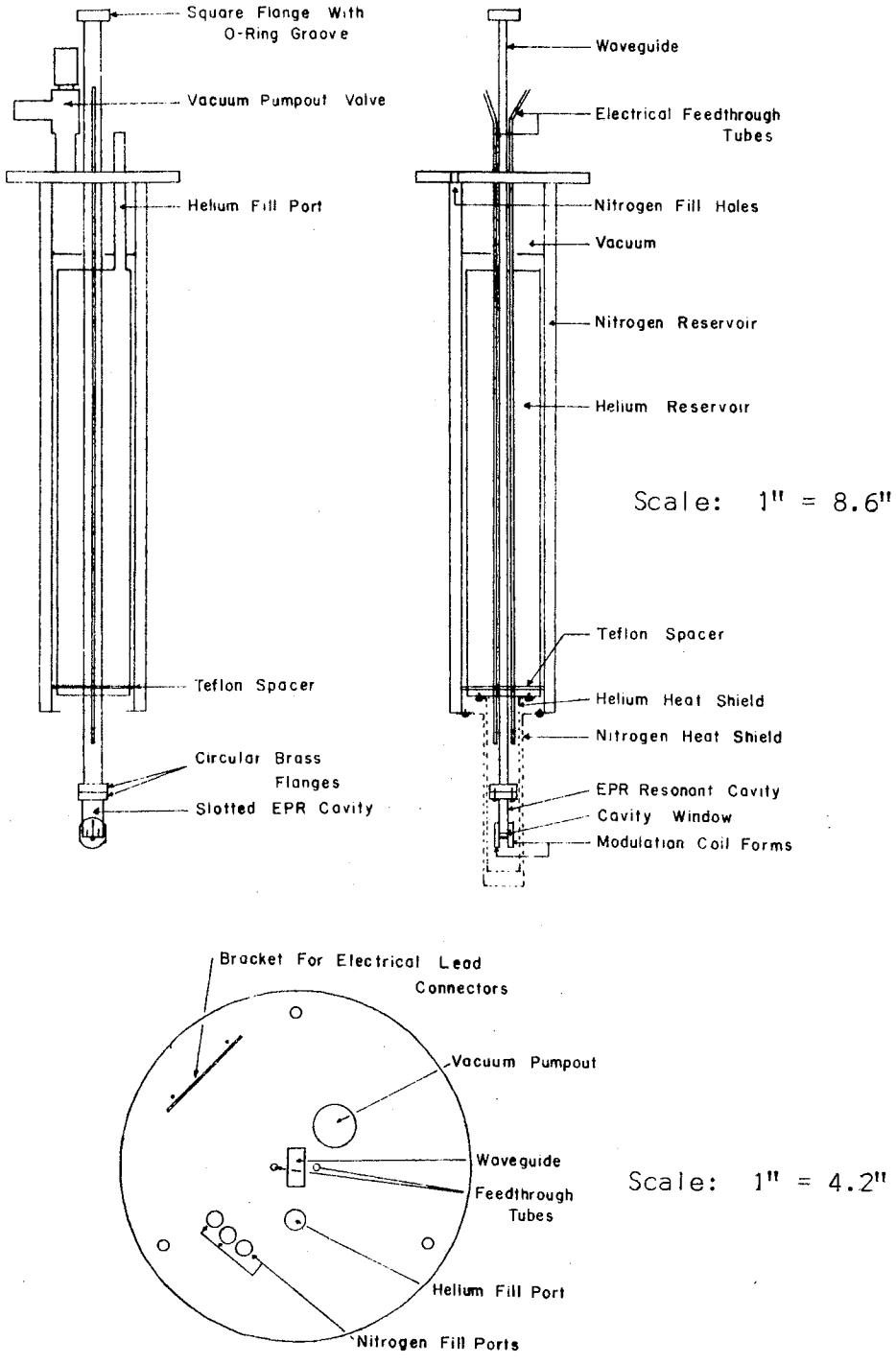

Figure 20. Cross-Sectional Views and Layout of Top Plate of Stainless Steel Helium Cryostat

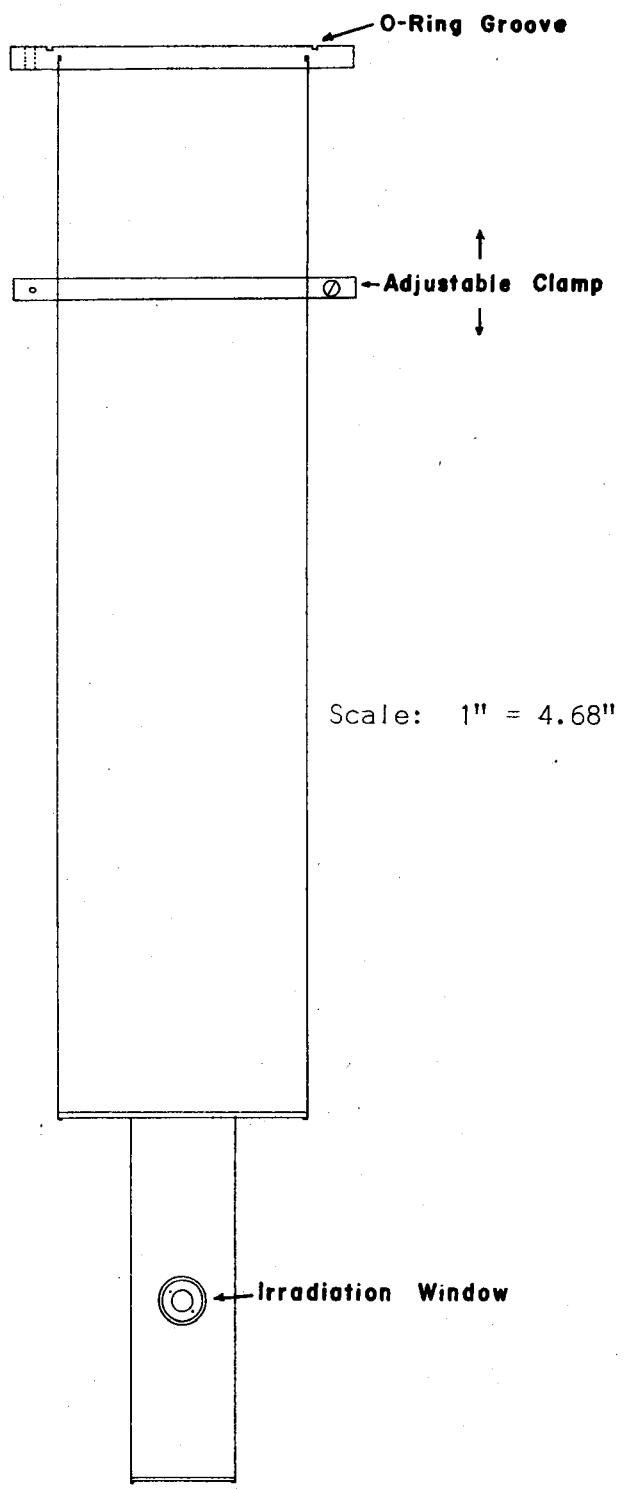

Figure 21. Outer Stainless Steel Jacket of Helium Cryostat

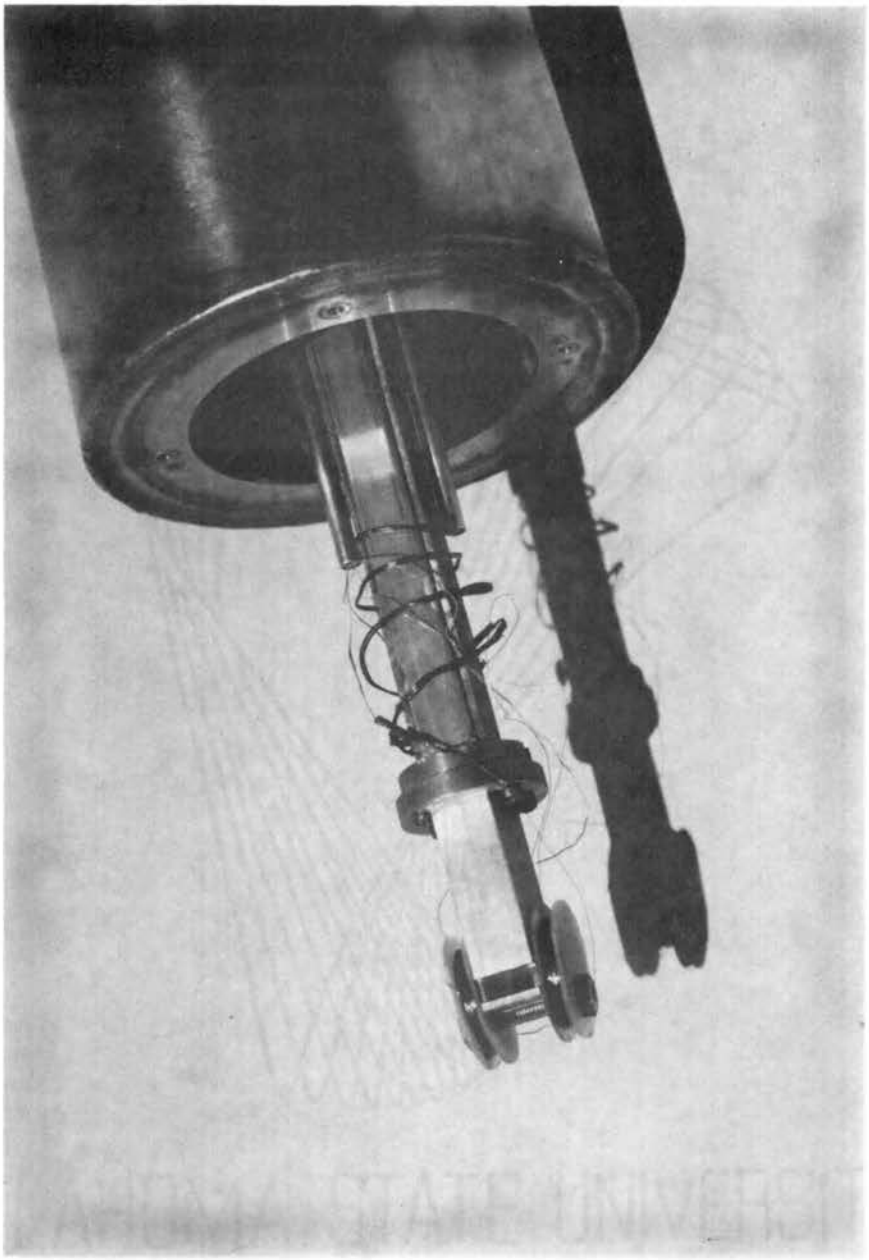

Figure 22. Close View of EPR Rectangular TE_{102} Resonant Cavity of the Helium Cryostat: The modulation coil forms are seen mounted on the broad walls of the cavity.

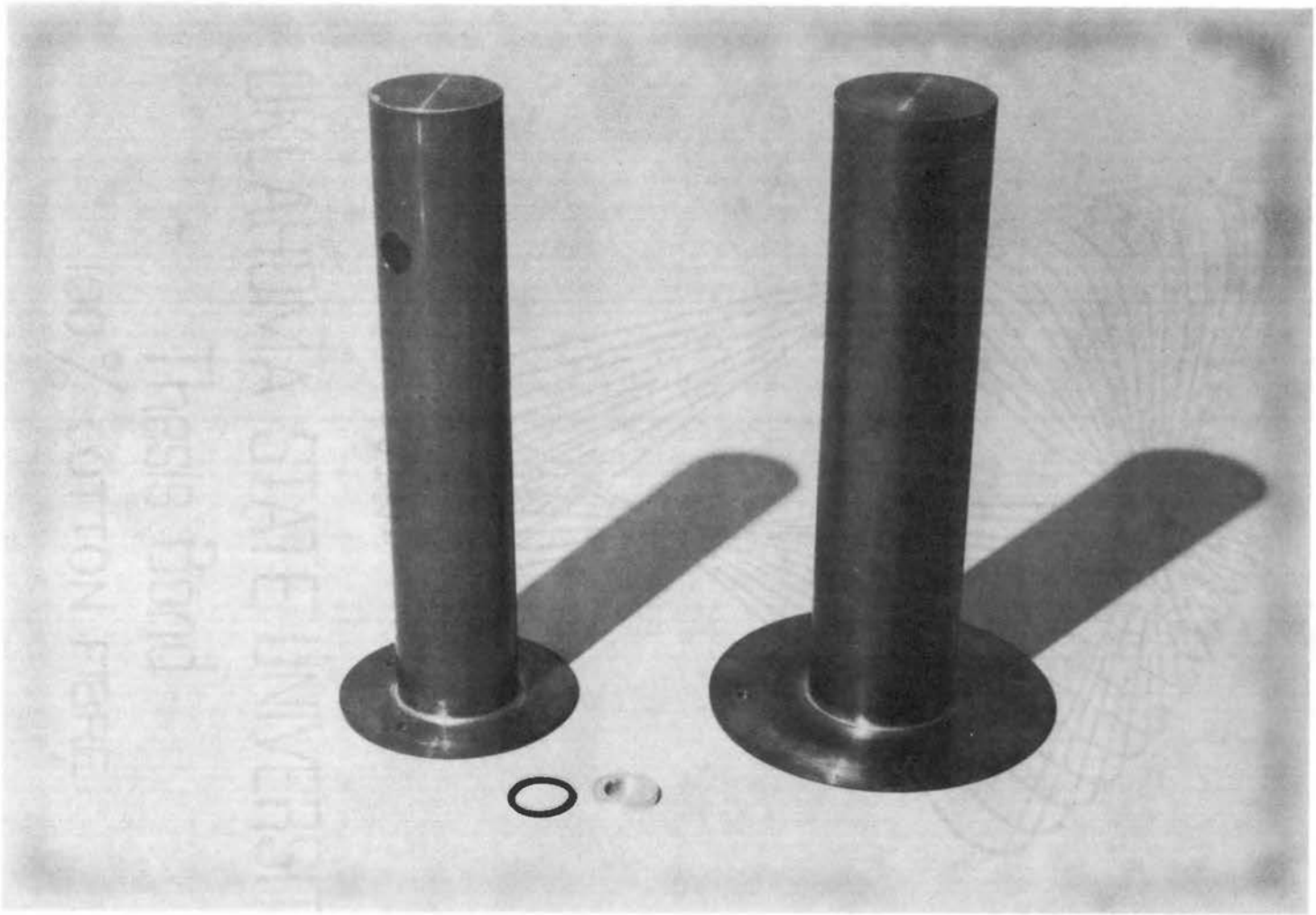

Figure 23. The Liquid Nitrogen and Helium Heat Shields: The aluminum irradiation window is shown in the foreground.

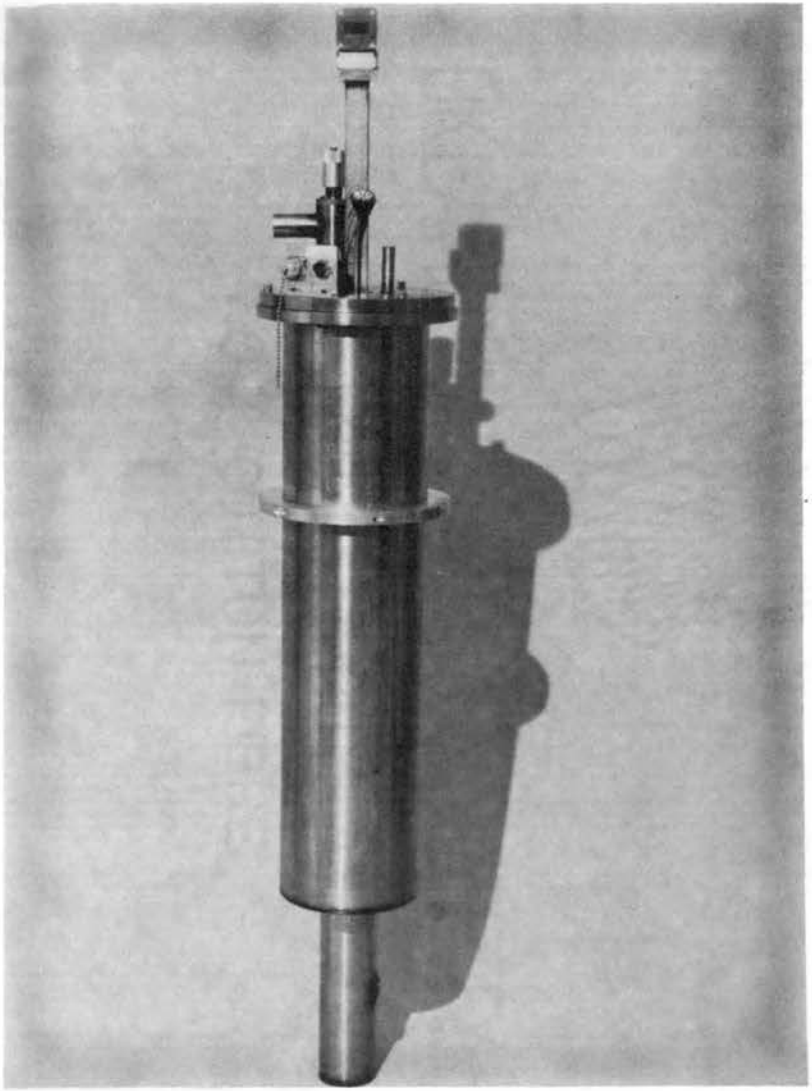

Figure 24(a). View of Entire Cryostat

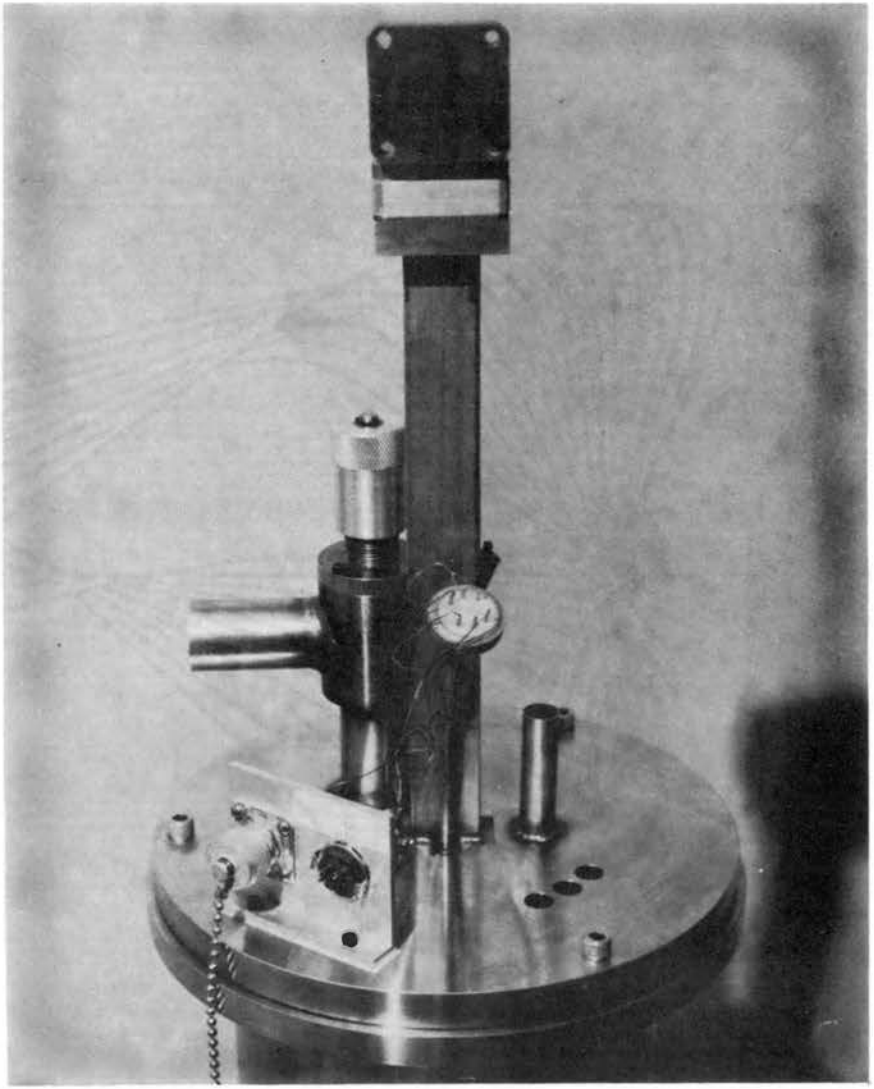

Figure 24(b). View of Top Plate of Cryostat

and its resonant frequency was in the neighborhood of 9000 MHz. The cavity had a 3/16" x 0.400" window milled out at the bottom of one of the narrow walls of the cavity (Figure 22). This window allowed irradiation of a sample in situ in the resonant cavity. The effect of this window upon the Q of the cavity was slight. This window aligned with holes in the copper heat shields (one such hole is shown in the helium heat shield of Figure 23) and the 0.006" aluminum window on the outer jacket of the Dewar.

Modulation of the static magnetic field was accomplished with modulation coils mounted on one-inch teflon or nylon forms which were in turn mounted low on the broad sides of the resonant cavity. To allow penetration of the 100 KHz modulating field into the cavity, three slots were cut through the bottom plate of the cavity and up the broad sides: a central one cut up to a height of 3/8" from the inside bottom of the cavity, and two outer ones, each ¼" from the center slot, were cut up to a height of 1/8". More and/or deeper slots had a deleterious effect on the Q of the resonant cavity. The coils themselves consisted of 225 turns each of B & S gauge 36 nyclad copper wire.

The Dewar had an excellent overall performance. Routinely both helium and nitrogen reservoirs were filled with liquid nitrogen and the EPR resonant cavity and the sample mounted on the bottom plate would remain at the equilibrium temperature of approximately 85 K for upwards of 18 hours before the reservoirs would need

refilling. During such periods of storage of an irradiated sample, the Dewar would normally be put back onto the pumping station.

Before transferring helium into the Dewar it was customary to first cool the helium reservoir with liquid nitrogen. Once cooled, the nitrogen was expelled and the helium transfer was then performed. This technique appeared to be much more efficient in terms of the amount of helium required to fill the Dewar. With a normal helium transfer, the Dewar would routinely maintain its equilibrium temperature at the bottom of the EPR cavity of approximately 10 K for something on the order of 12 hours, sufficient time to do many experiments.

The Dewar was not without improvable points, and in fact modification was required before the equilibrium temperatures quoted above could be obtained. This problem was due to the thermal gradient which developed along the stainless steel waveguide between the bottom of the helium reservoir and the bottom of the resonant cavity. The difference in temperature between these two points was attributed to the rather poor thermal conductivity of the thin-walled stainless steel waveguide and to the flange-iris plate-flange junctions. This difference was reduced by soft soldering two 1/16" x 13/16" x 4¼" copper plates to the broad sides of the waveguide from the bottom of the helium reservoir to the top of the cavity (Figure 22). Before introducing this copper, the equilibrium temperature at the bottom of the cavity with liquid helium in the helium reservoir was approximately 30 K. This problem could have been avoided by utilizing heavy

brass or perhaps even copper waveguide to extend from the helium reservoir down to the resonant cavity. However, a degree of thermal isolation was intended in the original design of this Dewar, for it was hoped that the entire resonant cavity could be electrically heated and hence the cryostat could serve as a variable temperature device. This was never attempted.

The second most severe minor problem was that of modulation amplitude. The home wrapped coils were found to be sufficient for this study, but the EPR signals encountered in this study (eight to ten Gauss linewidth) could not be over-modulated. This was due to the fact that the resonant cavity brass walls have a skin depth of 0.016" at 100 KHz, whereas the walls were 0.050" thick. The slots alleviated somewhat this problem, but 0.005" - 0.010" walls would have helped even more.

Rotation of the magnet to make angular studies was accompanied by a loss in signal intensity. This effect was inherent in the rectangular cavity as used. Space requirements dictated by a 2.7 inch magnet gap required that the cavity be "upright" rather than in the "on-its-side" configuration utilized in the commercial Varian cavity where this effect is eliminated. The same space requirements ruled out the possibility of using a cylindrical cavity. Too, the constructing of modulation coils for use at 100 KHz with a thick-walled cylindrical cavity would have been even more of a problem than it was for a rectangular cavity simply because the coils would have been

inherently further from the sample.

Filling the warm helium reservoir with nitrogen presented another minor problem since there was only the one fill hole. The evaporated cryogenic gas had a strong tendency to blow the entering cryogenic liquid back out the fill hole. A vent hole could have alleviated this problem.

Usable capacities were quoted above for the helium and nitrogen reservoirs. The actual capacities were actually much larger. However, filling the nitrogen reservoir completely to the top plate would have invited freezing of the O-ring at the top plate, causing a loss of the vacuum. Even filling to the usable capacity caused a great deal of bothersome but not harmful condensation on the top plate.

Finally, the sheer weight of the Dewar could perhaps have been lessened. When filled with cryogenics the Dewar weighed close to 45 pounds.

APPENDIX C

NUCLEAR MAGNETIC RESONANCE (NMR)

MARGINAL OSCILLATOR

NUCLEAR MAGNETIC RESONANCE (NMR)

MARGINAL OSCILLATOR

The solid state field effect transistor (FET) marginal oscillator described by this appendix was constructed using the circuit prescribed by Idoine and Brandenberger, Review of Scientific Instruments, 42, 716 (1971). What is included here are: slight changes made to the basic circuit description, a copy of the circuit board mask and component placement diagram, implications for extending the range of the oscillator, conversion to an external B^+ and B^- power supply (rather than the battery pack now incorporated), and NMR probe and Helmholtz coil construction.

The circuit was constructed as near as possible to that described by the reference. The changes that were made in components were (using the component designations of the reference):

C_4: 47pf instead of 45pf

R_5: 51Ω instead of 50Ω

F_1, F_2, F_3: GE-FET-1 instead of TI2N4221

B^+: Mallory TR-236 instead of Mallory TR-238 (The Mallory TR-238 is apparently no longer produced)

The circuit board used for this oscillator was of the glass-backed type, copper clad one side only. This type was the suggested

preference over phenolic type circuit board. In the rf portions of this circuit, silver mica and ceramic disc capacitors were employed. A double bearing variable capacitor (C_1) was preferred to provide additional stability for this circuit but could not be obtained. Hence, a single bearing Hammarlund capacitor was used.

In order to span a larger frequency range with this oscillator a rotary switch S_2 and a 100pf silver mica capacitor (C_{14}) were placed in parallel with the variable capacitor C_1:

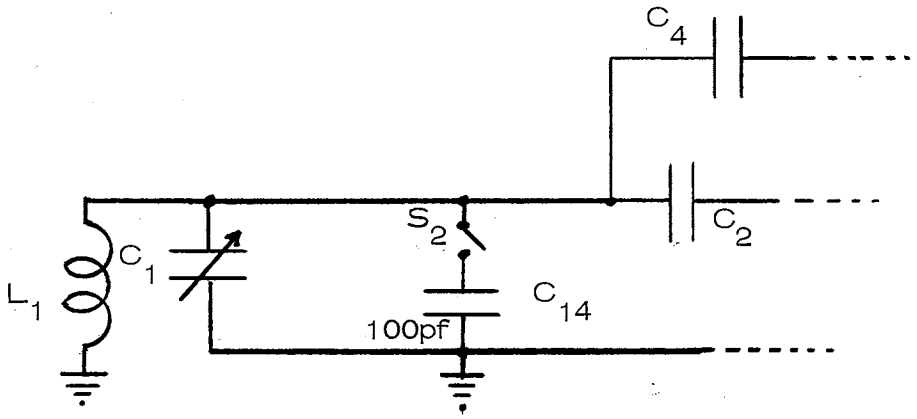

Closing S_2 lowers the frequency at which the oscillator will oscillate but the variable capacitor then no longer comprises the total capacitance for the tank circuit and hence, when varied, has less effect on the resonant frequency of the circuit. The result is that with the additional capacitor switched in, the range of oscillator frequencies is much smaller.

The circuit board mask is reproduced in Figure 25. The two islands A and B were etched so that separate power supplies could be used to serve the drain of F_1 and F_2, respectively, if the need arose to do so. This need did not arise, and a connection (jumper) was

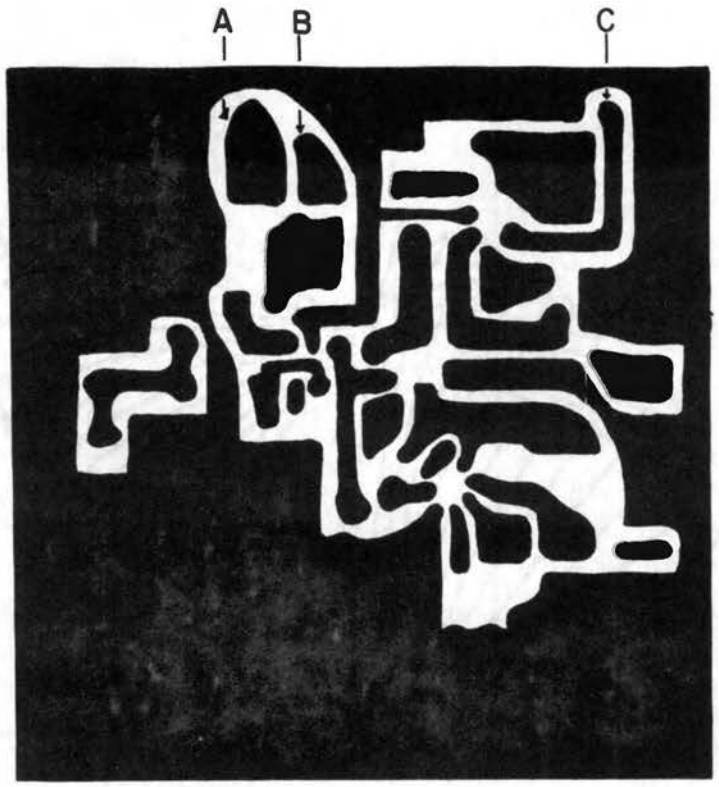

Scale: 1" = 1.65"

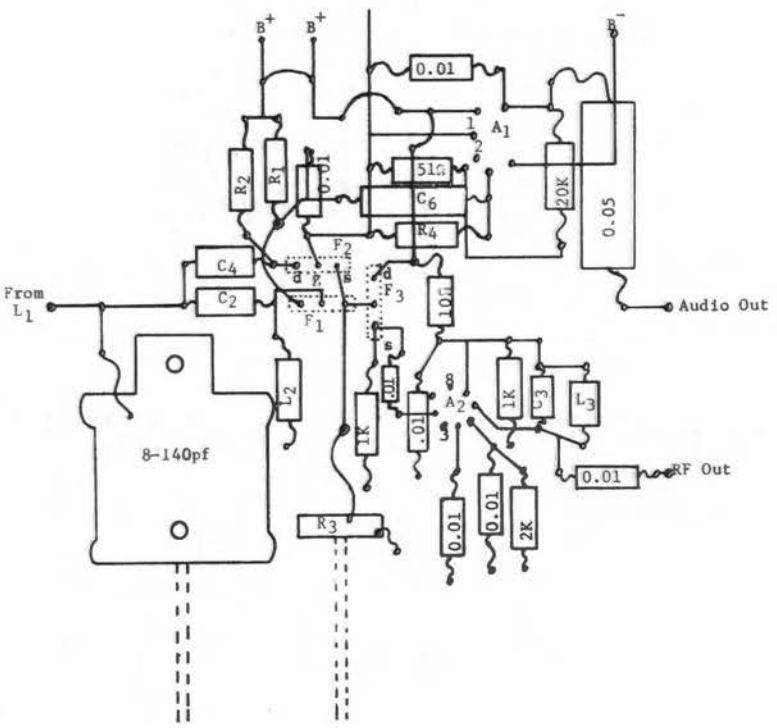

Figure 25. Circuit Board Mask and Component Placement for Marginal Oscillator

made between them and a common B^+ used; however, use of this facility could perhaps improve the stability of the oscillator. Obviously, it is at these islands and at that denoted by C (B^-) that connections may be made to either batteries or a power supply for B^+ and B^- voltages. Figure 25 also provides a description of component placement on the circuit board. The circuit board itself was mounted on the bottom plate of a 6" x 6½" x 3" aluminum box having 3/8" walls. A partial interior view of the completed arrangement is shown in Figure 26. Note that R_3 was not mounted on the circuit board. It was mounted on the front wall of the aluminum box.

The NMR probe is also shown in Figure 26. It essentially consisted of coaxial cable surrounded by a brass tube ¼" O.D., which furnished mechanical support as well as further electrostatic shielding. At the top a rigid BNC connector was provided for connecting the probe to the oscillator via 3"-4" of coaxial cable. At the other end of the probe, the coaxial lead ended in an inductor L_1 which consisted of 18-20 turns of B & S gauge 29 nyclad copper wire wound on and epoxied to a cylindrical 6 mm diameter sealed glass capsule (~14 mm long) containing the NMR standard sample. The inductor L_1 was grounded by soldering it to the teflon-lined brass electrostatic shield which covered the inductor and the NMR sample capsule. This shield (7/16" O.D.) was afixed to the ¼" rod by means of a set screw. It was found that the inductor L_1 had a large effect upon the frequency of oscillation; for example, one additional turn would lower the

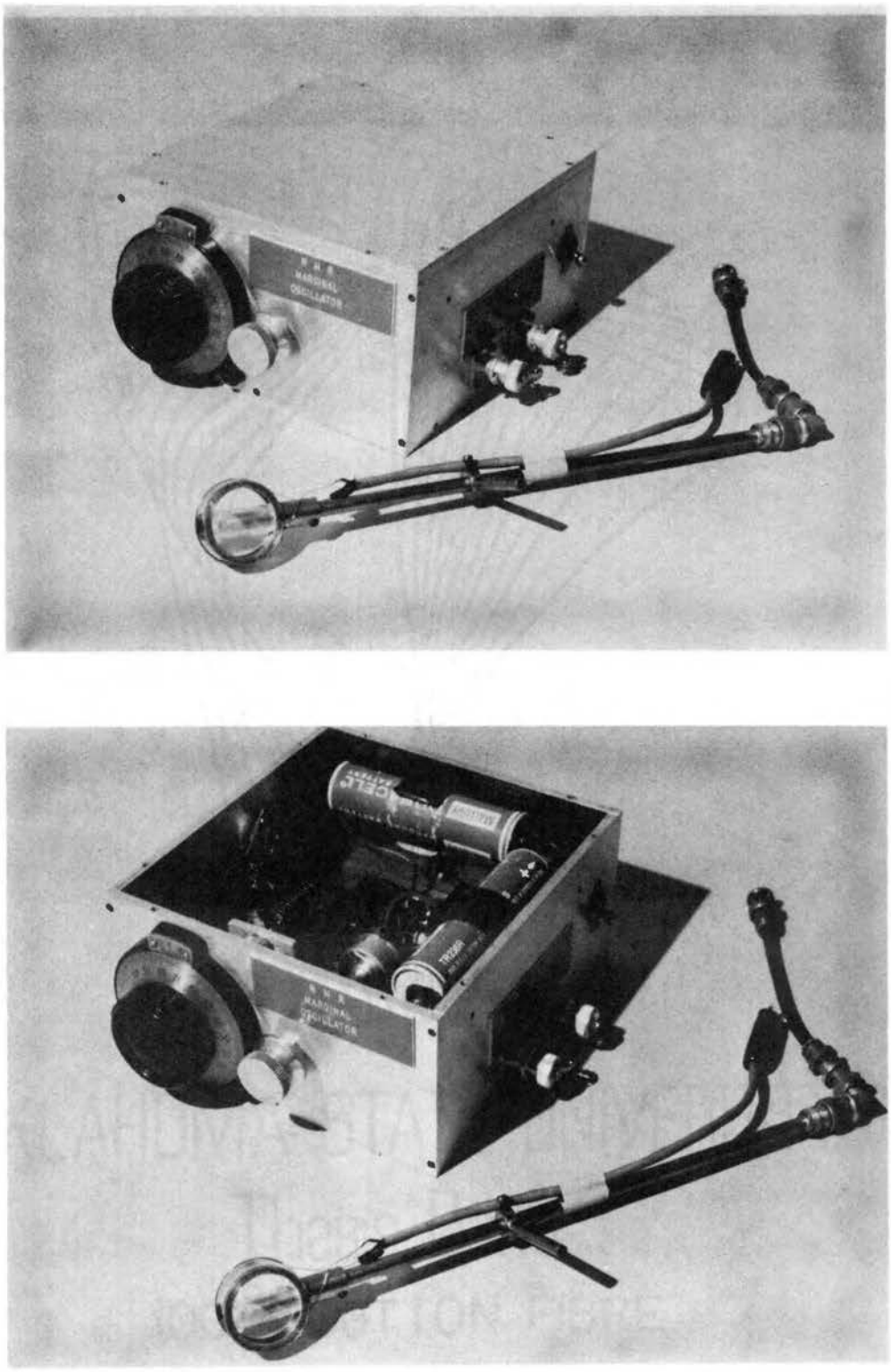

Figure 26. Views of the Marginal Oscillator and NMR Probe

oscillator frequency range by approximately 2 MHz.

The NMR standard sample which was called for, $FeNO_3$, was found not to be a well recognized NMR standard. No conversion factor could be found which would relate NMR frequency to magnetic field strength for the suggested solution. It was also pointed out that the nomenclature should be $Fe(NO_3)_2$. The standard chosen was pure white glycerin, $C_3H_8O_3$, from Fisher Scientific which has a resonant frequency ν MHz in a magnetic field H Gauss (Abragam and Bleany, Electron Paramagnetic Resonance of Transition Ions, Oxford, Clarendon Press, 1970) which are related as:

$$H = 234.87 * \nu \text{ Gauss, MHz}$$

If more information concerning $Fe(NO_3)_2$ becomes available, better signal/noise ratios may be obtained by its use.

The modulation coils were constructed in the Helmholtz configuration. A cylindrical plexiglas form of radius 5/8" and height 9/16" was made into which grooves ½" apart, 1/16" wide, and 1/8" deep were cut. A 7/16" hole was drilled through the side of the cylinder and was press fitted onto the brass shield mentioned above (see Figure 26). Using B & S gauge 30 nyclad copper wire, the coils, consisting of 30 turns each, were wrapped into the grooves. For a 10 Gauss modulation field the required current was approximately ½ ampere. Using a step-down transformer (United Transformer Company, UTC-S-55, 6.3 volts) and power resistors in series with the Helmholtz coils, this current was obtained from an AC 120 volts,

60 Hz line source.

The performance of the oscillator was excellent with regard to stability against drift. Typically, the frequency would drift from 30-70 Hz/min. (0.007-0.016 Gauss/min.), the better stability being observed at the lower frequencies. The range was observed to be from approximately 10.268 MHz to 18.260 MHz (2412-4288 Gauss) with new batteries. When switch S_2 was closed, the range was reduced to 8.626 MHz to 11.377 MHz (2025-2670 Gauss). The signal to noise ratio was only fair, being on the order of 5 to 1 over the range of the oscillator. It should be pointed out that stability and range were somewhat dependent upon the value of the variable resistor R_3. Hence, all the above values are approximate.

Parts List

1. Six (6) 0.01 μf ceramic disc capacitors (75v) CRL (C_5)
2. One (1) 0.05 μf ceramic disc capacitor (75v) CRL
3. One (1) 0.15 mfd 50 vdc WMF 05P15 tubular capacitor (C_6)
4. One (1) 0.05 mfd 600 vdc 6TM-550 Sprague tubular capacitor
5. One (1) 8→140 pf variable air gap capacitor, Hammarlund HFA-140-A, single bearing (C_1)
6. Silver mica capacitors:
   (a) Two (2) 30 pf (C_2 and C_3)
   (b) One (1) 47 pf (C_4)
   (c) One (1) 100 pf (C_{14})

7. One (1) 15 μh 75 ma RF choke (L_2)
8. Three (3) GE-FET-1 N channel silicon field effect transistors 10 mamp gate current, 200 mw, 25 volts, 2000 min μmho. (F_1, F_2, and F_3)
9. Resistors, carbon, 0.5 watt, 5%: 2.2 KΩ (R_1); 6.8 KΩ (R_2); 3 KΩ (R_4); 51 Ω, 20 KΩ, 1 KΩ, 10 Ω, 2 KΩ
10. One (1) wire wound variable 1 KΩ resistor (R_3). (This resistor should be a carbon type variable resistor.)
11. One (1) RCA CA 3015 (A_1)
12. One (1) RCA CA 3028A (A_2)
13. Two (2) Mallory mercury batteries TR236R 2200 mah (B^+ and B^-)
14. One (1) double pole single throw (dpst) toggle switch (S_1)
15. One (1) rotary switch (S_2)
16. One (1) flexible shaft connector
17. One (1) 2 7/8" vernier dial variable capacitor drive (Argonne)
18. Three (3) BNC male connectors RG - 290/U
19. Two (2) battery holders
20. One (1) 3/8" wall box: Inside dimensions: 6 5/16" x 6" x 3"
21. Kepro copper clad laminate circuit board: 6" x 6" x 0.062", G-10 2 oz., 1 side, unsensitized catalogue number P12-665G
22. Archer etch resist lacquer and Archer etchant (Radio Shack)

APPENDIX D

MICROWAVE SYSTEM

MICROWAVE SYSTEM

A. Ten and one-half inch section flexible waveguide

B. Differential Phase Shift Circulator (Microwave Associates 126)

C. Precision Low Power Terminator (Microwave Associates 684)

D. Variable Attenuator (Hewlett-Packard X382A)

E. H-Plane Folded Hybrid Tee (Microwave Associates 5110)

F. Variable Attenuator (Narda 730)

G. Waveguide Twist (90^{o}) (Waveline 690)

H. Phase Shifter (Waveline 608C)

I. Ferrite Isolator (Micro Radionics, Inc., Van Nuys, CA, PN C994-100-102)

J. Magic Tee (Waveline 657)

K. Adjustable Isolator (Caswell Electronics X-100-A)

L. Cross Guide Directional Coupler (Microwave Associates 886)

M. Tunable Crystal Mount (Microwave Associates 536C)

N. Frequency Meter - reference cavity (Narda 810)

O. Microwave Crystal Detector (Microwave Associates 40075)

APPENDIX E

PROGRAM TO CALCULATE FIELD POSITIONS FOR $[F_2^-]_A$ RESONANCES

```
C
C     * * * * * * * * * * VKA RESONANT FIELD POSITIONS * * * * * * * * * *
C
C
C      THIS PROGRAM CALCULATES THE FIELD POSITIONS OF EPR RESONANCES OF THE
C     VKA-CENTER IN KMGF3 FOR FIELD ORIENTATIONS ALONG (100) AND (110)
C     DIRECTIONS. FOR THESE TWO DIRECTIONS OF THE MAGNETIC FIELD THERE ARE
C     A TOTAL OF SIX DISTINGUISHABLE SPECTRA CORRESPONDING TO THE VARIOUS
C     ORIENTATIONS OF THE VKA CENTERS FOR THESE FIELD DIRECTIONS. WITH
C     MINOR MODIFICATIONS (IE, CHANGING THE ANGLES THETA AND PHI) THIS
C     PROGRAM WILL PREDICT FIELD POSITIONS FOR ARBITRARY MAGNETIC FIELD
C     DIRECTIONS. AS INDICATED THE DIRECTION OF THE MAGNETIC FIELD IS SPECIFIED
C     BY THE EULER ANGLES (GOLDSTEIN CONVENTION) RELATIVE TO THE Z-AXIS,
C     WHICH LIES ALONG THE VKA MOLECULAR AXIS. SEE CHAPTER FOUR FOR MORE
C     DETAILS ON THESE AXES.
C
C      AS INPUT THE FOLLOWING INFORMATION IS NEEDED:
C         1)THE HYPERFINE PARAMETERS AX,AY,AZ, EXPRESSED IN MHZ
C         2)THE G-VALUES GX,GY,GZ.
C         3)THE ANGLES ALPHA AND ELTA, EXPRESSED IN DEGREES.
C         4)A MICROWAVE FREQUENCY (FREQ), EXPRESSED IN MHZ.
C
C
      IMPLICIT REAL*8 (A-H,O-Z)
      REAL*8 NUMHZ,NU
      REAL * 8 MATRXR,MATRXI
      COMMON/MATRIX/MATRXR(8,8),MATRXI(8,8),D(8),E(8),E2(8),TAU(2,8),N,I
     1ERR
C
      B= 9.2740960-21
      BN=5.0509510-24
      GN = 5.2547415
      PSC = 6.6261965D-27                                          ERG*SEC
      PC  = 6.6261965D-21                                          H*10**6
      X= 1.00-6
      N = 8
      THETA = 0.0D0
      PHI   = 0.0D0
C
      J2 = 1
C
C        THE INDEX J2 IS USED TO CHANGE THE DIRECTION OF THE MAGNETIC FIELD
C        SEE STATEMENT 700 AND SUBSEQUENT
C
      H = 2400
C
C
C         THE VALUE OF THE PARAMETERS ARE ASSUMED TO BE:
C
C
      GX    = 2.024
      GY    = 2.018
      GZ    = 2.0024
      AX    = 128.0
      AY    = 128.0
      AZ    = 2495.0
      ALPHA = 8.00
      ELTA  = 6.80
C
C        THE MICROWAVE FREQUENCY IS GIVEN THE FOLLOWING VALUE IN MHZ:
C
      FREQ = 9210.20
C
      AX  = AX * PC                                                MHZ   --
      AY  = AY * PC                                                  TO
      AZ  = AZ * PC                                                -- ERGS
      ALPHA = ALPHA * 0.017453292519943                            DEGREES
      ELTA  = ELTA  * 0.017453292519943                            TO RADNS
C
   10 B11 = DCOS(PHI - ELTA)
      B12 = DSIN(PHI - ELTA)
      B13 = 0.0D0
      B21 =-DCOS(THETA) * DSIN(PHI - ELTA)
      B22 = DCOS(THETA) * DCOS(PHI - ELTA)
      B23 = DSIN(THETA)
      B31 = DSIN(THETA) * DSIN(PHI - ELTA)
      B32 =-DSIN(THETA) * DCOS(PHI - ELTA)
      B33 = DCOS(THETA)
      I  = 0
      BETA31 = GX*B11*B31 + GY*B12*B32
      BETA32=GX*B31*B21 +GY*B32*B22 +GZ*B23*B33
      BETA33=GX*B31**2 +GY*B32**2 +GZ*B33**2
      W11=AX*DCOS(ALPHA)**2 + AZ*DSIN(ALPHA)**2
      W13=(AX-AZ)*DSIN(ALPHA)*DCOS(ALPHA)
      W33=AX*DSIN(ALPHA)**2 + AZ*DCOS(ALPHA)**2
      W22=AY
      Z11P=B11**2*W11 +B12**2*W22 +B13**2*W33 +2.*B11*B13*W13
      Z11M=B11**2*W11 +B12**2*W22 +B13**2*W33 -2.*B11*B13*W13
      Z12P=B11*B21*W11+B12*B22*W22+B13*B23*W33+W13*(B13*B21+B11*B23)
      Z12M=B11*B21*W11+B12*B22*W22+B13*B23*W33-W13*(B13*B21+B11*B23)
      Z22P=B21**2*W11+B22**2*W22+B23**2*W33 +2.*B21*B23*W13
      Z22M=B21**2*W11+B22**2*W22+B23**2*W33 -2.*B21*B23*W13
      Z13P=B11*B31*W11+B12*B32*W22+B13*B33*W33 +W13*(B13*B31+B11*B33)
      Z13M=B11*B31*W11+B12*B32*W22+B13*B33*W33 -W13*(B13*B31+B11*B33)
      Z23P=B21*B31*W11+B22*B32*W22+B23*B33*W33 +W13*(B31*B23+B21*B33)
      Z23M=B21*B31*W11+B22*B32*W22+B23*B33*W33 -W13*(B31*B23+B21*B33)
      Z33P=B31**2*W11 +B32**2*W22 +B33**2*W33 +2.*W13*B31*B33
      Z33M=B31**2*W11 +B32**2*W22 +B33**2*W33 -2.*W13*B31*B33
C
C
C      THE MATRIX ELEMENTS ARE DEFINED BELOW IN TERMS OF THE QUANTITIES
C     DEFINED ABOVE.
C
C
   50 DO 349 L = 1,15
   51 DO 52 M=1,8,1
      DO 52 J=1,8,1
      MATRXR(M,J) = 0.0D0
```

```
      52 MATRXI(M,J) = 0.0D0
         MATRXR(1,1)=0.5*B*H*BETA33 -GN*BN*H +0.25*(Z33P+Z33M)
         MATRXR(2,1)=0.25*Z13M
         MATRXI(2,1)=0.25*Z23M
         MATRXR(2,2)=0.5*B*H*BETA33 + 0.25*(Z33P-Z33M)
         MATRXR(3,1)=0.25*Z13P
         MATRXI(3,1)=0.25*Z23P
         MATRXR(3,3)=0.5*B*H*BETA33 -0.25*(Z33P-Z33M)
         MATRXR(4,2)=0.25*Z13P
         MATRXI(4,2)=0.25*Z23P
         MATRXR(4,3)=0.25*Z13M
         MATRXI(4,3)=0.25*Z23M
         MATRXR(4,4)=0.5*B*H*BETA33 +GN*BN*H -0.25*(Z33P+Z33M)
         MATRXR(5,1)=0.5*B*H*BETA31 +0.25*(Z13P +Z13M)
         MATRXI(5,1)=0.5*B*H*BETA32 +0.25*(Z23P +Z23M)
         MATRXR(5,2)=0.25*(Z11M + Z22M)
         MATRXR(5,3)=0.25*(Z11P + Z22P)
         MATRXR(5,5)=-0.5*B*H*BETA33 -GN*BN*H -0.25*(Z33P+Z33M)
         MATRXR(6,1)=0.25*(Z11P-Z22P)
         MATRXI(6,1)=0.5*Z12P
         MATRXR(6,3)=0.5*B*H*BETA31 -0.25*(Z13P - Z13M)
         MATRXI(6,3)=0.5*B*H*BETA32 -0.25*(Z23P - Z23M)
         MATRXR(6,4)=0.25*(Z11M + Z22M)
         MATRXR(6,5)=-0.25*Z13P
         MATRXI(6,5)=-0.25*Z23P
         MATRXR(6,6)=-0.5 *B*H*BETA33 +0.25*(Z33P - Z33M)
         MATRXR(7,1)=0.25*(Z11M - Z22M)
         MATRXI(7,1)=0.5*Z12M
         MATRXR(7,2)=0.5*B*H*BETA31 + 0.25*(Z13P - Z13M)
         MATRXI(7,2)=0.5*B*H*BETA32 + 0.25*(Z23P - Z23M)
         MATRXR(7,4)=0.25*(Z11P+Z22P)
         MATRXR(7,5)=-0.25*Z13M
         MATRXI(7,5)=-0.25*Z23M
         MATRXR(7,7)=-0.5*B*H*BETA33 -0.25*(Z33P - Z33M)
         MATRXR(8,2)=0.25*(Z11P - Z22P)
         MATRXI(8,2)=0.5*Z12P
         MATRXR(8,3)=0.25*(Z11M - Z22M)
         MATRXI(8,3)=0.5*Z12M
         MATRXR(8,4)=0.5*B*H*BETA31 -0.25*(Z13P + Z13M)
         MATRXI(8,4)=0.5*B*H*BETA32 -0.25*(Z23P + Z23M)
         MATRXR(8,6)=-0.25*Z13M
         MATRXI(8,6)=-0.25*Z23M
         MATRXR(8,7)=-0.25*Z13P
         MATRXI(8,7)=-0.25*Z23P
         MATRXR(8,8)=-0.5*B*H*BETA33 +GN*BN*H  +0.25*(Z33P + Z33M)
C
      60 CALL HTRIDI
C
         CALL IMTQL1
C
         IF(IERR)309,309,70
      70 WRITE(6,71) IERR
      71 FORMAT(' IERR IS ZERO FOR A NORMAL RETURN FROM SUBROUTINE IMTQL1 A
        1ND IS SET TO AN INTEGER J OTHERWISE. THE VALUE OF IERR=',I2)
         GO TO 1000
     309 WRITE(6,310) H
     310 FORMAT(' *****  THE CALCULATED FIELD IN GAUSS FOR THIS ITERATION I
        1S:',D15.6)
C
C
C     THE FOLLOWING STEPS CALCULATE THE APPROPRIATE MICROWAVE FREQUENCY,
C     CONVERT IT TO MHZ, AND COMPARE IT TO THE EXPERIMENTAL MICROWAVE
C     FREQUENCY.
C
C
         NU=(D(8-I) -D(I+1))/PSC
         NUMHZ=  NU * X
         FRQUIF  = DABS(NUMHZ - FREQ)
         IF(FRQUIF.LE.0.5) GO TO 350
C
     349 H = H*FREQ/NUMHZ
     348 FORMAT(' AFTER FIFTEEN ITERATIONS OF THE FIELD WE STILL DO NOT HAV
        1E A SOLUTION WITHIN OUR ERROR LIMITS')
     347 WRITE(6,348)
         GO TO 1000
     350 WRITE(6,351)
     351 FORMAT(' **********  THE CALCULATED MAGNETIC FIELD AT WHICH THIS P
        1ARTICULAR LINE FALLS IS GIVEN DIRECTLY ABOVE  **********')
         I = I+1
         IF(I-4) 361,700,700
     361 WRITE(6,360)
     360 FORMAT(//' HAVING CALCULATED ONE FIELD POSITION WE NOW WISH TO CAL
        1CULATE ANOTHER.TO DO SO REQUIRES THAT THE INDEX I BE'/ ' ADVANCED
        2BY ONE SO THAT THE APPROPRIATE NU IS COMPUTED.THIS HAS BEEN DONE')
     400 NU = (D(8-I)-D(I+1))/PSC
         NUMHZ = NU*X
         H = H * FREQ/NUMHZ
         GO TO 50
C
C
     700 IF(5 - J2) 711,709,750
     750 IF(4 - J2)1000,707,751
     751 IF(3 - J2)1000,705,752
     752 IF(2 - J2)1000,703,753
     753 IF(1 - J2)1000,701,1000
C
     701 WRITE(6,702)
     702 FORMAT(/' *****  THE FOUR CALCULATED FIELD POSITIONS ABOVE ARE FOR
        1 THE ZERO DEGREE LINES IN THE (110) SPECTRUM  *****')
         J2 = J2 + 1
         THETA =-1.57079632
         PHI   = 1.57079632
         H = H * FREQ/((( D(8) - D(1))/PSC) * X)
         GO TO 10
C
     703 WRITE(6,704)
     704 FORMAT(/' *****  THE FOUR CALCULATED FIELD POSITIONS ABOVE ARE FOR
        1 THE NINETY DEGREE LINES IN THE (110) SPECTRUM  *****')
```

```
      J2 = J2 + 1
      THETA = 1.04719255                                              60 DGRS
      PHI   =-0.61577640                                              35.3 DGS
      H = H * FREQ/((( D(8) - D(1))/PSC) * X)
      GO TO 10
C
  705 WRITE(6,706)
  706 FORMAT(/' *****  THE FOUR CALCULATED FIELD POSITIONS ABOVE ARE FOR
     1 ONE SET OF SIXTY DEGREE LINES IN THE (110) SPECTRUM  *****')
      J2 = J2 + 1
      ELTA =-ELTA
      H = H * FREQ/((( D(8) - D(1))/PSC) * X)
      GO TO 10
C
  707 WRITE(6,708)
  708 FORMAT(/' *****  THE FOUR CALCULATED FIELD POSITIONS ABOVE ARE FOR
     1 THE SECOND SET OF SIXTY DEGREE LINES IN THE (110) SPECTRUM  *****
     2')
      J2 = J2 + 1
      THETA = 0.78539816
      PHI   = 1.57079632
      H = H * FREQ/((( D(8) - D(1))/PSC) * X)
      GO TO 10
C
  709 WRITE(6,710)
  710 FORMAT(/' *****  THE FOUR CALCULATED FIELD POSITIONS ABOVE ARE FOR
     1 THE FORTY-FIVE DEGREE LINES IN THE (100) SPECTRUM  *****')
      J2 = J2 + 1
      THETA = 1.57079632
      PHI   = 0.0D0
      H = H * FREQ/((( D(8) - D(1))/PSC) * X)
      GO TO 10
C
  711 WRITE(6,712)
  712 FORMAT(/' *****  THE FOUR CALCULATED FIELD POSITIONS ABOVE ARE FOR
     1 THE NINETY DEGREE LINES IN THE (100) SPECTRUM  *****')
 1000 STOP
      END
C
C     * * * * * * * * * * * *  HTRIDI  * * * * * * * * * * * * * * * * * *
C
      SUBROUTINE HTRIDI
C
C
C     THIS SUBROUTINE IS A TRANSLATION OF A COMPLEX ANALOGUE OF
C     THE ALGOL PROCEDURE TRED1, NUM. MATH. 11, 181-195(1968)
C     BY MARTIN, REINSCH, AND WILKINSON.
C     HANDBOOK FOR AUTO. COMP., VOL.II-LINEAR ALGEBRA, 212-226(1971).
C
C     THIS SUBROUTINE REDUCES A COMPLEX HERMITIAN MATRIX
C     TO A REAL SYMMETRIC TRIDIAGONAL MATRIX USING
C     UNITARY SIMILARITY TRANSFORMATIONS.
C
C     ON INPUT:
C
C        N IS THE ORDER OF THE MATRIX;
C
C        AR AND AI CONTAIN THE REAL AND IMAGINARY PARTS,
C          RESPECTIVELY, OF THE COMPLEX HERMITIAN INPUT MATRIX.
C          ONLY THE LOWER TRIANGLE OF THE MATRIX NEED BE SUPPLIED.
C
C     ON OUTPUT:
C
C        AR AND AI CONTAIN INFORMATION ABOUT THE UNITARY TRANS-
C          FORMATIONS USED IN THE REDUCTION IN THEIR FULL LOWER
C          TRIANGLES.  THEIR STRICT UPPER TRIANGLES AND THE
C          DIAGONAL OF AR ARE UNALTERED;
C
C        D CONTAINS THE DIAGONAL ELEMENTS OF THE THE TRIDIAGONAL MATRIX;
C
C        E CONTAINS THE SUBDIAGONAL ELEMENTS OF THE TRIDIAGONAL
C          MATRIX IN ITS LAST N-1 POSITIONS.  E(1) IS SET TO ZERO;
C
C        E2 CONTAINS THE SQUARES OF THE CORRESPONDING ELEMENTS OF E.
C          E2 MAY COINCIDE WITH E IF THE SQUARES ARE NOT NEEDED;
C
C        TAU CONTAINS FURTHER INFORMATION ABOUT THE TRANSFORMATIONS.
C
C     ARITHMETIC IS REAL EXCEPT FOR THE USE OF THE SUBROUTINES
C     CDABS AND DCMPLX IN COMPUTING COMPLEX ABSOLUTE VALUES.
C
C     QUESTIONS AND COMMENTS SHOULD BE DIRECTED TO B. S. GARBOW,
C     APPLIED MATHEMATICS DIVISION, ARGONNE NATIONAL LABORATORY
C
C     ------------------------------------------------------------------
      IMPLICIT REAL * 8 (A-H,O-Z)
      COMMON/MATRIX/AR(8,8),AI(8,8),D(8),E(8),E2(8),TAU(2,8),N,IERR
      COMPLEX*16 DCMPLX
C
      TAU(1,N) = 1.0D0
      TAU(2,N) = 0.0D0
C
      DO 100 I = 1, N
  100 D(I) = AR(I,I)
C
C     ********** FOR I=N STEP -1 UNTIL 1 DO -- **********
      DO  300 II = 1, N
         I = N + 1 - II
         L = I - 1
         H = 0.0D0
         SCALE = 0.0D0
         IF (L .LT. 1) GO TO 130
C     ********** SCALE ROW (ALGOL TOL THEN NOT NEEDED) **********
         DO 120 K = 1, L
  120    SCALE = SCALE + DABS(AR(I,K)) + DABS(AI(I,K))
C
         IF (SCALE .NE. 0.0D0) GO TO 140
         TAU(1,L) = 1.0D0
```

```
      TAU(2,L) = C.ODO
  130 E(I) = 0.000
      E2(I) = 0.0D0
      GO TO 290
C
  140 DO 150 K = 1, L
         AR(I,K) = AR(I,K) / SCALE
         AI(I,K) = AI(I,K) / SCALE
         H = H + AR(I,K) * AR(I,K) + AI(I,K) * AI(I,K)
  150 CONTINUE
C
      E2(I) = SCALE * SCALE * H
      G = DSQRT(H)
      E(I) = SCALE * G
      F = CDABS(DCMPLX(AR(I,L),AI(I,L)))
C     :::::::::: FORM NEXT DIAGONAL ELEMENT OF MATRIX T ::::::::::
      IF (F .EQ. C.0DO) GO TO 160
      TAU(1,L) = (AI(I,L) * TAU(2,I) - AR(I,L) * TAU(1,I)) / F
      SI = (AR(I,L) * TAU(2,I) + AI(I,L) * TAU(1,I)) / F
      H = H + F * G
      G = 1.0D0 + G / F
      AR(I,L) = G * AR(I,L)
      AI(I,L) = G * AI(I,L)
      IF (L .EQ. 1) GO TO 270
      GO TO 170
  160 TAU(1,L) = -TAU(1,I)
      SI = TAU(2,I)
      AR(I,L) = G
  170 F = 0.0D0
C
      DO 240 J = 1, L
         G = 0.0D0
         GI = 0.0D0
C     :::::::::: FORM ELEMENT OF A*U ::::::::::
         DO 180 K = 1, J
            G = G + AR(J,K) * AR(I,K) + AI(J,K) * AI(I,K)
            GI = GI - AR(J,K) * AI(I,K) + AI(J,K) * AR(I,K)
  180    CONTINUE
C
         JP1 = J + 1
         IF (L .LT. JP1) GO TO 220
C
         DO 200 K = JP1, L
            G = G + AR(K,J) * AR(I,K) - AI(K,J) * AI(I,K)
            GI = GI - AR(K,J) * AI(I,K) - AI(K,J) * AR(I,K)
  200    CONTINUE
C     :::::::::: FORM ELEMENT OF P ::::::::::
  220    E(J) = G / H
         TAU(2,J) = GI / H
         F = F + E(J) * AR(I,J) - TAU(2,J) * AI(I,J)
  240 CONTINUE
C
      HH = F / (H + H)
C     :::::::::: FORM REDUCED A ::::::::::
      DO 260 J = 1, L
         F = AR(I,J)
         G = E(J) - HH * F
         E(J) = G
         FI = -AI(I,J)
         GI = TAU(2,J) - HH * FI
         TAU(2,J) = -GI
C
         DO 260 K = 1, J
            AR(J,K) = AR(J,K) - F * E(K) - G * AR(I,K)
     X                        + FI * TAU(2,K) + GI * AI(I,K)
            AI(J,K) = AI(J,K) - F * TAU(2,K) - G * AI(I,K)
     X                        - FI * E(K) - GI * AR(I,K)
  260 CONTINUE
C
  270 DO 280 K = 1, L
         AR(I,K) = SCALE * AR(I,K)
         AI(I,K) = SCALE * AI(I,K)
  280 CONTINUE
C
      TAU(2,L) = -SI
  290 HH = D(I)
      D(I) = AR(I,I)
      AR(I,I) = HH
      AI(I,I) = SCALE * SCALE * H
  300 CONTINUE
C
      RETURN
C     :::::::::: LAST CARD OF HTRIDI ::::::::::
      END
C
C     * * * * * * * * * * * * IMTQL1 * * * * * * * * * * * * * * * * * *
C
      SUBROUTINE IMTQL1
C
C
C     THIS SUBROUTINE IS A TRANSLATION OF THE ALGOL PROCEDURE IMTQL1,
C     NUM. MATH. 12, 377-383(1968) BY MARTIN AND WILKINSON,
C     AS MODIFIED IN NUM. MATH. 15, 450(1970) BY DUBRULLE.
C     HANDBOOK FOR AUTO. COMP., VOL.II-LINEAR ALGEBRA, 241-248(1971).
C
C     THIS SUBROUTINE FINDS THE EIGENVALUES OF A SYMMETRIC
C     TRIDIAGONAL MATRIX BY THE IMPLICIT QL METHOD.
C
C     ON INPUT:
C
C        N IS THE ORDER OF THE MATRIX;
C
C        D CONTAINS THE DIAGONAL ELEMENTS OF THE INPUT MATRIX;
C
C        E CONTAINS THE SUBDIAGONAL ELEMENTS OF THE INPUT MATRIX
C          IN ITS LAST N-1 POSITIONS.  E(1) IS ARBITRARY.
C
C     ON OUTPUT:
```

```
C
C        D CONTAINS THE EIGENVALUES IN ASCENDING ORDER.  IF AN
C          ERROR EXIT IS MADE, THE EIGENVALUES ARE CORRECT AND
C          ORDERED FOR INDICES 1,2,...IERR-1, BUT MAY NOT BE
C          THE SMALLEST EIGENVALUES;
C
C        E HAS BEEN DESTROYED;
C
C        IERR IS SET TO
C          ZERO       FOR NORMAL RETURN,
C          J          IF THE J-TH EIGENVALUE HAS NOT BEEN
C                     DETERMINED AFTER 30 ITERATIONS.
C
C     QUESTIONS AND COMMENTS SHOULD BE DIRECTED TO B. S. GARBOW,
C     APPLIED MATHEMATICS DIVISION, ARGONNE NATIONAL LABORATORY
C
C     ------------------------------------------------------------------
      IMPLICIT REAL * 8 (A-H,O-Z)
      REAL * 8 MACHEP
      COMMON/MATRIX/AR(8,8),AI(8,8),D(8),E(8),E2(8),TAU(2,8),N,IERR
C
C     ********** MACHEP IS A MACHINE DEPENDENT PARAMETER SPECIFYING
C                THE RELATIVE PRECISION OF FLOATING POINT ARITHMETIC.
C                MACHEP = 16.0D0**(-13) FOR LONG FORM ARITHMETIC
C                ON S360 **********
      DATA MACHEP/Z341C000000000000/
C
      IERR = 0
      IF (N .EQ. 1) GO TO 1001
C
      DO 100 I = 2, N
  100 E(I-1) = E(I)
C
      E(N) = 0.0D0
C
      DO 290 L = 1, N
         J = 0
C     ********** LOOK FOR SMALL SUB-DIAGONAL ELEMENT **********
  105    DO 110 M = L, N
            IF (M .EQ. N) GO TO 120
            IF (DABS(E(M)) .LE. MACHEP * (DABS(D(M)) + DABS(D(M+1))))
     X         GO TO 120
  110    CONTINUE
C
  120    P = D(L)
         IF (M .EQ. L) GO TO 215
         IF (J .EQ. 30) GO TO 1000
         J = J + 1
C     ********** FORM SHIFT **********
         G = (D(L+1) - P) / (2.0D0 * E(L))
         R = DSQRT(G*G+1.0D0)
         G = D(M) - P + E(L) / (G + DSIGN(R,G))
         S = 1.0D0
         C = 1.0D0
         P = 0.0D0
         MML = M - L
C     ********** FOR I=M-1 STEP -1 UNTIL L DO -- **********
         DO 200 II = 1, MML
            I = M - II
            F = S * E(I)
            B = C * E(I)
            IF (DABS(F) .LT. DABS(G)) GO TO 150
            C = G / F
            R = DSQRT(C*C+1.0D0)
            E(I+1) = F * R
            S = 1.0D0 / R
            C = C * S
            GO TO 160
  150       S = F / G
            R = DSQRT(S*S+1.0D0)
            E(I+1) = G * R
            C = 1.0D0 / R
            S = S * C
  160       G = D(I+1) - P
            R = (D(I) - G) * S + 2.0D0 * C * B
            P = S * R
            D(I+1) = G + P
            G = C * R - B
  200    CONTINUE
C
         D(L) = D(L) - P
         E(L) = G
         E(M) = 0.0D0
         GO TO 105
C     ********** ORDER EIGENVALUES **********
  215    IF (L .EQ. 1) GO TO 250
C     ********** FOR I=L STEP -1 UNTIL 2 DO -- **********
         DO 230 II = 2, L
            I = L + 2 - II
            IF (P .GE. D(I-1)) GO TO 270
            D(I) = D(I-1)
  230    CONTINUE
C
  250    I = 1
  270    D(I) = P
  290 CONTINUE
C
      GO TO 1001
C     ********** SET ERROR -- NO CONVERGENCE TO AN
C                EIGENVALUE AFTER 30 ITERATIONS **********
 1000 IERR = L
 1001 RETURN
C     ********** LAST CARD OF IMTQL1 **********
      END
```

APPENDIX F

PROGRAM TO CALCULATE PARAMETERS FOR $[F_2^-]_A$

```
C
C
C       ******* VKA-CENTER PARAMETER FITTING PROGRAM *******
C
C
C     THIS PROGRAM IS DESIGNED TO CALCULATE THE EIGHT PARAMETERS OF
C     INTEREST IN THE VKA-CENTER MODEL IN KMGF3. AS INPUT ONE NEED
C     FURNISH THE FOLLOWING:
C
C       1)THE FIELD POSITIONS OF THE VARIOUS EPR RESONANCES, ENTERED
C         IN THE FOLLOWING MANNER. FIELD POSITIONS WILL BE DIMENSIONALIZED
C         IN A ONE DIMENSIONAL ARRAY HFP(L). FOR FORTY-FIVE DEGREE LINES
C         IN THE (100) SPECTRUM L=1,4, HFP(1) BEING THE LOWEST FIELD
C         RESONANCE WHILE HFP(4) IS THE HIGHEST; THE NINETY DEGREE LINES
C         HAVE L=5,8. IN THE (110) SPECTRUM, THE ZERO DEGREE LINES ARE
C         LABELED BY L=9,12 AND THE NINETY DEGREE LINES HAVE L=13,16.
C         BECAUSE OF THE PERTURBATION THERE ARE TWO DISTINCT SETS OF
C         SIXTY DEGREE LINES. THE FIRST, SECOND, FIFTH, AND SIXTH
C         RESONANCES COMPRISE ONE SET WITH L=17,20. THE OTHER SET CONSISTS
C         OF THE FIRST, THIRD, FOURTH, AND SIXTH RESONANCES LABELED
C         BY L=21,24. IF A LINE COULD NOT BE MEASURED, A ZERO IS TO
C         BE ENTERED FOR THAT HFP(L). ENTER ALL HFP IN GAUSS.
C       2)INTERNALLY A SET OF ANGLES IS SPECIFIED FOR EACH OF THE MOLECULAR
C         ORIENTATIONS (A TOTAL OF SIX SETS) RELATIVE TO THE EXTERNAL
C         MAGNETIC FIELD ( THE EULER ANGLES)
C       3)THE EXPERIMENTAL MICROWAVE FREQUENCY MUST BE ENTERED IN MHZ.
C       4)AN INITIAL SET OF PARAMETERS MUST BE FURNISHED: AX,AY,AZ,GX,GY,
C         GZ,ALPHA,AND ELTA. BOTH ANGLES ARE ENTERED AS DEGREES,ALL HYPERFINE
C         PARAMETERS ARE EXPRESSED AS MHZ.
C       5)THE INDICATED PROGRAM TIME LIMIT MINUS XX SECONDS (USED FOR
C         COMPILATION,ETC) NEEDS BE SUPPLIED IN MILLISECONDS FOR USE IN
C         CONJUNCTION WITH THE ELAPSE SUBROUTINE. THIS NUMBER IS TO BE
C         SUPPLIED IN THE IF STATEMENTS(#'S 333 AND 92) OF THE FUNCTN SUBROUTINE
C         AS A CONSTANT AT THE RIGHT PARENTHESES. THIS PREVENTS EXCESSIVE
C         OUTPUT YET PROVIDES AN INDICATION AS TO WHAT POINT IN A DETERMINATION
C         OF THE PARAMETERS THE PROGRAM HAS REACHED IF IT FAILS TO
C         CULMINATE IN THE ALLOTTED TIME LIMIT.
C
C     AS OUTPUT ONE SHOULD HAVE THE PARAMETERS OF INTEREST, ANGLES IN DEGREES,
C     HYPERFINE PARAMETERS IN MHZ.
C
C
      IMPLICIT REAL*8 (A-H,O-Z)
      COMMON/PSYFH/PSYFHI(2,8),SS,NTIME
      COMMON/HUNTR/RHO(8),STEP(8),STOP(8),NP,IPASS
C
C
      READ(5,200) RHO,STEP,STOP
  200 FORMAT(8D10.7))
C
C     'THE PARAMETERS ARE INITIALIZED AS FOLLOWS:
C
      GX    = 2.025
      GY    = 2.020
      GZ    = 2.00295
      AX    = 85
      AY    = 96
      AZ    = 2495.0
      ALPHA = 8.18
      ELTA  = 6.17
C
      PSYFHI(1,1) = ALPHA/57.29578
      PSYFHI(1,2) =  ELTA/57.29578
      PSYFHI(1,3) = GX
      PSYFHI(1,4) = GY
      PSYFHI(1,5) = GZ
      PSYFHI(1,6) = AX*6.626196D-21
      PSYFHI(1,7) = AY*6.626196D-21
      PSYFHI(1,8) = AZ*6.626196D-21
      NTIME  = 0
      NP = 8
      CALL HUNTER
      WRITE(6,202) NTIME,IPASS
  202 FORMAT(///' THE NUMBER OF TIMES THAT FUNCTN WAS CALCULATED, WHICH'/
     1' INVOLVES SOLVING THE 8 X 8 MATRIX ONCE PER NONZERO HFP(L), IS'/'
     2 GIVEN BY NTIME:',I5,' . THE VALUE OF IPASS IS:',I3,' .'/)
C
      DO 210 J = 1,8
  210 STOP(J) = STEP(J) * DABS(PSYFHI(1,J))
      DO 211 J = 1,2
      PSYFHI(1,J) = PSYFHI(1,J) * 57.29578                                  RADS2DGR
  211 STOP(J) = STOP(J) * 57.29578                                          RADS2DGR
C
C     THE FOLLOWING CALCULATION CONVERTS THE A'S FROM ERG TO MHZ UNITS
C
      DO 212 J = 6,8
      PSYFHI(1,J) = PSYFHI(1,J)/6.626196D-21
  212 STOP(J) = STOP(J)/6.626196D-21
      WRITE(6,213) (PSYFHI(1,J),STOP(J), J = 1,8)
  213 FORMAT(' :::::::::  THE FITTED SET OF PARAMETERS FOLLOW  ::::::::
     1::'//'              ALPHA    =',1PD15.7,'  + OR -',0PD15.8,'  DEGREE
     2S'//'              ELTA     =',1PD15.7,'  + OR -',0PD15.8,'  DEGREES
     3'//'               GX       =',1PD14.7,'  + OR -',-2PD15.8//'
     4      GY       =',1PD14.7,'  + OR -',-2PD15.8//'                  GZ
     5 =',1PD15.8,'  + OR -',-3PD16.9//'            AX       =',3PD16.7,
     6'  + OR -',1PD15.8,'  MHZ'//'              AY       =',3PD16.7,'  +
     7OR -',1PD15.8,'  MHZ'//'              AZ       =',4PD18.8,'  + OR -'
     8,2PD17.9,'  MHZ')
      STOP
      END
C
C
C     * * * * * * * * * * * * FUNCTN SUBROUTINE * * * * * * * * * * * * *
C
C     THIS FUNCTN SUBROUTINE MAKES USE OF THE KNOWN FIELD POSITIONS (HFP)
C     OF THE EXPERIMENTALLY OBSERVED VKA RESONANCES. USING A TRIAL
C     SET OF PARAMETERS, ONE WILL CALCULATE A SET OF EIGHT ENERGY LEVELS.
C     USING THE TWO THAT ARE APPROPRIATE TO THE OBSERVED RESONANCE UNDER
```

```
C     CONSIDERATION, ONE CALCULATES WHAT THE MICROWAVE FREQUENCY (NUMHZ)
C     SHOULD BE FOR THIS TRANSITION. NEXT A DELTA(I) IS CALCULATED (AFTER
C     STATEMENT #66) FOR THIS LINE, DELTA(I) = NUMHZ - MWFRQ, WHERE
C     MWFRQ IS THE EXPERIMENTALLY DETERMINED KLYSTRON FREQUENCY. THIS
C     PROCEDURE IS REPEATED FOR EACH OF THE POSSIBLE TWENTY-FOUR LINES.
C     THEN FUNCTN IS CALCULATED AS THE SUM OF SQUARES OF THE DELTAS.
C
      DOUBLE PRECISION FUNCTION FUNCTN(LA)
C
      IMPLICIT REAL*8 (A-H,O-Z)
      DIMENSION T(6), P(6)
C
C
C      THIS DATA REPRESENTS THE APPROPRIATE EULER ANGLES WHICH ARE ASSIGNED
C     TO THETA AND PHI IN STATEMENT 46
C
      DATA T/0.78539816,1.57079632,0.0,-1.57079632,1.04719255,1.04719255
     1/,P/1.57079632,0.0,0.0,1.57079632,-0.61577640,-0.61577640/
      REAL * 8 NUMHZ, MWFRQ
      REAL * 8 HFP(24), DELTA(24)
      REAL * 8 MATRXR, MATRXI
      COMMON/MATRIX/MATRXR(8,8),MATRXI(8,8),D(8),E(8),E2(8),TAU(2,8),N
      COMMON/PSYFH/PSYFHI(2,8),SS,NTIME
      M = LA
      IF(NTIME)199,199,58
  199 READ(5,200) HFP
  200 FORMAT(5(D12.5,4X))
C
C     THE EXPERIMENTAL MICROWAVE FREQUENCY IS GIVEN BELOW IN MHZ:
      MWFRQ = 9210.20
C
      B  = 9.274096D-21
      BN = 5.050951D-24
      GN = 5.2547415
      N  = 8
      PSC= 6.626196D-27                                          ERG*SEC
      X  = 1.0D-6
      MSEC = 0
      CALL ELAPSE(MTLAPS)
C
   58 J2 = 0
C
C      J2 INDEXES THE HFP(J2) AS WELL AS THE DELTA(J2)
C
      ALPHA = PSYFHI(M,1)
      ELTA  = PSYFHI(M,2)
      GX    = PSYFHI(M,3)
      GY    = PSYFHI(M,4)
      GZ    = PSYFHI(M,5)
      AX    = PSYFHI(M,6)
      AY    = PSYFHI(M,7)
      AZ    = PSYFHI(M,8)
C
   45 DO 61 J3 = 1,6
      IF(J3 - 6) 46,47,47
   47 ELTA = -ELTA
   46 THETA = T(J3)
      PHI   = P(J3)
      INDEX = 0
C
   10 B11 = DCOS(PHI - ELTA)
      B12 = DSIN(PHI - ELTA)
      B13 = 0.0D0
      B21 =-DCOS(THETA) * DSIN(PHI - ELTA)
      B22 = DCOS(THETA) * DCOS(PHI - ELTA)
      B23 = DSIN(THETA)
      B31 = DSIN(THETA) * DSIN(PHI - ELTA)
      B32 =-DSIN(THETA) * DCOS(PHI - ELTA)
      B33 = DCOS(THETA)
      BETA31 = GX*B11*B31 + GY*B12*B32
      BETA32 = GX*B21*B31 + GY*B22*B32 + GZ*B23*B33
      BETA33 = GX*B31**2  + GY*B32**2  + GZ*B33**2
      W11 = AX*DCOS(ALPHA)**2 + AZ*DSIN(ALPHA)**2
      W13 = (AX - AZ)*DSIN(ALPHA)*DCOS(ALPHA)
      W33 = AX*DSIN(ALPHA)**2 + AZ*DCOS(ALPHA)**2
      W22 = AY
      Z11P=B11**2*W11 +B12**2*W22 +B13**2*W33 +2.*B11*B13*W13
      Z11M=B11**2*W11 +B12**2*W22 +B13**2*W33 -2.*B11*B13*W13
      Z12P=B11*B21*W11+B12*B22*W22+B13*B23*W33+W13*(B13*B21+B11*B23)
      Z12M=B11*B21*W11+B12*B22*W22+B13*B23*W33-W13*(B13*B21+B11*B23)
      Z22P=B21**2*W11+B22**2*W22+B23**2*W33 +2.*B21*B23*W13
      Z22M=B21**2*W11+B22**2*W22+B23**2*W33 -2.*B21*B23*W13
      Z13P=B11*B31*W11+B12*B32*W22+B13*B33*W33 +W13*(B13*B31+B11*B33)
      Z13M=B11*B31*W11+B12*B32*W22+B13*B33*W33 -W13*(B13*B31+B11*B33)
      Z23P=B21*B31*W11+B22*B32*W22+B23*B33*W33 +W13*(B31*B23+B21*B33)
      Z23M=B21*B31*W11+B22*B32*W22+B23*B33*W33 -W13*(B31*B23+B21*B33)
      Z33P=B31**2*W11 +B32**2*W22 +B33**2*W33 +2.*W13*B31*B33
      Z33M=B31**2*W11 +B32**2*W22 +B33**2*W33 -2.*W13*B31*B33
      DO 61 J4 = 1,4
      J2 = J2 + 1
   65 IF(HFP(J2))68,68,72
   68 DELTA(J2) = 0.0D0
      GO TO 61
   72 H = HFP(J2)
C
C      THE MATRIX ELEMENTS ARE DEFINED BELOW IN TERMS OF THE QUANTITIES
C     DEFINED ABOVE.
C
   51 DO 52 MU = 1,8
      DO 52 J  = 1,8
      MATRXR(MU,J) = 0.0D0
   52 MATRXI(MU,J) = 0.0D0
      MATRXR(1,1)=0.5*B*H*BETA33 -GN*BN*H +0.25*(Z33P+Z33M)
      MATRXR(2,1)=0.25*Z13M
      MATRXI(2,1)=0.25*Z23M
      MATRXR(2,2)=0.5*B*H*BETA33 + 0.25*(Z33P-Z33M)
      MATRXR(3,1)=0.25*Z13P
      MATRXI(3,1)=0.25*Z23P
```

```
      MATRXR(3,3)=0.5*B*H*BETA33 -0.25*(Z33P-Z33M)
      MATRXR(4,2)=0.25*Z13P
      MATRXI(4,2)=0.25*Z23P
      MATRXR(4,3)=0.25*Z13M
      MATRXI(4,3)=0.25*Z23M
      MATRXR(4,4)=0.5*B*H*BETA33 +GN*BN*H -0.25*(Z33P+Z33M)
      MATRXR(5,1)=0.5*B*H*BETA31 +0.25*(Z13P +Z13M)
      MATRXI(5,1)=0.5*B*H*BETA32 +0.25*(Z23P +Z23M)
      MATRXR(5,2)=0.25*(Z11M + Z22M)
      MATRXR(5,3)=0.25*(Z11P + Z22P)
      MATRXR(5,5)=-0.5*B*H*BETA33 -GN*BN*H -0.25*(Z33P+Z33M)
      MATRXR(6,1)=0.25*(Z11P-Z22P)
      MATRXI(6,1)=0.5*Z12P
      MATRXR(6,3)=0.5*B*H*BETA31 -0.25*(Z13P - Z13M)
      MATRXI(6,3)=0.5*B*H*BETA32 -0.25*(Z23P - Z23M)
      MATRXR(6,4)=0.25*(Z11M + Z22M)
      MATRXR(6,5)=-0.25*Z13P
      MATRXI(6,5)=-0.25*Z23P
      MATRXR(6,6)=-0.5 *B*H*BETA33 +0.25*(Z33P - Z33M)
      MATRXR(7,1)=0.25*(Z11M - Z22M)
      MATRXI(7,1)=0.5*Z12M
      MATRXR(7,2)=0.5*B*H*BETA31 + 0.25*(Z13P - Z13M)
      MATRXI(7,2)=0.5*B*H*BETA32 + 0.25*(Z23P - Z23M)
      MATRXR(7,4)=0.25*(Z11P+Z22P)
      MATRXR(7,5)=-0.25*Z13M
      MATRXI(7,5)=-0.25*Z23M
      MATRXR(7,7)=-0.5*B*H*BETA33 -0.25*(Z33P - Z33M)
      MATRXR(8,2)=0.25*(Z11P - Z22P)
      MATRXI(8,2)=0.5*Z12P
      MATRXR(8,3)=0.25*(Z11M - Z22M)
      MATRXI(8,3)=0.5*Z12M
      MATRXR(8,4)=0.5*B*H*BETA31 -0.25*(Z13P + Z13M)
      MATRXI(8,4)=0.5*B*H*BETA32 -0.25*(Z23P + Z23M)
      MATRXR(8,6)=-0.25*Z13M
      MATRXI(8,6)=-0.25*Z23M
      MATRXR(8,7)=-0.25*Z13P
      MATRXI(8,7)=-0.25*Z23P
      MATRXR(8,8)=-0.5*B*H*BETA33 +GN*BN*H  +0.25*(Z33P + Z33M)
C
   60 CALL HTRIDI
C
      CALL IMTQL1(IERR)
C
      IF(IERR)67,66,67
   67 WRITE(6,70)
   70 FORMAT(' WE HAD AN ABNORMAL RETURN FROM SUBROUTINE IMTQL1 IN THAT
     1IERR WAS NOT ZERO')
      STOP
C
C      THE FOLLOWING STEPS CALCULATE THE APPROPRIATE MICROWAVE FREQUENCY,
C     CONVERT IT TO MHZ, AND COMPARE IT TO THE EXPERIMENTAL MICROWAVE
C     FREQUENCY.
C
   66 NUMHZ = ((D(8-INDEX) - D(INDEX+1))/PSC)* X
      DELTA(J2) = NUMHZ - MWFRQ
      CALL ELAPSE(MTLAPS)
      MSEC = MSEC + MTLAPS
  333 IF(MSEC.LT.XX*1000)GO TO 61
      WRITE(6,203) INDEX,(D(MEN),MEN=1,8),NUMHZ,J2,DELTA(J2)
  203 FORMAT(' THE PARTICULAR LINE OF THE PARTICULAR SPECTRUM AS SPECIFI
     1ED BY J2, IS SPECIFIED BY INDEX:',I3/' THE EIGENVALUES AT THIS FIE
     2LD VALUE WITH THIS PARTICULAR SET OF PARAMETERS ARE GIVEN IN ASCEN
     3DING ORDER BY:'//4(D20.10,2X)//4(D20.10,2X)//' THE CALCULATED NUMH
     4Z IS:',D20.10,'   AND DELTA(',I2,' ) IS:',D20.10)
   61 INDEX = INDEX+ 1
      FUNCTN = 0.000
      DO 90 KL = 1,24
C
C
   90 FUNCTN = DELTA(KL)**2 + FUNCTN
C
C
C     IT IS THIS FUNCTN THAT MUST BE BROUGHT TO ITS ABSOLUTE MINIMUM BY A
C     VARIATION OF THE EIGHT PARAMETERS.
C
C
   92 IF(MSEC.LT.XX*1000)GO TO 998
      WRITE(6,204) FUNCTN, (PSYFHI(M,I),I=1,8), NTIME
  204 FORMAT(/' *****  THE VALUE OF FUNCTN HAS BEEN CALCULATED TO BE:',
     1D20.10//'         FOR THE FOLLOWING SET OF PARAMETERS(ALPHA,BETA,GX
     2,GY,GZ,AX,AY,AND AZ):'//8X,4(D14.7,2X)/8X,4(D14.7,2X)//'          N
     3TIME IS:',I3)
  998 NTIME = NTIME + 1
  999 RETURN
      END
C
C     * * * * * * * * * * * *  HUNTER  * * * * * * * * * * * * * * * * * *
C
      SUBROUTINE HUNTER
C
C     TWELFTH VERSION -- PROPER PATTERN SEARCH
C     DIRECT SEARCH -- HOOKE, JEEVES, KAUPE
C     TRANSLATION OF ALGORITHM 178, A.F. KAUPE, JR.
C     COMM. ACM  VOL.6, P.313 (1963)
C
C     THIS SUBROUTINE IS USED TO FIND THE MINIMUM OF A FUNCTION OF NP
C     VARIABLES ARRANGED IN AN ARRAY PSYFHI
C     STEP IS AN INITIAL STEP SIZE,A FRACTION. THE INCREMENTING OF THE VARIABLES
C       IS DONE IN TERMS OF A DELT(K) = STEP(K) * PSYFHI(M,K)
C     RHO IS A STEP REDUCTION FACTOR. IT ALSO IS A FRACTION. AFTER A MINIMUM HAS
C       BEEN FOUND USING STEP, STEP IS REPLACED BY RHO*STEP.
C     STOP IS A STEP SIZE TERMINATOR. STEP IS REDUCED ONLY TO THIS VALUE,NO MORE
C     RHO, STEP, AND STOP ARE SPECIFIC FOR EACH VARIABLE.
C
C
      IMPLICIT REAL*8(A-H,O-Z)
      COMMON/HUNTR/RHO(8),STEP(8),STOP(8),NP,IPASS
      COMMON/PSYFH/PSYFHI(2,8),SS,NTIME
```

```
C
      IPASS = 0
    1 SPSI = FUNCTN(1)
      SS=SPSI
    7 DO 10 K=1,NP
   10 PSYFHI(2,K) = PSYFHI(1,K)
C
C     THE FIRST TIME HUNT IS CALLED, EXPLORATORY MOVES ARE MADE
C
      CALL HUNT
      IF(SS-SPSI)2,3,3
    2 IPASS = IPASS + 1
C
C     STATEMENTS 11 THROUGH 20 CONSTITUTE THE BASIS OF THE PATTERN MOVE,
C       WHICH IS ACCOMPLISHED IN SUBSEQUENT STEPS
C
   11 DO 20 K=1,NP
      THET  = PSYFHI(1,K)
      PSYFHI(1,K) = PSYFHI(2,K)
   20 PSYFHI(2,K)  = 2D0*PSYFHI(2,K) - THET
      SPSI = SS
  150 SS = FUNCTN(2)
      IF(SS-SPSI)151,151,1
C
C     THE SECOND TIME HUNT IS CALLED, EXPLORATORY MOVES ARE MADE FOLLOWING THE
C       PATTERN MOVE.
C
  151 CALL HUNT
C
C     IF THE PATTERN MOVE WAS A SUCCESS,RETURN TO STATEMENT 2 FOR ANOTHER
C       PATTERN MOVE.  OTHERWISE RETURN TO STATEMENT 1 FOR EXPLORATORY MOVES.
C
  661 IF(SS-SPS1)2,1,1
    3 LUV = 0
      DO 33 NI = 1,NP
      IF(STEP(NI)-STOP(NI))33,33,32
   32 STEP(NI) = RHO(NI)* STEP(NI)
      LUV = LUV + 1
   33 CONTINUE
      IF(LUV)30,30,1
   30 CONTINUE
   99 RETURN
      END
C
C     * * * * * * * * * * * *   HUNT   * * * * * * * * * * * * * * * * * *
C
      SUBROUTINE HUNT
C     SUBSIDIARY OF HUNTER
C
      IMPLICIT REAL*8(A-H,O-Z)
      COMMON/PSYFH/PSYFHI(2,8),SS,NTIME
      DIMENSION DELT(8)
      COMMON/HUNTR/RHO(8),DEL(8),STOP(8),NP,IPASS
      DO 20 K = 1, NP
      DELT(K) = DEL(K) * DABS(PSYFHI(2,K))
      IF(DELT(K))102,101,102
  101 DELT(K) = DEL(K)
  102 PSYFHI(2,K) = PSYFHI(2,K) + DELT(K)
      SPHI = FUNCTN(2)
      IF(SPHI-SS)12,16,16
   12 SS = SPHI
      GO TO 20
   16 PSYFHI(2,K) = PSYFHI(2,K) - 2D0*DELT(K)
      SPHI = FUNCTN(2)
      IF(SPHI-SS)14,18,18
   14 SS = SPHI
      GO TO 20
   18 PSYFHI(2,K) = PSYFHI(2,K) + DELT(K)
   20 CONTINUE
      RETURN
      END
C
C     * * * * * * * * * * * *  HTRIDI  * * * * * * * * * * * * * * * * * *
C
      SUBROUTINE HTRIDI
C          ( SEE APPENDIX E )
C
C     * * * * * * * * * * * *  IMTQL1  * * * * * * * * * * * * * * * * * *
C
      SUBROUTINE IMTQL1(IERR)
C          ( SEE APPENDIX E )
```

APPENDIX G

PROGRAM TO CALCULATE FIELD POSITIONS FOR H_A CENTER RESONANCES

```
C
C
C     * * * * * * * * * * H-CENTER PROBLEM * * * * * * * * * * * * * * * * * * *
C
C
C      THIS PROGRAM IS TO CALCULATE THE FIELD POSITIONS OF EPR RESONANCES
C     OF THE H-TYPE CENTER IN CUBIC PEROVSKITE STRUCTURED MATERIALS.  THE
C     DIRECTION OF THE MAGNETIC FIELD WITH RESPECT TO THE CRYSTALOGRAPHIC
C     COORDINATE SYSTEM IS TO BE SPECIFIED BY ANGLES THETA AND PHI.  THE
C     PLANE OF THE PROPOSED THREE-ION CENTER COINCIDES WITH A (010) PLANE
C     OF THE CRYSTAL.  THE CRYSTALOGRAPHIC Y-AXIS IS NORMAL TO THIS PLANE(010)
C     AND THE Z-AXIS (001) IS ALONG THE GENERAL DIRECTION OF THE THREE-CENTER
C     MOLECULE, FROM THE NUMBER TWO ION TO THE NUMBER THREE, THE X-AXIS(100) IS
C     OF COURSE NORMAL TO BOTH THESE DIRECTIONS FORMING A RIGHT HANDED
C     COORDINATE SYSTEM.  THETA IS MEASURED AS A COUNTERCLOCKWISE ROTATION
C     ABOUT THE Y-AXIS (LOOKING DOWN THE NEGATIVE Y-AXIS), WHEREAS PHI IS
C     MEASURED AS A CLOCKWISE ROTATION ABOUT THE NEW X'-AXIS.  THESE ROTATIONS
C     TRANSFORM ALL QUANTITIES INTO THE MAGNETIC FIELD COORDINATE SYSTEM
C     WHERE H LIES ALONG THE Z-AXIS.  FOR EACH SUCH THETA AND PHI SPECIFICATION,
C     SIXTEEN ENERGY LEVELS ARE CALCULATED, HENCE EIGHT FIELD POSITIONS ARE
C     PREDICTED.
C
C
C
C      THERE ARE SIXTEEN PARAMETERS WHICH MUST BE FURNISHED TO THIS PROGRAM
C     BEFORE THE CALCULATION CAN PROCEED.  THESE ARE:
C       1) THE HYPERFINE PARAMETERS RELEVANT TO EACH OF THE THREE ION  OF
C          THE DEFECT.  THESE ARE A1X, A1Y, AND A1Z FOR THE INTERSTITIAL ATOM,
C          A2X, A2Y, AND A2Z FOR WHAT IS BEING CALLED ION TWO, AND A3X, A3Y,
C          AND A3Z FOR ION THREE.  ALL HYPERFINE PARAMETERS ARE TO BE
C          ENTERED IN MHZ.
C       2) THE G-VALUES:  GX, GY, AND GZ
C       3) A SET OF ANGLES.  THESE ARE: CHI, ALPHA1, ALPHA2, AND ALPHA3 WHICH
C          REPRESENT, RESPECTIVELY, THE ANGLES BETWEEN THE Z-AXIS OF THE CRYSTAL
C          AND THE Z-AXIS OF THE COORDINATE SYSTEMS IN WHICH THE G, A1, A2, AND
C          A3 TENSORS ARE DIAGONAL.  THE ANGLES ARE TO BE ENTERED IN DEGREES.
C          ALL ANGLES ARE SUCH THAT A CCW ROTATION BY ALPHAJ BRINGS THE AJ
C          TENSOR COORDINATE SYSTEM INTO COINCIDENCE WITH THE CRYSTALOGRAPHIC
C          COORDINATE SYSTEM.
C
C
C      ALSO TO BE FURNISHED TO THE PROGRAM ARE THE FOLLOWING:  AN INITIAL
C     MAGNETIC FIELD VALUE H; A MICROWAVE FREQUENCY, ENTERED IN MHZ; AND OF
C     COURSE AN INITIAL THETA AND PHI VALUE.
C
C
      IMPLICIT REAL*8 (A-H,O-Z)
      REAL*8 NUMHZ,NU
      REAL * 8 MATRXR,MATRXI
      COMMON/MATRIX/MATRXR(16,16),MATRXI(16,16),D(16),E(16),E2(16),TAU(2
     1,16),N,IERR
C
C
      N = 16
      B = 9.274096D-21
      BN = 5.050951D-24
      GN = 5.2547415
      PSC = 6.6261965D-27                                          ERG SEC
      PC  = 6.626196500-21                                         H *10**a
      X = 1.0D-6
      DG2RAD = 0.017453292519943
      THETA = 0.0D0
      PHI   = 0.0D0
C
      J2 = 1
C
C        THE INDEX J2 IS USED TO CHANGE THE DIRECTION OF THE MAGNETIC FIELD
C        SEE STATEMENT 700 AND SUBSEQUENT
C
      H = 2400
C
C        THE VALUE OF THE PARAMETERS ARE ASSUMED TO BE:
C
      GX     = 2.033269
      GY     = 2.025910
      GZ     = 2.00184809
      CHI    = 12.06
      A1X    = 508.37
      A1Y    = 542.18
      A1Z    = 3121.40
      ALPHA1 = 12.3568
      A2X    = 181.80
      A2Y    = 193.04
      A2Z    = 1680.38
      ALPHA2 = 22.28
      A3X    = 13.05
      A3Y    = 17.07
      A3Z    = 141.72
      ALPHA3 =-22.97
C
C     THE MICROWAVE FREQUENCY IS GIVEN THE FOLLOWING VALUE IN MHZ:
C
      FREQ  = 9070.08
C
      A1X = A1X* PC                                                ---------
      A1Y = A1Y* PC
      A1Z = A1Z* PC
      A2X = A2X* PC                                                MHZ TO
      A2Y = A2Y* PC
      A2Z = A2Z* PC                                                  ERGS
      A3X = A3X* PC
      A3Y = A3Y* PC
      A3Z = A3Z* PC                                                ---------
      CHI = CHI * DG2RAD                                           ---------
      ALPHA1 = ALPHA1 * DG2RAD                                     DEGREES
      ALPHA2 = ALPHA2 * DG2RAD                                       TO
      ALPHA3 = ALPHA3 * DG2RAD                                     RADIANS
```

```
C                                                                       --------
   10 G13 = 0.5*(GX-GZ)*DSIN(2*(THETA+CHI))*DCOS(PHI)
      G23 =-0.5*DSIN(2*PHI)*(GX*(DSIN(THETA+CHI))**2 -GY
C
     1                                          + GZ*(DCOS(THETA + CHI))**2)
C
      G33 = (GX*(DSIN(THETA + CHI))**2 + GZ*(DCOS(THETA +CHI))**2)*
C
     1                                    DCOS(PHI)**2 + GY*DSIN(PHI)**2
      I = 0
      A111 = A1X*(DCOS(THETA + ALPHA1))**2 + A1Z*(DSIN(THETA+ALPHA1))**2
      A211 = A2X*(DCOS(THETA + ALPHA2))**2 + A2Z*(DSIN(THETA+ALPHA2))**2
      A311 = A3X*(DCOS(THETA + ALPHA3))**2 + A3Z*(DSIN(THETA+ALPHA3))**2
      A112 = 0.5*(A1Z - A1X)*DSIN(PHI)*DSIN(2*(THETA + ALPHA1))
      A212 = 0.5*(A2Z - A2X)*DSIN(PHI)*DSIN(2*(THETA + ALPHA2))
      A312 = 0.5*(A3Z - A3X)*DSIN(PHI)*DSIN(2*(THETA + ALPHA3))
      A113 = 0.5*(A1X - A1Z)*DCOS(PHI)*DSIN(2*(THETA + ALPHA1))
      A213 = 0.5*(A2X - A2Z)*DCOS(PHI)*DSIN(2*(THETA + ALPHA2))
      A313 = 0.5*(A3X - A3Z)*DCOS(PHI)*DSIN(2*(THETA + ALPHA3))
      A122 = (A1X*(DSIN(THETA + ALPHA1))**2 +A1Z*(DCOS(THETA+ALPHA1))**2
C
     1                                    )*DSIN(PHI)**2  + A1Y*DCOS(PHI)**2
C
      A222 = (A2X*(DSIN(THETA + ALPHA2))**2 +A2Z*(DCOS(THETA+ALPHA2))**2
C
     1                                    )*DSIN(PHI)**2  + A2Y*DCOS(PHI)**2
C
      A322 = (A3X*(DSIN(THETA + ALPHA3))**2 +A3Z*(DCOS(THETA+ALPHA3))**2
C
     1                                    )*DSIN(PHI)**2  + A3Y*DCOS(PHI)**2
C
      A123 = DSIN(PHI)*DCOS(PHI)*(-A1X*(DSIN(THETA + ALPHA1))**2  +A1Y
C
     1                                  - A1Z*(DCOS(THETA + ALPHA1))**2)
C
      A223 = DSIN(PHI)*DCOS(PHI)*(-A2X*(DSIN(THETA + ALPHA2))**2  + A2Y
C
     1                                  - A2Z*(DCOS(THETA + ALPHA2))**2)
C
      A323 = DSIN(PHI)*DCOS(PHI)*(-A3X*(DSIN(THETA + ALPHA3))**2  + A3Y
C
     1                                  - A3Z*(DCOS(THETA + ALPHA3))**2)
C
      A133 = (A1X*(DSIN(THETA + ALPHA1))**2 +A1Z*(DCOS(THETA+ALPHA1))**2
C
     1                                    )*DCOS(PHI)**2  + A1Y*DSIN(PHI)**2
C
      A233 = (A2X*(DSIN(THETA + ALPHA2))**2 +A2Z*(DCOS(THETA+ALPHA2))**2
C
     1                                    )*DCOS(PHI)**2  + A2Y*DSIN(PHI)**2
C
      A333 = (A3X*(DSIN(THETA + ALPHA3))**2 +A3Z*(DCOS(THETA+ALPHA3))**2
C
     1                                    )*DCOS(PHI)**2  + A3Y*DSIN(PHI)**2
```

```
   50 DO 349 L =1,15
C
C
C     THE MATRIX ELEMENTS ARE DEFINED BELOW IN TERMS OF THE QUANTITIES
C     DEFINED ABOVE.
C
C
   51 DO 52 M= 1,16
      DO 52 J= 1,16
      MATRXR(M,J) = 0.0D 00
   52 MATRXI(M,J) = 0.0D 00
      MATRXR(1,1) = 0.5*G33*B*H +0.25*(A133+A233+A333)-1.5*GN*BN*H
      MATRXR(2,1) = C.25*A313
      MATRXI(2,1) = C.25*A323
      MATRXR(2,2) = C.5*(G33*B -GN*BN)*H +0.25*(A133+A233-A333)
      MATRXR(3,1) = C.25*A213
      MATRXI(3,1) = 0.25*A223
      MATRXR(3,3) = C.5*H*(G33*B - GN*BN) +0.25*(A133-A233+A333)
      MATRXR(4,1) = C.25*A113
      MATRXI(4,1) = C.25*A123
      MATRXR(4,4) = C.5*H*(G33*B - GN*BN) +0.25*(-A133+A233+A333)
      MATRXR(5,2) = C.25*A213
      MATRXI(5,2) = C.25*A223
      MATRXR(5,3) = C.25*A313
      MATRXI(5,3) = C.25*A323
      MATRXR(5,5) = C.5*H*(G33*B + GN*BN) +0.25*(A133-A233-A333)
      MATRXR(6,2) = C.25*A113
      MATRXI(6,2) = C.25*A123
      MATRXR(6,4) = C.25*A313
      MATRXI(6,4) = 0.25*A323
      MATRXR(6,6) = C.5*H*(G33*B + GN*BN) + 0.25*(-A133+A233-A333)
      MATRXR(7,3) = C.25*A113
      MATRXI(7,3) = 0.25*A123
      MATRXR(7,4) = C.25*A213
      MATRXI(7,4) = 0.25*A223
      MATRXR(7,7) = C.5*H*(G33*B + GN*BN) + 0.25*(-A133-A233+A333)
      MATRXR(8,5) = C.25*A113
      MATRXI(8,5) = C.25*A123
      MATRXR(8,6) = 0.25*A213
      MATRXI(8,6) = C.25*A223
      MATRXR(8,7) = 0.25*A313
      MATRXI(8,7) = C.25*A323
      MATRXR(8,8) = 0.5*H*(G33*B +3*GN*BN)- 0.25*(A133+A233+A333)
      MATRXR(9,5) = 0.25*(A111 - A122)
      MATRXI(9,5) = C.5 *A112
      MATRXR(9,6) = 0.25*(A211 - A222)
      MATRXI(9,6) = C.5 *A212
      MATRXR(9,7) = C.25*(A311 - A322)
      MATRXI(9,7) = 0.5 *A312
      MATRXR(9,8) = C.5*G13*B*H - 0.25*(A113 + A213 + A313)
      MATRXI(9,8) = 0.5*G23*B*H - 0.25*(A123 + A223 + A323)
      MATRXR(9,9) =-0.5*H*(G33*B -3.0*GN*BN)+ 0.25*(A133+A233+A333)
      MATRXR(10,3)= C.25*(A111 - A122)
      MATRXI(10,3)= C.5 *A112
```

```
      MATRXR(10,4)= 0.25*(A211 - A222)
      MATRXI(10,4)= 0.5 *A212
      MATRXR(10,7)= C.5*G13*B*H - 0.25*(A113 + A213 - A313)
      MATRXI(10,7)= C.5*G23*B*H - 0.25*(A123 + A223 - A323)
      MATRXR(10,8)= C.25*(A311 + A322)
      MATRXR(10,9)=-0.25*A313
      MATRXI(10,9)= 0.25*A323
      MATRXR(10,10) =-0.5*H*(G33*B - GN*BN) +0.25*(A133+A233-A333)
      MATRXR(11,2)  = 0.25*(A111 - A122)
      MATRXI(11,2)  = 0.5 * A112
      MATRXR(11,4)  = 0.25*(A311 - A322)
      MATRXI(11,4)  = 0.5 * A312
      MATRXR(11,6)  = 0.5 *G13*B*H - 0.25*(A113 - A213 + A313)
      MATRXI(11,6)  = 0.5 *G23*B*H - 0.25*(A123 - A223 + A323)
      MATRXR(11,8)  = 0.25*(A211 + A222)
      MATRXR(11,9)  =-0.25*A213
      MATRXI(11,9)  = 0.25*A223
      MATRXR(11,11) =-0.5*H*(G33*B - GN*BN) + 0.25*(A133-A233+A333)
      MATRXR(12,2)  = C.25*(A211 - A222)
      MATRXI(12,2)  = 0.5 *A212
      MATRXR(12,3)  = C.25*(A311 - A322)
      MATRXI(12,3)  = 0.5 * A312
      MATRXR(12,5)  = 0.5*G13*B*H + 0.25*(A113 - A213 - A313)
      MATRXI(12,5)  = 0.5*G23*B*H + 0.25*(A123 - A223 - A323)
      MATRXR(12,8)  = 0.25*(A111 + A122)
      MATRXR(12,9)  =-C.25* A113
      MATRXI(12,9)  = 0.25* A123
      MATRXR(12,12) =-0.5*H*(G33*B - GN*BN) + 0.25*(-A133+A233+A333)
      MATRXR(13,1)  = C.25*(A111 - A122)
      MATRXI(13,1)  = C.5 * A112
      MATRXR(13,4)  = 0.5*G13*B*H + 0.25*(-A113+A213+A313)
      MATRXI(13,4)  = 0.5*G23*B*H + 0.25*(-A123+A223+A323)
      MATRXR(13,6)  = 0.25*(A311 + A322)
      MATRXR(13,7)  = 0.25*(A211 + A222)
      MATRXR(13,10) =-C.25*A213
      MATRXI(13,10) = 0.25*A223
      MATRXR(13,11) =-0.25*A313
      MATRXI(13,11) = 0.25*A323
      MATRXR(13,13) =-0.5*H*(G33*B + GN*BN) + 0.25*(A133-A233-A333)
      MATRXR(14,1)  = 0.25*(A211 - A222)
      MATRXI(14,1)  = 0.5 * A212
      MATRXR(14,3)  = 0.5*G13*B*H +0.25*(A113 - A213 + A313)
      MATRXI(14,3)  = 0.5*G23*B*H +0.25*(A123 - A223 + A323)
      MATRXR(14,5)  = C.25*(A311+ A322)
      MATRXR(14,7)  = 0.25*(A111+ A122)
      MATRXR(14,10) =-C.25* A113
      MATRXI(14,10) = 0.25* A123
      MATRXR(14,12) =-0.25* A313
      MATRXI(14,12) = 0.25* A323
      MATRXR(14,14) =-0.5*H*(G33*B + GN*BN) + 0.25*(-A133+A233-A333)
      MATRXR(15,1)  = 0.25*(A311 - A322)
      MATRXI(15,1)  = 0.5 * A312
      MATRXR(15,2)  = 0.5*G13*B*H + 0.25*(A113 + A213 - A313)
      MATRXI(15,2)  = 0.5*G23*B*H + 0.25*(A123 + A223 - A323)
      MATRXR(15,5)  = 0.25*(A211 + A222)
      MATRXR(15,6)  = 0.25*(A111 + A122)
      MATRXR(15,11) =-C.25* A113
      MATRXI(15,11) = 0.25* A123
      MATRXR(15,12) =-0.25* A213
      MATRXI(15,12) = C.25* A223
      MATRXR(15,15) =-0.5*H*(G33*B + GN*BN) + 0.25*(-A133-A233+A333)
      MATRXR(16,1)  = 0.5*G13*B*H + 0.25*(A113 +A213 +A313)
      MATRXI(16,1)  = C.5*G23*B*H + 0.25*(A123 +A223 +A323)
      MATRXR(16,2)  = 0.25*(A311 + A322)
      MATRXR(16,3)  = C.25*(A211 + A222)
      MATRXR(16,4)  = C.25*(A111 + A122)
      MATRXR(16,13) =-0.25* A113
      MATRXI(16,13) = C.25* A123
      MATRXR(16,14) =-0.25* A213
      MATRXI(16,14) = 0.25* A223
      MATRXR(16,15) =-C.25* A313
      MATRXI(16,15) = 0.25* A323
      MATRXR(16,16) =-0.5*H*(G33*B + 3.0*GN*BN) - 0.25*(A133+A233+A333)
C
   60 CALL HTRIDI
C
      CALL IMTQL1
C
      IF(IERR)309,3C9,70
   70 WRITE(6,71)IERR
   71 FORMAT(' IERR IS ZERO  FOR A NORMAL RETURN FROM SUBROUTINE IMTQL1 A
     1ND IS SET TO AN INTEGER J OTHERWISE THE VALUE OF IERR:',I2)
      GO TO 1000
  309 WRITE(6,310) H
  310 FORMAT(' *****  THE CALCULATED FIELD IN GAUSS FOR THIS ITERATION I
     1S:',D13.6)
C
C
C      THE FOLLOWING STEPS CALCULATE THE APPROPRIATE MICROWAVE FREQUENCY,
C     CONVERT IT TO MHZ, AND COMPARE IT TO THE EXPERIMENTAL MICROWAVE
C     FREQUENCY.
C
C
      NU = (D(16 -I) - D(I+1))/PSC
      NUMHZ = NU * X
      FRQDIF = DABS(NUMHZ - FREQ)
      IF(FRQDIF.LE.0.5) GO TO 350
  349 H = H * FREQ/NUMHZ
  347 WRITE(6,348)
  348 FORMAT(' AFTER FIFTEEN ITERATIONS OF THE FIELD WE STILL DO NOT HAV
     1E A SOLUTION WITHIN OUR ERROR LIMIT')
      GO TO 1000
  350 WRITE(6,351)
  351 FORMAT(' **********   THE CALCULATED MAGNETIC FIELD AT WHICH THIS
     1PARTICULAR LINE FALLS IS GIVEN DIRECTLY ABOVE  **********')
      I = I + 1
      IF(I - 8) 361,7CC,700
  361 WRITE(6,360)
```

```
  360 FORMAT(//' HAVING CALCULATED ONE FIELD POSITION WE NOW WISH TO CAL
     1CULATE ANOTHER.TO DO SO REQUIRES THAT THE INDEX I BE'/ ' ADVANCED
     2BY ONE SO THAT THE APPROPRIATE NU IS COMPUTED.THIS HAS BEEN DONE')
  400 NU = (D(16 -I) - D(I +1))/PSC
      NUMHZ = NU * X
      H = H * FREQ/NUMHZ
      GO TO 50
C
C
  700 IF(6 - J2)713,711,750
  750 IF(5 - J2)1000,709,751
  751 IF(4 - J2)1000,707,752
  752 IF(3 - J2)1000,705,753
  753 IF(2 - J2)1000,703,754
  754 IF(1 - J2)1000,701,1000
C
  701 WRITE(6,702)
  702 FORMAT(/' ***** THE EIGHT CALCULATED FIELD POSITIONS ABOVE ARE FOR
     1 ORIENTATIONS A,B,C, AND D IN THE (100) SPECTRUM, GIVING ZERO DEGR
     2EE'/' LINES *****')
      J2 = J2 + 1
      THETA = 1.5707963Z
      H = H * FREQ/((( D(16) - D(1))/PSC) * X)
      GO TO 10
C
  703 WRITE(6,704)
  704 FORMAT(/' ***** THE EIGHT CALCULATED FIELD POSITIONS ABOVE ARE FOR
     1 ORIENTATIONS E,F,L, AND K IN THE (100) SPECTRUM, GIVING PSEUDO-NI
     2NETY'/' DEGREE LINES *****')
      J2 = J2 + 1
      PHI = THETA
      H = H * FREQ/((( D(16) - D(1))/PSC) * X)
      GO TO 10
C
  705 WRITE(6,706)
  706 FORMAT(/' ***** THE EIGHT CALCULATED FIELD POSITIONS ABOVE ARE FOR
     1 ORIENTATIONS G,H,I, AND J IN THE (100) SPECTRUM, GIVING RISE TO T
     2RUE'/' NINETY DEGREE LINES *****')
      J2 = J2 + 1
      PHI   = 2.3561944Z
      H = H * FREQ/((( D(16) - D(1))/PSC) * X)
      GO TO 10
C
  707 WRITE(6,708)
  708 FORMAT(/' ***** THE EIGHT CALCULATED FIELD POSITIONS ABOVE ARE FOR
     1 ORIENTATIONS I,J,K, AND L IN THE (110) SPECTRUM, GIVING NINETY DE
     2GREE'/' LINES  *****')
      J2 = J2 + 1
      PHI   = -PHI
      THETA = 0.000
      H = H * FREQ/((( D(16) - D(1))/PSC) * X)
      GO TO 10
C
  709 WRITE(6,710)
  710 FORMAT(/' ***** THE EIGHT CALCULATED FIELD POSITIONS ABOVE ARE FOR
     1 ORIENTATIONS C,D,G, AND H IN THE (110) SPECTRUM, GIVING FORTY-FIV
     2E'/' DEGREE LINES *****')
      J2 = J2 + 1
      THETA = 0.7853981636
      PHI   = 0.000
      H = H * FREQ/((( D(16) - D(1))/PSC) * X)
      GO TO 10
C
  711 WRITE(6,712)
  712 FORMAT(/' ***** THE EIGHT CALCULATED FIELD POSITIONS ABOVE ARE FOR
     1 ORIENTATIONS B AND F IN THE (110) SPECTRUM, GIVING INNER FORTY-FI
     2VE'/' DEGREE LINES *****')
      J2    =  J2 + 1
      THETA = -THETA
      H = H * FREQ/((( D(16) - D(1))/PSC) * X)
      GO TO 10
C
  713 WRITE(6,714)
  714 FORMAT(/' ***** THE EIGHT CALCULATED FIELD POSITIONS ABOVE ARE FOR
     1 ORIENTATIONS A AND E IN THE (110) SPECTRUM, GIVING OUTER FORTY-FI
     2VE'/' DEGREE LINES *****')
 1000 STOP
      END
C
C     * * * * * * * * * * * *  HTRIDI  * * * * * * * * * * * * * * * * * *
C
      SUBROUTINE HTRIDI
C          ( SEE APPENDIX E )
C
      COMMON/MATRIX/AR(16,16),AI(16,16),D(16),E(16),E2(16),TAU(2,16),N,
     1IERR
C
C     * * * * * * * * * * * *  IMTQL1  * * * * * * * * * * * * * * * * * *
C
      SUBROUTINE IMTQL1
C          ( SEE APPENDIX E )
C
      COMMON/MATRIX/AR(16,16),AI(16,16),D(16),E(16),E2(16),TAU(2,16),N,
     1IERR
```

APPENDIX H

PROGRAM TO CALCULATE PARAMETERS FOR H_A CENTER

```
C
C       ******* H-CENTER PARAMETER FITTING PROGRAM *******
C
C     THIS PROGRAM IS DESIGNED TO CALCULATE THE SIXTEEN PARAMETERS OF
C     INTEREST IN THE H-CENTER MODEL DEFECT IN KMGF3. AS INPUT ONE NEED
C     FURNISH THE FOLLOWING:
C
C       1)THE FIELD POSITIONS OF THE VARIOUS EPR RESONANCES,ENTERED IN
C         A SPECIFIC SYSTEMATIC MANNER. AT PRESENT THIS SYSTEM WILL
C         BE AS FOLLOWS. FIELD POSITIONS WILL BE DIMENSIONALIZED IN A ONE
C         DIMENSIONAL ARRAY HFP(L). FOR ZERO DEGREE LINES IN THE (100)
C         SPECTRUM (ORIENTATIONS A,B,C, AND D) L=1,8, HFP(1) BEING THE
C         LOWEST FIELD POSITION,HFP(8) THE HIGHEST; NINETY DEGREE LINES
C         (DUE TO ORIENTATIONS E,F,K,L) IN THE (100) SPECTRUM WILL BE
C         ASSIGNED L=9,16 (LOW TO HIGH FIELD); AND NINETY DEGREE LINES
C         (DUE TO ORIENTATIONS G,H,I,J) WILL HAVE L=17,24. FOR THE (110)
C         SPECTRUM: NINETY DEGREE LINES (DUE TO ORIENTATIONS I,J,K,L) WILL
C         HAVE L=25,32; FORTY-FIVE DEGREE LINES (DUE TO ORIENTATIONS B,F)
C         WILL HAVE L=33,40; FORTY-FIVE DEGREE LINES (DUE TO ORIENTATIONS
C         A,E) WILL HAVE L=41,48; AND FINALLY FORTY-FIVE DEGREE LINES
C         (DUE TO ORIENTATIONS C,D,G,H) WILL HAVE L=49,56. FOR LINES WHICH
C         COULD NOT BE OBTAINED, ENTER A ZERO FOR THAT HFP(L). ENTER ALL
C         HFP IN GAUSS.
C       2)INTERNALLY A SET OF ANGLES IS FURNISHED FOR EACH OF THE MOLECULAR
C         ORIENTATIONS ( A TOTAL OF SEVEN SETS OF ANGLES ) WITH
C         RESPECT TO THE MAGNETIC FIELD.
C       3)THE EXPERIMENTAL MICROWAVE FREQUENCY MUST BE ENTERED IN MHZ.
C       4)AN INITIAL SET OF PARAMETERS MUST BE FURNISHED: A1X,A1Y,A1Z,
C         ALPHA1,A2X,A2Y,A2Z,ALPHA2,A3X,A3Y,A3Z,ALPHA3,GX,GY,GZ,CHI.ALL
C         ANGLES ARE TO BE ENTERED IN DEGREES, ALL HYPERFINE PARAMETERS
C         IN MHZ.
C       5)THE INDICATED PROGRAM TIME LIMIT MINUS XX SECONDS (USED FOR
C         COMPILATION) NEEDS BE SUPPLIED IN MILLISECONDS FOR USE IN
C         CONJUNCTION WITH THE ELAPSE SUBROUTINE. THIS NUMBER MUST BE
C         SUPPLIED IN TWO IF STATEMENTS(#'S 333,92) OF THE FUNCTN SUBROUTINE
C         AS THE CONSTANT AT THE RIGHT PARENTHESIS. THIS PROCEDURE IS TO
C         PREVENT EXCESSIVE OUTPUT DATA YET PROVIDE AN INDICATION AS TO
C         WHAT POINT IN A DETERMINATION OF THE PARAMETERS THE PROGRAM HAS
C         REACHED IF IT FAILS TO CULMINATE IN THE ALLOTTED TIME LIMIT.
C
C     AS OUTPUT ONE SHOULD HAVE THE SIXTEEN PARAMETETERS OF INTEREST.
C
      IMPLICIT REAL * 8 (A-H,O-Z)
      COMMON/PSYFH/PSYFHI(2,16),SS,NTIME
      COMMON/HUNTR/RHO(16),STEP(16),STOP(16),NP,IPASS
C
      READ(5,200) RHO,STEP,STOP
  200 FORMAT(8(D10.7))
C
C     THE PARAMETERS ARE INITIALIZED AS FOLLOWS:
C
      GX     = 2.033269
      GY     = 2.025911
      GZ     = 2.0016C8
      CHI    = 12.06
      A1X    = 508.3746
      A1Y    = 545.5868
      A1Z    = 3119.8398
      ALPHA1 = 12.3588
      A2X    = 181.8
      A2Y    = 193.04
      A2Z    = 1680.38
      ALPHA2 = 22.28
      A3X    = 13.05
      A3Y    = 17.07
      A3Z    = 141.72
      ALPHA3 =-22.97
C
      PSYFHI(1,1)  = ALPHA1/57.29578
      PSYFHI(1,2)  = ALPHA2/57.29578
      PSYFHI(1,3)  = ALPHA3/57.29578
      PSYFHI(1,4)  = CHI/57.29578
      PSYFHI(1,5)  = GX
      PSYFHI(1,6)  = GY
      PSYFHI(1,7)  = GZ
      PSYFHI(1,8)  = A1X * 6.626196D-21
      PSYFHI(1,9)  = A1Y * 6.626196D-21
      PSYFHI(1,10) = A1Z * 6.626196D-21
      PSYFHI(1,11) = A2X * 6.626196D-21
      PSYFHI(1,12) = A2Y * 6.626196D-21
      PSYFHI(1,13) = A2Z * 6.626196D-21
      PSYFHI(1,14) = A3Z * 6.626196D-21
      PSYFHI(1,15) = A3Y * 6.626196D-21
      PSYFHI(1,16) = A3X * 6.626196D-21
      NTIME = 0
      NP    = 16
      CALL HUNTER
      WRITE(6,202) NTIME,IPASS
  202 FORMAT(///' THE NUMBER OF TIMES THAT FUNCTN WAS CALCULATED, WHICH'/
     1' INVOLVES SOLVING THE 16 X 16 MATRIX ONCE PER NONZERO HFP, IS'/'
     2GIVEN BY NTIME:',I5,' . THE VALUE OF IPASS IS:',I3,' .'/)
C
      DO 210 J =1,16
  210 STOP(J) = STEP(J) * DABS(PSYFHI(1,J))
      DO 211 J = 1,4
      PSYFHI(1,J) = PSYFHI(1,J) * 57.29578                              RADS2DGR
  211 STOP(J)= STOP(J)* 57.29578                                        RADS2DGR
C
C     THE FOLLOWING CALCULATION CONVERTS THE A'S FROM ERGS TO MHZ
C
      DO 212 J = 8,16
      PSYFHI(1,J) = PSYFHI(1,J)/6.626196D-21
  212 STOP(J)= STOP(J)/6.626196D-21
      WRITE(6,213) (PSYFHI(1,J),STOP(J), J = 1,16)
  213 FORMAT(' ::::::::::  THE FITTED SET OF PARAMETERS FOLLOW  ::::::::
     1::'//'              ALPHA1  =',2PD15.7,'  + OR -',0PD15.8,'  DEGREE
     2S'//'              ALPHA2  =',2PD15.7,'  + OR -',0PD15.8,'  DEGREES
     3'//'              ALPHA3  =',2PD15.7,'  + OR -',0PD15.8,'  DEGREES'
```

```
     4//'              CHI     =',1PD14.7,'  + OR -',0PD15.8,'  DEGREES'/
     5/'              GX      =',1PD14.7,'  + OR -',-2PD15.8//'
     6    GY      =',1PD14.7,'  + OR -',-2PD15.8//'                    GZ      =
     7',1PD15.8,'  + OR -',-3PD16.9//'              A1X     =',3PD16.7,'
     8 + OR -',1PD15.8,'  MHZ'//'                   A1Y     =',3PD16.7,'  + OR
     9 -',1PD15.8,'  MHZ'//'                  A1Z     =',4PD18.8,'  + OR -',2
     1PD17.9,'  MHZ'//'              A2X     =',3PD16.7,'  + OR -',1PD15.
     28,'  MHZ'//'              A2Y     =',3PD16.7,'  + OR -',1PD15.8,'
     3MHZ'//'              A2Z     =',4PD18.8,'  + OR -',2PD17.9,'  MHZ'/
     4/'              A3Z     =',3PD16.7,'  + OR -',1PD15.8,'  MHZ'//'
     5          A3Y     =',2PD15.7,'  + OR -',1PD15.8,'  MHZ'//'
     6      A3X     =',2PD15.7,'  + OR -',1PD15.8,'  MHZ')
      STOP
      END
C
C     * * * * * * * * * * FUNCTN SUBROUTINE  * * * * * * * * * * * * * * * *
C
C     THIS FUNCTN SUBROUTINE MAKES USE OF THE KNOWN FIELD POSITIONS (HFP)
C     OF THE EXPERIMENTALLY OBSERVED H-CENTER RESONANCES. USING A TRIAL
C     SET OF PARAMETERS, ONE WILL CALCULATE A SET OF SIXTEEN ENERGY LEVELS.
C     USING THE TWO THAT ARE APPROPRIATE TO THE OBSERVED RESONANCE UNDER
C     CONSIDERATION, ONE CALCULATES WHAT THE MICROWAVE FREQUENCY (NUMHZ)
C     SHOULD BE FOR THIS TRANSITION. NEXT A DELTA(I) IS CALCULATED (AFTER
C     STATEMENT #66) FOR THIS LINE, DELTA(I) = NUMHZ - MWFRQ  , WHERE
C     MWFRQ IS THE EXPERIMENTALLY DETERMINED KLYSTRON FREQUENCY. THIS
C     PROCEDURE IS REPEATED FOR EACH OF THE POSSIBLE FIFTY-SIX LINES. THEN
C     FUNCTN IS CALCULATED AS THE SUM OF SQUARES OF THE DELTAS.
C
      DOUBLE PRECISION FUNCTION FUNCTN(LA)
      IMPLICIT REAL * 8 (A-H,O-Z)
      DIMENSION T(7),P(7)
C
C
C      THIS DATA REPRESENTS THE APPROPRIATE ANGLES WHICH ARE ASSIGNED
C     TO THETA AND PHI IN STATEMENT 45 AND SUBSEQUENT
C
C
      DATA T/0.0,1.57079632,0.0,1.57079632,0.7853981636,-0.7853981636,0.
     1O/,P/0.0,0.0,-1.57079632,2.356194491,0.0,0.0,-2.356194491/
      REAL * 8 MWFRQ
      REAL * 8 HFP(56),DELTA(56)
      REAL * 8 MATRXR,MATRXI
      COMMON/MATRIX/MATRXR(16,16),MATRXI(16,16),D(16),E(16),E2(16),TAU(2  ***
     1,16),N
      COMMON/PSYFH/PSYFHI(2,16),SS,NTIME
      M = LA
      IF(NTIME) 199,199,58
  199 READ(5,200) HFP
  200 FORMAT(5(D12.5,4X))
C
C     THE EXPERIMENTAL MICROWAVE FREQUENCY IS GIVEN BELOW IN MHZ:
      MWFRQ = 9070.08                                                    MHZ
C
      B  = 9.274096D-21
      BN = 5.050951D-24
      GN = 5.2547415
      N  = 16
      MSEC  = 0
      CALL ELAPSE(MTLAPS)
C
C      J2 INDEXES THE HFP(J2) AS WELL AS THE DELTA(J2)
C
   58 J2 = 0
      ALPHA1 = PSYFHI(M,1)
      ALPHA2 = PSYFHI(M,2)
      ALPHA3 = PSYFHI(M,3)
      CHI    = PSYFHI(M,4)
      GX     = PSYFHI(M,5)
      GY     = PSYFHI(M,6)
      GZ     = PSYFHI(M,7)
      A1X    = PSYFHI(M,8)
      A1Y    = PSYFHI(M,9)
      A1Z    = PSYFHI(M,10)
      A2X    = PSYFHI(M,11)
      A2Y    = PSYFHI(M,12)
      A2Z    = PSYFHI(M,13)
      A3Z    = PSYFHI(M,14)
      A3Y    = PSYFHI(M,15)
      A3X    = PSYFHI(M,16)
C
   45 DO 61 J3 =1,7
      THETA = T(J3)
      PHI   = P(J3)
      INDEX = 0
C
   10 G13 = 0.5*(GX-GZ)*DSIN(2*(THETA+CHI))*DCOS(PHI)
      G23 =-0.5*DSIN(2*PHI)*(GX*(DSIN(THETA+CHI))**2 -GY
C
     1                                    + GZ*(DCOS(THETA + CHI))**2)
C
      G33 = (GX*(DSIN(THETA + CHI))**2 + GZ*(DCOS(THETA +CHI))**2)*
C
     1                                   DCOS(PHI)**2 + GY*DSIN(PHI)**2
      A111 = A1X*(DCOS(THETA + ALPHA1))**2 + A1Z*(DSIN(THETA+ALPHA1))**2
      A211 = A2X*(DCOS(THETA + ALPHA2))**2 + A2Z*(DSIN(THETA+ALPHA2))**2
      A311 = A3X*(DCOS(THETA + ALPHA3))**2 + A3Z*(DSIN(THETA+ALPHA3))**2
      A112 = 0.5*(A1Z - A1X)*DSIN(PHI)*DSIN(2*(THETA + ALPHA1))
      A212 = 0.5*(A2Z - A2X)*DSIN(PHI)*DSIN(2*(THETA + ALPHA2))
      A312 = 0.5*(A3Z - A3X)*DSIN(PHI)*DSIN(2*(THETA + ALPHA3))
      A113 = 0.5*(A1X - A1Z)*DCOS(PHI)*DSIN(2*(THETA + ALPHA1))
      A213 = 0.5*(A2X - A2Z)*DCOS(PHI)*DSIN(2*(THETA + ALPHA2))
      A313 = 0.5*(A3X - A3Z)*DCOS(PHI)*DSIN(2*(THETA + ALPHA3))
      A122 = (A1X*(DSIN(THETA + ALPHA1))**2 +A1Z*(DCOS(THETA+ALPHA1))**2
C
     1                                  )*DSIN(PHI)**2  + A1Y*DCOS(PHI)**2
C
      A222 = (A2X*(DSIN(THETA + ALPHA2))**2 +A2Z*(DCOS(THETA+ALPHA2))**2
C
```

```
     1                                  )*DSIN(PHI)**2  + A2Y*DCOS(PHI)**2
C
      A322 = (A3X*(DSIN(THETA + ALPHA3))**2 +A3Z*(DCOS(THETA+ALPHA3))**2
C
     1                                  )*DSIN(PHI)**2  + A3Y*DCOS(PHI)**2
C
      A123 = DSIN(PHI)*DCOS(PHI)*(-A1X*(DSIN(THETA + ALPHA1))**2  +A1Y
C
     1                                  - A1Z*(DCOS(THETA + ALPHA1))**2)
C
      A223 = DSIN(PHI)*DCOS(PHI)*(-A2X*(DSIN(THETA + ALPHA2))**2  + A2Y
C
     1                                  - A2Z*(DCOS(THETA + ALPHA2))**2)
C
      A323 = DSIN(PHI)*DCOS(PHI)*(-A3X*(DSIN(THETA + ALPHA3))**2  + A3Y
C
     1                                  - A3Z*(DCOS(THETA + ALPHA3))**2)
C
      A133 = (A1X*(DSIN(THETA + ALPHA1))**2 +A1Z*(DCOS(THETA+ALPHA1))**2
C
     1                                  )*DCOS(PHI)**2  + A1Y*DSIN(PHI)**2
C
      A233 = (A2X*(DSIN(THETA + ALPHA2))**2 +A2Z*(DCOS(THETA+ALPHA2))**2
C
     1                                  )*DCOS(PHI)**2  + A2Y*DSIN(PHI)**2
C
      A333 = (A3X*(DSIN(THETA + ALPHA3))**2 +A3Z*(DCOS(THETA+ALPHA3))**2
C
     1                                  )*DCOS(PHI)**2  + A3Y*DSIN(PHI)**2
      DO 61 J4 = 1,8
      J2 = J2 + 1
   65 IF(HFP(J2))68,68,72
   68 DELTA(J2) = 0.CC 00
      GO TO 61
   72 H = HFP(J2)
C
C
C      THE MATRIX ELEMENTS ARE DEFINED BELOW IN TERMS OF THE QUANTITIES
C     DEFINED ABOVE.
C
C
   51 DO 52 MU = 1,16
      DO 52 J= 1,16
      MATRXR(MU,J) = 0.00  0
   52 MATRXI(MU,J) = C.00 00
      MATRXR(1,1) = G.5*G33*B*H +D.25*(A133+A233+A333)-1.5*GN*BN*H
      MATRXR(2,2) = C.5*(G33*B -GN*BN)*H +0.25*(A133+A233-A333)
      MATRXR(3,3) = C.5*H*(G33*B - GN*BN) +0.25*(A133-A233+A333)
      MATRXR(4,4) = 0.5*H*(G33*B - GN*BN) +0.25*(-A133+A233+A333)
      MATRXR(5,5) = C.5*H*(G33*B + GN*BN) +0.25*(A133-A233-A333)
      MATRXR(6,6) = 0.5*H*(G33*B + GN*BN) + 0.25*(-A133+A233-A333)
      MATRXR(7,7) = C.5*H*(G33*B + GN*BN) + 0.25*(-A133-A233+A333)
      MATRXR(8,8) = 0.5*H*(G33*B +3*GN*BN)- 0.25*(A133+A233+A333)
      MATRXR(9,9) =-C.5*H*(G33*B -3.0*GN*BN)+ 0.25*(A133+A233+A333)
```

```
MATRXR(10,10) =-0.5*H*(G33*B - GN*BN) +0.25*(A133+A233-A333)
MATRXR(11,11) =-0.5*H*(G33*B - GN*BN) + 0.25*(A133-A233+A333)
MATRXR(12,12) =-0.5*H*(G33*B - GN*BN) + 0.25*(-A133+A233+A333)
MATRXR(13,13) =-0.5*H*(G33*B + GN*BN) + 0.25*(A133-A233-A333)
MATRXR(14,14) =-0.5*H*(G33*B + GN*BN) + 0.25*(-A133+A233-A333)
MATRXR(15,15) =-0.5*H*(G33*B + GN*BN) + 0.25*(-A133-A233+A333)
MATRXR(16,16) =-0.5*H*(G33*B + 3.0*GN*BN) - 0.25*(A133+A233+A333)
MATRXR(9,8) = C.5*G13*B*H - 0.25*(A113 + A213 + A313)
MATRXI(9,8) = C.5*G23*B*H - 0.25*(A123 + A223 + A323)
MATRXR(10,7)= C.5*G13*B*H - 0.25*(A113 + A213 - A313)
MATRXI(10,7)= C.5*G23*B*H - 0.25*(A123 + A223 - A323)
MATRXR(11,6)  = 0.5 *G13*B*H - 0.25*(A113 - A213 + A313)
MATRXI(11,6)  = 0.5 *G23*B*H - 0.25*(A123 - A223 + A323)
MATRXR(12,5)  = C.5*G13*B*H + 0.25*(A113 - A213 - A313)
MATRXI(12,5)  = 0.5*G23*B*H + 0.25*(A123 - A223 - A323)
MATRXR(13,4)  = C.5*G13*B*H + 0.25*(-A113+A213+A313)
MATRXI(13,4)  = 0.5*G23*B*H + 0.25*(-A123+A223+A323)
MATRXR(14,3)  = 0.5*G13*B*H +0.25*(A113 - A213 + A313)
MATRXI(14,3)  = 0.5*G23*B*H +0.25*(A123 - A223 + A323)
MATRXR(15,2)  = 0.5*G13*B*H + 0.25*(A113 + A213 - A313)
MATRXI(15,2)  = 0.5*G23*B*H + 0.25*(A123 + A223 - A323)
MATRXR(16,1)  = C.5*G13*B*H + 0.25*(A113 +A213 +A313)
MATRXI(16,1)  = 0.5*G23*B*H + 0.25*(A123 +A223 +A323)
MATRXR(2,1) = C.25*A313
MATRXR(5,3)   = MATRXR(2,1)
MATRXR(6,4)   = MATRXR(2,1)
MATRXR(8,7)   = MATRXR(2,1)
MATRXR(10,9)  =-MATRXR(2,1)
MATRXR(13,11) =-MATRXR(2,1)
MATRXR(14,12) =-MATRXR(2,1)
MATRXR(16,15) =-MATRXR(2,1)
MATRXI(2,1) = C.25*A323
MATRXI(5,3)   = MATRXI(2,1)
MATRXI(6,4)   = MATRXI(2,1)
MATRXI(8,7)   = MATRXI(2,1)
MATRXI(10,9)  = MATRXI(2,1)
MATRXI(13,11) = MATRXI(2,1)
MATRXI(14,12) = MATRXI(2,1)
MATRXI(16,15) = MATRXI(2,1)
MATRXR(3,1) = C.25*A213
MATRXR(5,2)   = MATRXR(3,1)
MATRXR(7,4)   = MATRXR(3,1)
MATRXR(8,6)   = MATRXR(3,1)
MATRXR(11,9)  =-MATRXR(3,1)
MATRXR(13,10) =-MATRXR(3,1)
MATRXR(15,12) =-MATRXR(3,1)
MATRXR(16,14) =-MATRXR(3,1)
MATRXI(3,1) = C.25*A223
MATRXI(5,2)   = MATRXI(3,1)
MATRXI(7,4)   = MATRXI(3,1)
MATRXI(8,6)   = MATRXI(3,1)
MATRXI(11,9)  = MATRXI(3,1)
MATRXI(13,10) = MATRXI(3,1)
MATRXI(15,12) = MATRXI(3,1)
```

```
      MATRXI(16,14) = MATRXI(3,1)
      MATRXR(4,1) = 0.25*A113
      MATRXR(6,2)   = MATRXR(4,1)
      MATRXR(7,3)   = MATRXR(4,1)
      MATRXR(8,5)   = MATRXR(4,1)
      MATRXR(12,9)  =-MATRXR(4,1)
      MATRXR(14,10) =-MATRXR(4,1)
      MATRXR(15,11) =-MATRXR(4,1)
      MATRXR(16,13) =-MATRXR(4,1)
      MATRXI(4,1) = 0.25*A123
      MATRXI(6,2)   = MATRXI(4,1)
      MATRXI(7,3)   = MATRXI(4,1)
      MATRXI(8,5)   = MATRXI(4,1)
      MATRXI(12,9)  = MATRXI(4,1)
      MATRXI(14,10) = MATRXI(4,1)
      MATRXI(15,11) = MATRXI(4,1)
      MATRXI(16,13) = MATRXI(4,1)
      MATRXR(9,5) = 0.25*(A111 - A122)
      MATRXR(10,3)  = MATRXR(9,5)
      MATRXR(11,2)  = MATRXR(9,5)
      MATRXR(13,1)  = MATRXR(9,5)
      MATRXI(9,5) = 0.5 *A112
      MATRXI(10,3)  = MATRXI(9,5)
      MATRXI(11,2)  = MATRXI(9,5)
      MATRXI(13,1)  = MATRXI(9,5)
      MATRXR(9,6) = 0.25*(A211 - A222)
      MATRXR(10,4)  = MATRXR(9,6)
      MATRXR(12,2)  = MATRXR(9,6)
      MATRXR(14,1)  = MATRXR(9,6)
      MATRXI(9,6) = 0.5 *A212
      MATRXI(10,4)  = MATRXI(9,6)
      MATRXI(12,2)  = MATRXI(9,6)
      MATRXI(14,1)  = MATRXI(9,6)
      MATRXR(9,7) = 0.25*(A311 - A322)
      MATRXR(11,4)  = MATRXR(9,7)
      MATRXR(12,3)  = MATRXR(9,7)
      MATRXR(15,1)  = MATRXR(9,7)
      MATRXI(9,7) = 0.5 *A312
      MATRXI(11,4)  = MATRXI(9,7)
      MATRXI(12,3)  = MATRXI(9,7)
      MATRXI(15,1)  = MATRXI(9,7)
      MATRXR(10,8)= 0.25*(A311 + A322)
      MATRXR(13,6)  = MATRXR(10,8)
      MATRXR(14,5)  = MATRXR(10,8)
      MATRXR(16,2)  = MATRXR(10,8)
      MATRXR(11,8)  = 0.25*(A211 + A222)
      MATRXR(13,7)  = MATRXR(11,8)
      MATRXR(15,5)  = MATRXR(11,8)
      MATRXR(16,3)  = MATRXR(11,8)
      MATRXR(12,8)  = 0.25*(A111 + A122)
      MATRXR(14,7)  = MATRXR(12,8)
      MATRXR(15,6)  = MATRXR(12,8)
      MATRXR(16,4)  = MATRXR(12,8)
   60 CALL HTRIDI
C
      CALL IMTQL1(IERR)
C
      IF(IERR) 66,66,70
   70 WRITE(6,71)IERR
   71 FORMAT(' IERR IS ZERO  FOR A NORMAL RETURN FROM SUBROUTINE IMTQL1 A
     1ND IS SET TO AN INTEGER J OTHERWISE THE VALUE OF IERR:',I2)
      STOP
C
C      THE FOLLOWING STEP CALCULATES THE APPROPRIATE MICROWAVE FREQUENCY,
C     CONVERTS IT TO MHZ, COMPARES IT TO THE EXPERIMENTAL MICROWAVE
C     FREQUENCY, AND CALCULATES THE DELTA(J2)
C
   66 DELTA(J2) = (((D(16 - INDEX) - D(INDEX + 1))/6.6261960-27) *1.0D-0
     1)- MWFRQ
      CALL ELAPSE(MTLAPS)
      MSEC = MSEC + MTLAPS
  333 IF(MSEC.LT.XX*1000) GO TO 61
      WRITE(6,203) J2,DELTA(J2)
  203 FORMAT(' DELTA(',I2,' ) =',D20.10)
   61 INDEX = INDEX + 1
      FUNCTN= 0.00D 00
      DO 91 KL = 1,56
C
C
   91 FUNCTN  = DELTA(KL)**2 + FUNCTN
C
C     IT IS THIS FUNCTION THAT MUST BE BROUGHT TO AN ABSOLUTE MINIMUM BY
C     A SYSTEMATIC VARIATION OF THE SIXTEEN PARAMETERS.
C
C
   92 IF(MSEC.LT.XX*1000) GO TO 998
      WRITE(6,204)FUNCTN,(PSYFHI(M,I),I = 1,16),NTIME
  204 FORMAT(' ***** FUNCTN =',D20.10,5X,' FOR THE FOLLOWING PARAMETERS:
     2'//8X,6(D14.7,2X)//8X,6(D14.7,2X)//8X,4(D14.7,2X),10X,' NTIME=',I5
     3/)
  998 NTIME  = NTIME + 1
  999 RETURN
      END
C
C     * * * * * * * * * * * * HUNTER * * * * * * * * * * * * * * * * * * *
C
      SUBROUTINE HUNTER
C          ( SEE APPENDIX F )
C
      IMPLICIT REAL*8(A-H,O-Z)
      COMMON/HUNTR/RHO(16),STEP(16),STOP(16),NP,IPASS
      COMMON/PSYFH/PSYFHI(2,16),SS,NTIME
C
C
C     * * * * * * * * * * * * *  HUNT  * * * * * * * * * * * * * * * * * * *
C
      SUBROUTINE HUNT
```

```
C     SUBSIDIARY OF HUNTER
C          ( SEE APPENDIX F )
C
      IMPLICIT REAL*8(A-H,O-Z)
      COMMON/PSYFH/PSYFHI(2,16),SS,NTIME
      DIMENSION DELT(16)
      COMMON/HUNTR/RHO(16),DEL(16),STOP(16),NP,IPASS
C
C
C     * * * * * * * * * * * *  HTRIDI  * * * * * * * * * * * * * * * * * * *
C
      SUBROUTINE HTRIDI
C          ( SEE APPENDIX E )
C
      COMMON/MATRIX/AR(16,16),AI(16,16),D(16),E(16),E2(16),TAU(2,16),N
C
C     * * * * * * * * * * * *  IMTQL1  * * * * * * * * * * * * * * * * * * *
C
      SUBROUTINE IMTQL1(IERR)
C          ( SEE APPENDIX E )
C
      COMMON/MATRIX/MATRXR(16,16),MATRXI(16,16),D(16),E(16),E2(16),TAU(2
     1,16),N
```

VITA

John Everett Rhoads

Candidate for the Degree of

Doctor of Philosophy

Thesis: RADIATION DAMAGE IN $KMgF_3$

Major Field: Physics

Biographical:

Personal Data: Born in Decatur, Texas, July 13, 1946, the son of Mr. and Mrs. John L. Rhoads.

Education: Graduated from Wichita Falls Senior High School, Wichita Falls, Texas, in May, 1964; received the Bachelor of Science degree with a major in physics and a minor in mathematics from Midwestern University, Wichita Falls, Texas, in 1968; received Hardin Award, was a member of Alpha Chi (national honorary society), and was named to Who's Who in American Colleges and Universities while attending Midwestern University; received the Master of Science degree in physics from Oklahoma State University in December, 1972; was elected to Sigma Pi Sigma (physics honorary society) and Phi Kappa Phi while attending Oklahoma State University; completed requirements for the Doctor of Philosophy degree at Oklahoma State University in December, 1974.

Military Service: U. S. Army, 1968-1970 (Vietnam Service, 1969-1970); recipient of Army Commendation Award.